Study of Neuroprotective Effect of Cryptotanshinone, an Acetylcholinesterase Inhibitor, in Cell and Animal Models

By
WONG, Kin Kwan Kelvin

A Thesis Submitted in Partial Fulfillment of the Requirements for the Degree of Doctor of Philosophy in Biochemistry

June 2009

Thesis/assessment Committee

Professor Lau K. F. (Chair)
Professor Shaw P.C. (Thesis Supervisor)
Professor Wan C.C. (Thesis Supervisor)
Professor Tsang S. Y. (Committee Member)
Professor Han Y. F. (External Examiner)

I declare that the assignment here submitted is original except for source material explicitly acknowledged, and that the same or related material has not been previously submitted for another course. I also acknowledge that I am aware of University policy and regulations on honesty in academic work, and of the disciplinary guidelines and procedures applicable to breaches of such policy and regulations, as contained in the website http://www.cuhk.edu.hk/policy/academichonesty/

_____ _____18/6/2009 _____

Signature Date

__Wong Kin Kwan Kelvin _____ ____05025830_____

Name Student ID

Acknowledgements

First of all I would like to express my sincere gratitude to my supervisors Prof. P.C.Shaw and Prof. David C.C.Wan for giving me opportunity to have my PhD study under their guidance. Thanks for their continuous support and guidance throughout these years of my PhD study.

Thanks to Mr. Lin Huang Quan and Ms. Cheung Sau Wan for their help on the preparation, purification and identification of the compounds that used in this study. More thanks go to Dr. John Rudd for his valuable guidance on the animal study and the preparation of my manuscript. I also want to show my appreciation to Dr. K.F. Lau for his teaching on the technique of scientific writing.

Of course, without the love and patience of my parents, it is impossible for me to receive education and opportunity to attain higher achievement. I express my greatest gratitude to their perseverance love.

Last but not least, to the fellows in my lab, especially Mr. Li Ming and Ms. Judy Chan, for their help, friendship and encouragement in my study.

Abstract

Alzhemier's disease (AD) is a common form of dementia which is characterized by the deposition of amyloids in affected neurons and a cholinergic neurotransmission deficit in the brain. Current therapeutic intervention for AD is primarily based on inhibition of brain acetylcholinesterase (AChE) to restore the brain acetylcholine level. Cryptotanshinone (CT) is a diterprene which is extracted from the root of *Salvia miltiorrhiza,* an herb that is commonly prescribed in Chinese medicine to treat cardiovascular disease. The present study is aimed at verifying CT's property as an AChE inhibitor using different models. By AChE activity assay, CT was found to be a dual inhibitor which inhibits both human acetylcholinesterase (AChE) and butylcholinesterase (BuChE) with similar IC_{50}. CT inhibited human AChE in a reversible manner, and the inhibition showed the characteristics of mixed-type. To human BuChE, CT is an uncompetitive inhibitor. CT can also inhibit AChE from rat cortical neurons. Apart from AChE inhibition, CT was demonstrated to have ameliorating effect on glutamate excitotoxicity, which is a cause of neuron death in AD. Further study showing that CT treatment can reduce cellular tau phosphorylation, which is the downstream effector of glutamate-induced excitotoxicity. In animal model, the

effect of CT on learning impairment in scopolamine-treated rats was also evaluated by the acquisition protocol of Morris water maze. The task learning ability of scopolamine-treated rats was significantly reversed by CT, and the CT-fed rats were able to develop spatial searching strategy comparable to the control animals. Chronic administration of CT at effective doses did not cause significant hepatotoxicity. Cholinergic side effect of muscle weakness was not observed in CT treated rats. On the contrary CT was found to increase the locomotor activity of NIH mice in forced swimming test through reducing the lactic acid in the circulation. Data in this study gives further support on CT's potential as a therapeutic drug for treating AD.

摘要

老人性痴呆症(AD) 是一種導致老年人痴呆的慢性神經退化疾病。該病的特徵是amyloid 蛋白在受影響的腦細胞周邊簇集成團與及大腦在神經衝動傳輸過程中缺乏乙醯膽鹼(ACh)。現行的 AD 治療方法主要基於應用乙酰膽鹼酯酶(AChE)抑制劑來增加大腦的 ACh 的含量,增強中樞膽鹼能系統的功能。丹參是一種傳統上用以治療心血管疾病的藥品，在這次研究中，其二萜醌類抽取物隱丹參酮(CT)的膽鹼酯酶抑制作用會用不同的生物模型加以查證。在膽鹼酯酶活性實驗中發現 CT 同樣為 AChE 與丁酰膽鹼酯酶(BuChE)抑制劑，兩者擁有相近的 IC_{50} 值。對於 AChE，CT 是一種可逆轉性抑混合型抑制劑，而對於 BuChE 則是一種反競爭性抑制劑。CT 同樣能抑制大鼠大腦皮質神經元的 AChE。除了 AChE 抑制作用之外，在大鼠大腦皮質神經元的模型中 CT 亦能緩和穀胺酸引起的興奮毒性(其中一種在 AD 導致神經凋亡的原因)。進一步研究顯示 CT 能減低細胞內 Tau 蛋白的磷酸化，而 Tau 蛋白的磷酸化是穀胺酸引起的興奮毒性的下游過程。用在實驗動物模型中，CT 能明顯地緩和由東莨菪鹼 (scopolamine) 所引發的水迷宮認知障礙，及建立與對照組相似的搜索策略。慢性給葯實驗中 CT 沒有引起明顯的肝毒性，亦沒有觀察到明顯的外周膽鹼能效應如肌肉無力。相反地, CT 能通過減低循環系統中的乳酸量，增強 NIH 小鼠在負重游泳實驗中所表現的活動力。所有實驗數據顯示 CT 有被發展為治療 AD 藥物的潛質。

Content

List of Abbreviations

ACh	Acetylcholine
AChE	Acetylcholinesterase
AChE-E	Erythrocytic AChE
AChE-R	Readthrough AChE
AChE-S	Synaptic AChE
ACPI	Atmospheric pressure chemical Ionization mode
ACTI	Acetylthiocholine iodide
AD	Alzheimer's disease
ALT	Alanine aminotransferase
AMPK	AMP-activated protein kinase
APP	Amyloid precursor protein
Aβ	Beta-amyloid
BuChE	Butyrylcholinesterase
CMM	Chinese Medicinal Material
CNS	Central nervous system
CT	Cryptotanshinone
DTNB	5'5-dithio-bis-(2-nitrobenzoate)
ECL	Enhanced chemiluminescence
FDA	US Food and Drug Administration
Gal	Galantamine
GSK-3β	Glycogen synthase kinase 3β
HPLC	High performance liquid chromatography
HRP	Horseradish peroxidase
HupA	Huperzine A
JNK	c-Jun-N-terminal kinase
LC-MS	Liquid chromatography-mass spectrometry
MRM	Multiple reaction monitoring
NFT	Neurofibrillary tangles
NMDA	N-methyl D-aspartate
PHF	Paired helical filaments
PI3	phosphatidylinositol 3-kinase
PP2A	Protein-phosphatase 2A
S/D rat	Sprague Dawleey rat
SC-CO2	Super-critical carbon dioxide
Scop	Scopolamine
SDS-PAGE	Sodium dodecyl sulfate polyacrylamide gel electrophoresis

TBS	Tris-buffer saline
TEMED	N,N,N,N-tetramethyl ethylene diamine
TLC	Thin-layer chromatography

List of Figures

List of Tables

Chapter 1 Introduction

1.1 Alzheimer's disease

Alzheimer 's disease (AD) is first documented in the medical literature in 1907 by a German clinician Alois Alzheimer. It is a neurodegenerative disorder which accounts for up to 75% of all cases of dementia. AD is a heterogeneous group of dementias that shares common clinical symptoms. These symptoms of AD include progressive cognitive impairments, abnormalities of memory, problem solving, language, calculation, visual-spatial perceptions, judgment, and behavior (Sisodia et al., 1995). There would also be psychotic symptoms in some cases, such as hallucinations and delusions. In late stage of the disease, patients are often muted, incontinent, bedridden and usually die of intercurrent medical illnesses (Price et al., 1998). Cognitive alterations in AD are associated with widespread neurodegeneration throughout the association cortex and hippocampus.

1.1.1 Pathology

Neuronal death in AD patients appears in brain area which associates in higher mental function. They are usually neocortex and hippocampus. Neuron

loss in AD is observed along with the neuropathological hallmarks. They are neuritic plaques and neurofibrillary tangles (NFT), preferentially located in limbic and cortical areas of the brain (Yankner, 1996).

1.1.1.1 Neuritic plaques

The neuritic plaques are spherical, multicellular lesions containing extracellular deposits of beta-amyloid (Aβ) protein in fibrillar form. Neuritic plaques are surrounded by degenerating axons and dendrites, activated microglia, and reactive astrocytes (Zhao et al., 2002). Aβ is produced from alternative splicing of Amyloid Precursor Protein (APP) (Fig 1.1). In AD, pathological processing of APP resulted in a deposition of insoluble Aβ. Aβ produced undergoes self-aggregation into Aβ fibrils. Aβ fibrils exert its neurotoxic effect on inducing glucose deprivation, increasing oxidative stress, damaging cell membrane, inducing inflammation, binding to receptor and altered signal transduction resulting in apoptosis (Yankner, 1996).

1.1.1.2 Neurofibrillary tangles (NFT)

A major characteristic lesion observed in AD is the accumulation of intracellular NFT in the affected brain regions. NFT composes of damaged

microtubule and paired helical filaments (PHF), which mainly consist of hyperphosphorylated tau protein (Imahori and Uchida, 1997). Tau protein is a microtubule-associated protein. In AD, hyperphosphorylation of tau into PHF-tau would cause it to lose its normal physiological function (Mandelkow et al., 1995). PHF-tau is disintegrated from microtubules and polymerized with straight filament to form PHF (Fig 1.2).

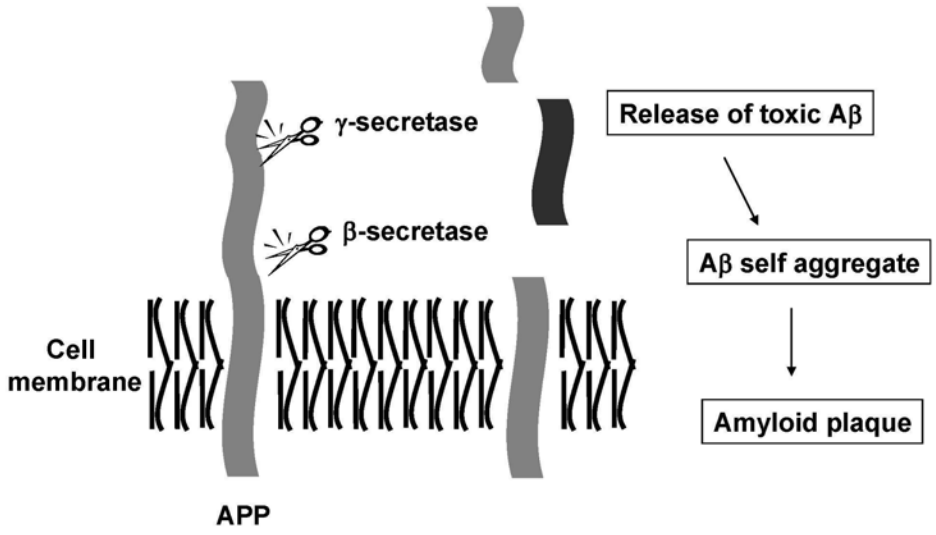

Fig 1.1 Amyoidosis in AD. APP is cleaved by β-secretase and γ-secretase forming Ab42. Ab42 fragment aggregates in extracellular space resulting in amyloid plaque.

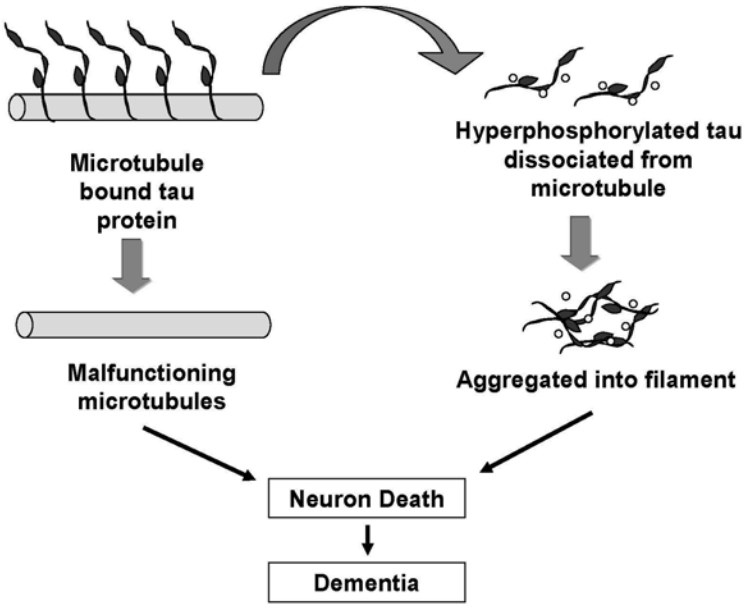

Fig 1.2 Tauopathy in AD. Hyperphosphorylation of tau protein leads to its disassembly from microtubule. The phosphorylated tau undergoes self-aggregation into neurotoxic intermediate. Some of them forming stable filament and resulting in intracellular deposit.

1.1.1.3 Loss of cholinergic function in AD patients

By systematic biochemical investigation on patient's brain it was found that the damage of brain cholinergic system contributes significantly to the deterioration of learning and memory in AD patients (Esiri, 1996). Scientist discovered that the AD brain was deficient in acetylcholine, and this led to the inability to transmit neurological impulses across cholinergic synapses, causing cognitive, functional and behavioral dysfunction. Brain biopsies and autopsy studies revealed that AD patients are suffered from a loss of cholinergic neuron and a reduced activity of cortical choline acetyltransferase, an enzyme that synthesizes acetylcholine from choline (Perry et al., 1978b). Subsequent discoveries of the decrease in choline acetyltransferase activity (Perry et al., 1977), reduced choline uptake (Rylett et al., 1983), ACh efflux (Nilsson et al., 1986) and loss of cholinergic perikarya from the nucleus basalis of Meynert (Giacobini, 2003; Perry et al., 1978a; Perry et al., 1978b) confirmed a substantial presynaptic cholinergic deficit.

1.1.2 Cholinergic hypothesis

As cognitive deterioration in AD is significantly associated with the loss of cholinergic neuron and cholinergic transmission, drugs that can increase brain

cholinergic activity may ameliorate cognitive dysfunctions. This assumption is referred as the cholinergic hypothesis (Contestabile and Ciani, 2008). This hypothesis provides a direction for designing drugs against memory deterioration in neurodegenerative diseases such as AD.

1.2 Acetylcholinesterase (AChE)

AChE is the enzyme that degrades synaptic ACh into choline and an acetate group (Fig 1.3). AChE can be found in vertebrates and invertebrates, from insects, fish, reptiles birds to animals. AChEs from different species share similar sequences. Crystal structures from mouse (Bourne et al., 1995), *Drosophila* (Harel et al., 2000) and man (Kryger et al., 2000) are also found to be similar. Isoforms of AChE are produced by alternative splicing of pre-mRNA. There are three isoforms: the synaptic (AChE-S), erythrocytic (AChE-E) and readthrough (AChE-R). Except AChE-E, which attaches at the outer membrane of erythrocyte, AChE-S and AChE-R are found in the neuromuscular junctions and the central nervous system (CNS). AChE-S is a tetramer that possesses a collagen-like tail, which allows its direct attachment to neuromuscular junction (Bon et al., 1997). AChE-R is a free monomer that does not possess attachment feature and remains soluble within synaptic cleft.

During signal transduction in cholinergic neuron, ACh released by presynaptic neuron first binds to either muscarinic M1 or M2 receptor, triggering action potential, and then quickly hydrolyzed by either AChE-R or AChE-S. This degradation mechanism is important in preventing over-activation of post-synaptic membrane. The choline molecule produced is then returned to presynaptic neuron for recycling.

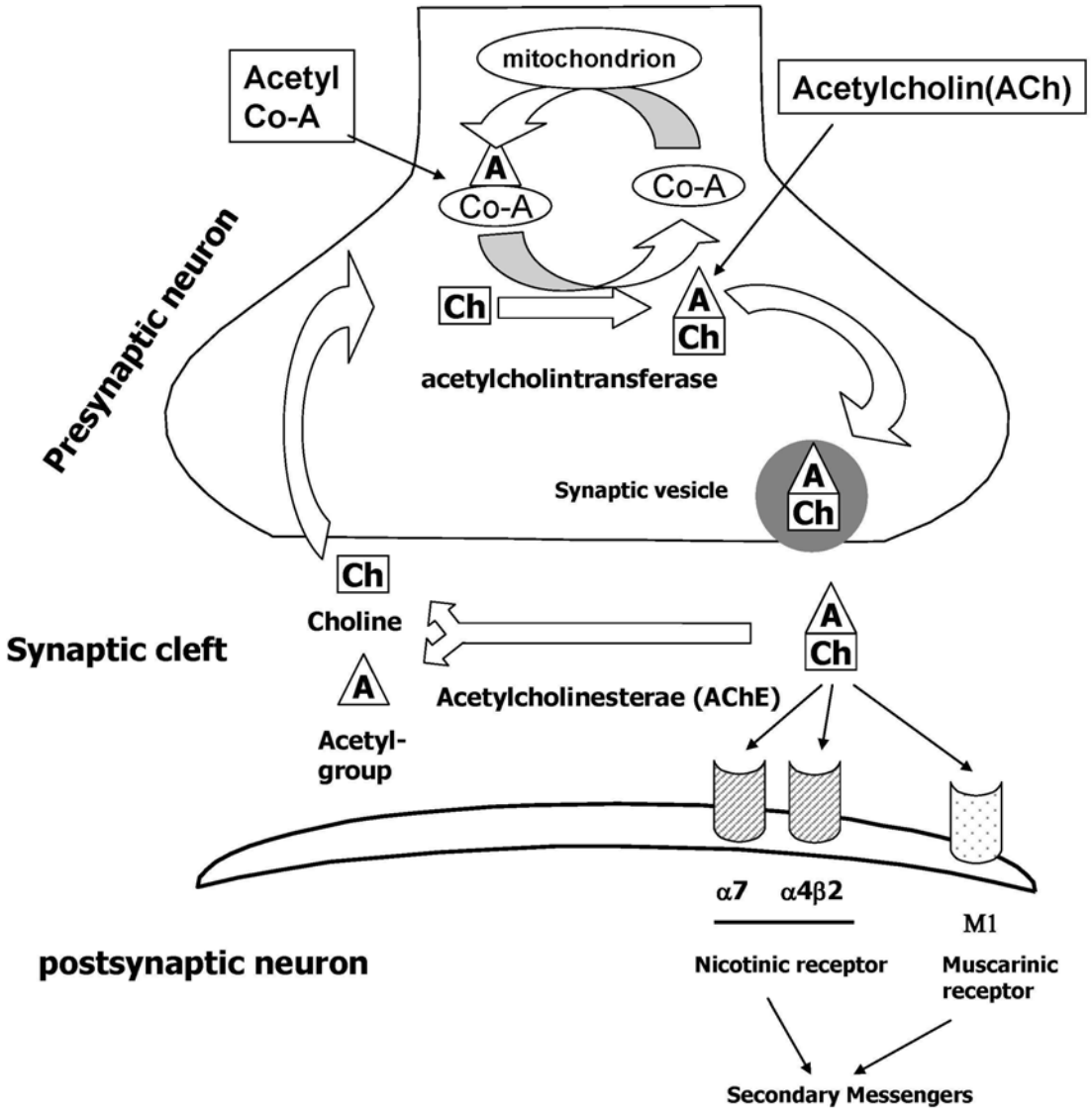

Fig 1.3 Cycling of ACh in synapse. In the presynaptic neuron, choline acetyltransferase catalyses the synthesis of acetylcholine (ACh) from choline and acetyl-coenzyme A. ACh is released to synaptic cleft via synaptic vesicle. Action potential triggers when ACh binds to nicotinic or muscarinic receptors located on the post synaptic membrane. ACh is then hydrolyzed by AChE, either soluble AChE-S or membrane-bound AChE-R, at the synaptic cleft. The choline molecule is then recycled back to presynaptic neuron.

1.2.1 Regulation of AChE

AChE is regulated in transcriptional, post-transcriptional and in post-translational levels. AChE expression can be either up-regulated by physiological condition or external stimulation. Physiological condition like cell differentiation, expression of AChE is increased as an indication of axonal growth (Rotundo, 1990). External stimulation including ACh-mediated excitation is a major stimulation of AChE expression. Long term exposure to anti-cholinergic agents including AChE inhibitor would increase AChE expression (Parnetti et al., 2002). Traumatic insult, which induces excessive ACh release, is another stimulation of AChE expression (Kaufer et al., 1998). The plasticity of AChE expression level is an important mechanism in response to the environment and self protection. For example, AChE expression elevation in response to cholinergic toxins (Ashani et al., 1991) can prevent the organism from poisoning.

1.2.2 Role of AChE in AD

In the brain of AD patients, there is a general loss in cholinergic neuron causing a selective downregulation of AChE-R. In certain brain region, the reduction may up to 90% due to the loss of presynaptic terminals, while the

amount AChE-S remain unchanged (Siek et al., 1990). Although there is an overall loss in AChE activity detected due to neuron loss, the activity of AChE increases around beta-amyloid plaques (Garcia-Ayllon et al., 2008). AChE can accelerate Aβ formation *in vitro* and the ability of AChE-amyloid complex on inducing neurodegeneration is even higher than Aβ alone (Inestrosa et al., 2005). Additionally, AChE binds to non-amyloidogenic form of amyloid and acts as a pathological chaperone inducing a conformational transition to the amyloidogenic form (De Ferrari et al., 2001).

1.2.3 Inhibition of AChE in AD

AD involves selective loss of cholinergic neurons in the brain. The reduction in cholinergic activity is correlated with the degree of cognitive impairment and is associated with decreased levels of ACh. To compensate the loss of cholinergic neurons, inhibition of AChE, the degradating enzyme of ACh, is used as a treatment to maintain the synaptic concentration of ACh of the surviving cholinergic system. So far, AChE inhibitors have been a major type of anti-AD drugs approved by the US Food and Drug Administration (FDA). Current treatment relies much on prolonged administration of AChE inhibitor to delay disease progression, in particular, the memory deficit.

1.2.4 Current available AChE inhibitor-type AD drugs

There are four AChE inhibitors that approved by the US Food and Drug Administration (FDA) as an anti-AD drug. They are Tacrine, Donepezil, Rivastigmine and Galantamine (Fig 1.4).

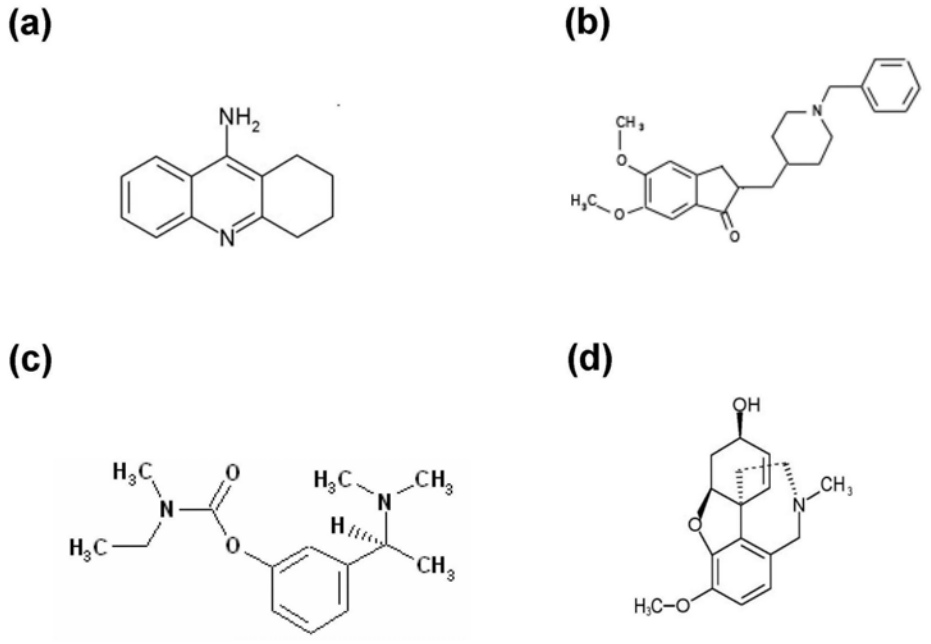

Fig 1.4 AChE inhibitor-type AD drugs. a) Tacrine, b) Donepezil, c) Rivastigmine, d) Galantamine

1.2.4.1 Tacrine

Tacrine (marketed under the trade name of Cognex®) is the first synthetic drugs approved by FDA in 1993 for treating mild to moderate AD. However, clinical uses have been limited due to associated cholinergic, hepatic, and gastrointestinal adverse reactions which lead to its withdrawal (Knapp et al., 1994; Summers, 2006). Recently, intranasal delivery has been suggested as an alternative way to prevent peripheral side effect of tacrine (Jogani et al., 2008). Analogues of tacrine like tacrine dimer or chemically linking tacrine with another molecule have been introduced as a mean of AD drug design (Savini et al., 2001). These tacrine-based analogues provides a alternative AChE inhibitor with higher potency (Wang et al., 1999b), less hepatotoxicity (Fang et al., 2008), and with additional neuroprotective effect (Fu et al., 2006; Leon et al., 2008).

1.2.4.2 Donepezil

Donepezil (marketed under the trade name of Aricept®) is the second drug for treating AD which was approved in 1996 by the FDA. It was first discovered in an attempt to synthesize a non-toxic tacrine derivative (Sugimoto et al., 2002). Comparing with tacrine, donepezil shows improved brain selectivity (Kosasa et

al., 1999), reduced hepatotoxicity (Rogers et al., 2000) and increased bioavailability (Nordberg and Svensson, 1998). Donepezil has been described as the second generation of anti-AD drug that possesses both anti-AChE and disease-modifying effect: donepezil treatment balances APP processing and reduced non-amyloidogenic cleavage of APP in AD patients (Zimmermann et al., 2005); it also protects cultured neuronal cell form Aβ toxicity (Svensson and Nordberg, 1998); donepezil treatment increases nicotinic receptor expression in culture thus increases the brain sensitivity to ACh.

1.2.4.3 Rivastigimine

Rivastigmine (marketed under the trade name Exelon®) is approved by the FDA in 1997. It is a special type of AChE inhibitor. Unlike tacrine and donepezil, which inhibit AChE by competing the catalytic site with ACh, It is a carbamate which inhibits AChE through carbamylation and de-carbamylation of the esteratic site of AChE (Fig 1.5). It is a slow process and thereby rivastigmine is classified as an intermediate-acting or pseudo-irreversible agent due to its long inhibition on AChE of up to 10 hours (Jann, 2000). Rivastigmine is not a selective AChE inhibitor. It also inhibits BuChE (Cutler et al., 1998). This dual inhibiting property is believed to be responsible for the higher incident of

cholinergic side effect reported in clinical cases (Farlow and Lilly, 2005). However, in some cases that patient has developed tolerance on AChE-specific drugs like donepezil and tacrine, rivastigmine is effective on restoring the drug efficacy (Inglis, 2002).

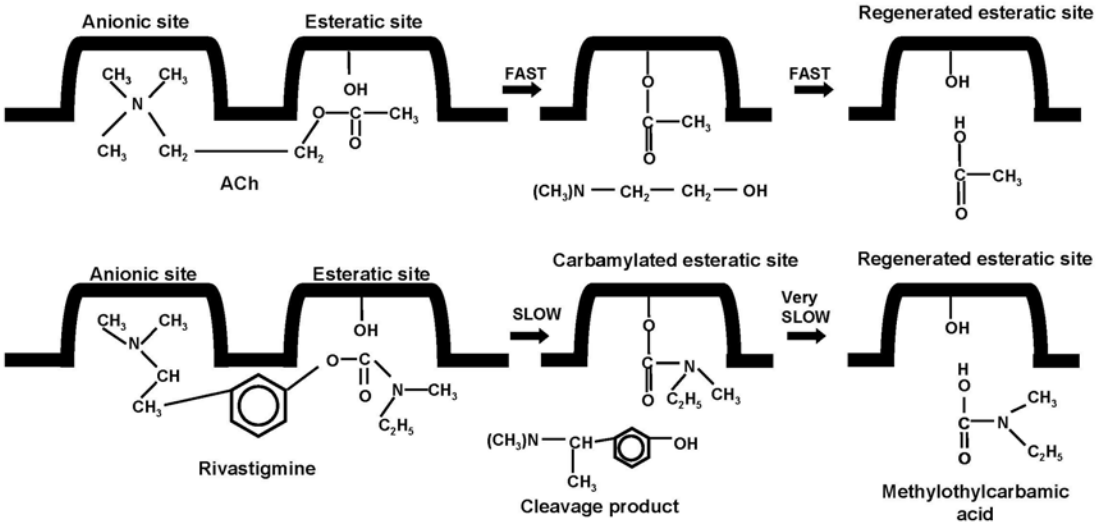

Fig 1.5 Binding of ACh (upper panel) and rivastigmine (lower panel) to the active site of AChE. After binding to the active site, a cabamate group is left behind. This occupies the active site of AChE and results in longer inhibition time (Jann, 2000).

1.2.4.4 Galantamine

Galantamine (marketed under the trade name Reminyl®) is an alkaloid isolated from *Galanthus woronowii* (Bores et al., 1996). It is the first approved as anti-AD drug. Galantamine, in addition to its inhibitory effect on AChE, is an

allosterically potentiating ligand of nicotinic receptor. It binds to the allosteric site of nicotinic ACh receptor and potentiating nicotinic ACh receptor activity in response to ACh (Samochocki et al., 2003). Long term treatment of galantamine can upregulate the amount of brain nicotinic receptor (Woodruff-Pak et al., 2001). Galantamine can protect neuron from glutamate-induced excitotoxicity, which is a major event of neurodegeneration caused by Ab toxicity (Takada-Takatori et al., 2006). Galantamine exerts its protection effect against Ab toxicity through upregulation of the protective protein bcl-2 and via α7 nicotinic ACh receptors (Geerts, 2005). Galantamine and Donepezil are two AChE-type anti-AD drugs that are said to be disease-modifying.

1.2.5 Search of AChE inhibitors from plant

Successful cases of the above AChE inhibitors have raised the interest on the search of AChE inhibitors from natural products that are prescribed in folk medicine. The search of AChE inhibitors from traditional remedy, which has proven its effect on memory-improving, becomes a method for developing lead compounds for treating AD. Previous effort from our group to screen for AChE inhibitors from Chinese Medicinal Materials (CMM) has come up with several

candidates. One of them is the 95% ethanol extract of “Danshen”, which is the dried roots of *Salvia miltiorrhiza Bunge.* (Ho T.W., 2003)

“Danshen” is a popular traditional Chinese herb. It has been included in medicinal formulae for treating aging problems for its action of heart nourishing and spirit pacifying. Clinical studies on these formulae have proven their effectiveness against memory depletion and blood stasis in the elderly (Cheng et al., 2004; Liao and Li, 1996; Wang et al., 2005). The 95% ethanol extract of Danshen contains lipophilic components with more than 30 diterpenoid tanshinones; the major active constituents include tanshinone I, IIA, B, cryptotanshinone, dihydrotanshinone, methylenetanshinone, and isotanshinone IIA. By activity guided fractionation, cryptotanshinone (CT) is selected for further study by its anti-AChE activity.

1.2.6 Cryptotanshinone (CT), AChE inhibitor from *Salvia miltiorrhiza Bge.*

CT (Fig 1.6) is found to possess various biological activities including anti-cyclooxygenase-2 activity, antibacterial activity, anti-atherosclerosis and anti-neointimal formation activity (Jin et al., 2006; Lee et al., 1999; Suh et al., 2006). Pharmacokinetic studies of CT showed that it can be absorbed through

intestine into blood and distributed in a short time ($T_{1/2\alpha}$ = 2.36 min). It can pass through blood brain barrier (Xie and Shen, 1983; Zhang et al., 2006). CT absorbed is then metabolized into tanshinone IIA by liver (Xue et al., 1999). As CT is able to pass through different cellular barriers, from intestine to brain. It can be available as an oral-administrating drug.

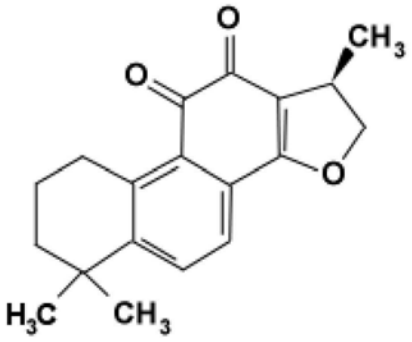

Fig 1.6 Structure of CT

1.3 Project objective

This study works on evaluating the potential of CT as an anti-AD drug. The present study aimed at 1) Characterizing the AChE inhibiting property of CT *in-vitro*, 2) Studying *in-vivo* efficacy of CT on protecting scopolamine-induced memory impairment of the rats in Morris water maze task, and 3) Exploring other beneficial effects of CT for AD pathology.

Chapter 2 Purification of cryptotanshinone

2.1 Introduction

Danshen and its active components are widely used in pharmaceutical and cosmetic industry. In the past, tanshinones, including cryptotanshinone (CT), was obtained by reflux in 95% ethanol and then followed by column purification. With this method, CT can be easily purified from the crude drug. However, this traditional method has a shortcoming. High temperature and prolonged heating would cause a great yield reduction. In order to improve the efficiency of the extraction procedure, a method called Super-critical-carbon-dioxide (Sc-CO_2) fluid extraction was introduced (Li et al., 2002). Nowadays, the Sc-CO_2 extraction of CT has been adopted for large scale preparation of CT in industry because of its high speed, less pollution and relatively high yield. Supercritical fluid extraction of crude Danshen using supercritical CO_2 and 95% ethanol as co-solvent yields extract containing 42% tanshinones, with 33% of CT content (Luo et al., 2006).

We have obtained a batch of Sc-CO_2 extract of Danshen from a commercial

source. In this chapter, purification procedure using chromatography technique was applied and the product quality was verified by high performance liquid chromatography (HPLC) and liquid chromatography-mass spectrometry (LC-MS) method. CT content of final product was found to be >90% pure.

2.2 Materials and Methods

2.2.1 Silica gel chromatography

Sc-CO_2 Danshen extract was purchased from Guangzhou Masson Pharmaceutical Co., Ltd. Specification sheet of the extract is listed in Table 2.1.

Table 2.1 Information on specification sheet of CT from Guangzhou Masson Pharmaceutical Co., Ltd.

Appearance	Salmon pink or scarlet Crystalline Powder
Content of cryptotanshinone (HPLC)	48% ~ 90%
Particle Size	60 mesh
Moisture	≤5%
Sulphated Ash	≤1%
Heavy metals	≤20PPM
Pesticides	Negative
Total Plate Count	≤1000cfu/g
Yeast & Mold	≤100cfu/g
Salmonella	Negative
E.Coli	Negative
Stock Spec	50%、60%、90%

Sc-CO_2 extract of Danshen was first dissolved in absolute methanol (AR grade, SCHARLAU, Spain) in concentration 5 ml/g. To prepare the column, slurry of

40 g silica gel (silica gel 60:70-230 mesh, Sigma, China) was loaded into a 40 cm x 3.5 cm diameter glass column. Slurry of gel was prepared by adding 40 g silica gel to 80 ml initial elution buffer which is 100% petroleum ether (AR grade, LAB-SCAN, Thailand). The column was allowed to settle in 100% petroleum ether overnight. Danshen Sc-CO_2 extract in methanol was mixed with 0.5 g of silica gel. The mixture was swirled until all solvent evaporated. Two ml of hexane was added to the dried powder mixture. This slurry of mixture was then transferred to the top of the prepared column. 20 ml of hexane was used to rinse the CT mixture onto the column. Separation of CT was started by eluting with petroleum ether:ethyl acetate in ratio 10:1. Fractions collected were monitored by Thin-layer chromatography (TLC) (silica gel 60 F254, 0.25 mm, Sigma, China). In TLC, petroleum ether:ethyl acetate in ratio 10:1, which was the same as the eluent above, was used as developing solvent. Fraction collected from the column was directly spotted onto the TLC plate. CT standard (>99% purity, National Institute for the Control of Pharmaceutical and Biological Products, State Drug Administration, China) was run in parallel to identify the CT. Several fractions, guided by preliminary TLC result, were joined together for purity evaluation as below.

2.2.2 Analysis by HPLC

Fractions from silica gel chromatography were dried using a rotary evaporater (Rotavapor. BÜCHI, Switzerland). Dried powder of fractions was then re-dissolved in absolute methanol in concentration 50 mg/ ml. To make sure all powder was completely dissolved, 30 minutes low-power sonication (Model -1510. BRANSON, USA) is applied. Before injecting into an HPLC column, fractions were filtered through a 0.22 μm filter (Millipore, China). Reverse-phase HPLC column (Symmetry C-18 5.0 μm, 4.6 mm x 150 mm. Waters, USA) was used for the analysis. Mixure of 20% H_2O with 0.5% acetic acid and 80% absolute methanol (LAB-SCAN Thailand) with 0.05% trifluoroacetic acid (Sigma, China) was used as mobile phase. HPLC analysis was started by injecting 5 μl of sample into the column, and then run for 20 minutes in the mobile phase. The flow rate was 1.0 ml/min with the column kept at ambient temperature. The detection wavelength was set to 254nm.

2.2.3 Analysis by LC-MS-MS

Electrospray mass spectra were acquired using an Agilent 1100 Series LC/MSD Trap mass spectrometer (Agilent Technologies, CA, USA). High purity nitrogen was used as a nebulizing gas. The Atmospheric Pressure

Chemical Ionization mode (ACPI) was used as interface. The mass spectrometer was operated in the positive ion multiple reaction monitoring (MRM) mode with the discharge current set at 4.0μA. Vaporizer temperature was 500℃, nitrogen sheath and auxiliary gas were set at 50 psi. Full scan mass spectra were acquired by scanning over the range m/z 50 - 2200 at a scan cycle time of 300ms.

2.3 Results

2.3.1 Silica gel purification of Danshen Sc-CO_2 extract

After the first round of purification, fractions with similar TLC profile were pooled as a single fraction. Collected fractions were spotted on silica gel TLC plate and developed in a development vessel saturated with a developing solution containing petroleum ether:ethyl acetate in ratio 10:1 (Fig 2.1). The only orange spot in lane 1, which is CT, was found in lane 5, which is the collected fraction F3. This F3 was further subjected to purification by another round of silica gel column purification. CT obtained after second round of purification were in high purity. Purity of CT was checked by HPLC analysis.

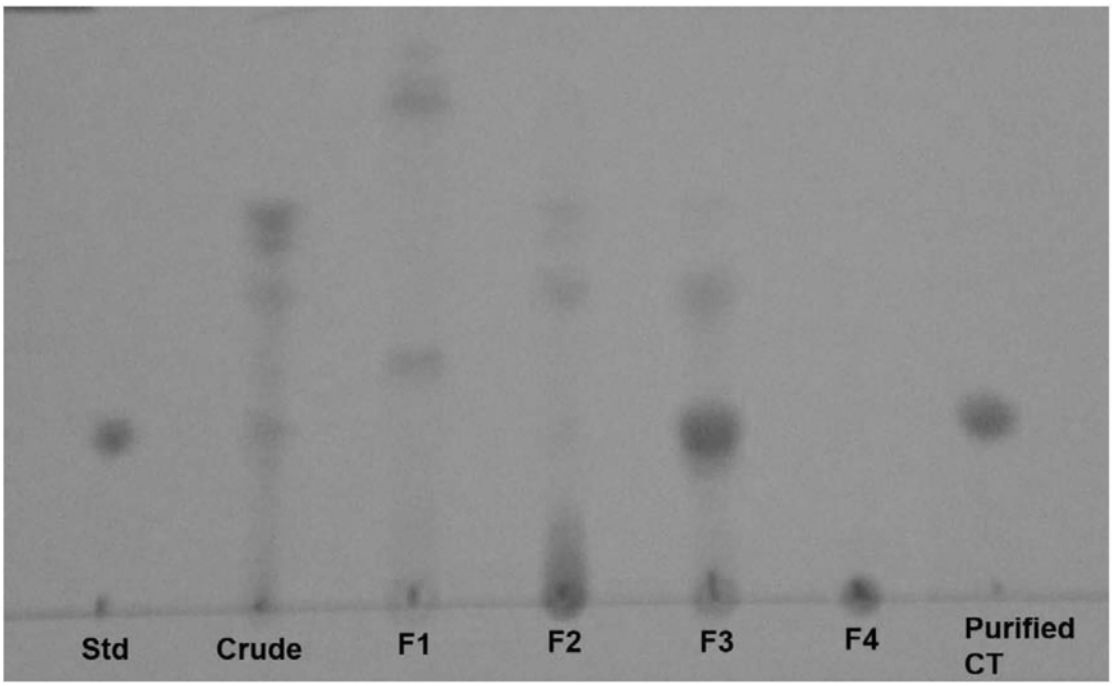

Fig 2.1 TLC profiles of CT standard (Std); Sc-CO2 extract of Danshen (Crude); fractions collected from silica-gel column purification (F1, F2, F3, F4); final CT obtained after two rounds of column purification (Purified CT)

2.3.2 HPLC analysis of purified fractions

HPLC chromatograms of CT standard (Fig 2.2a), Sc-CO_2 extract of Danshen (Fig 2.2b), fractions collected (Fig 2.2 c-f), and final purified CT (fig 2.2g) have been worked out to verify the purity of CT. The only peak in standard CT at retention time at 11.3 min (Fig 2.2a; Fig 2.3) was used as a reference which indicated the present of CT in extracts. After first round of silica gel column purification of the SC-CO_2 extract, enriched content of CT was detected in fraction F3 (Fig 2.2e). Peak integration result of F3 chromatogram detected 72% CT content (Fig 2.4). Another round of column purification was then performed to obtain CT in higher purity. Final purified CT was obtained after second round of purification. Peak integration of its HPLC profile showed this final product contains 92.8% CT (Fig 2.5).

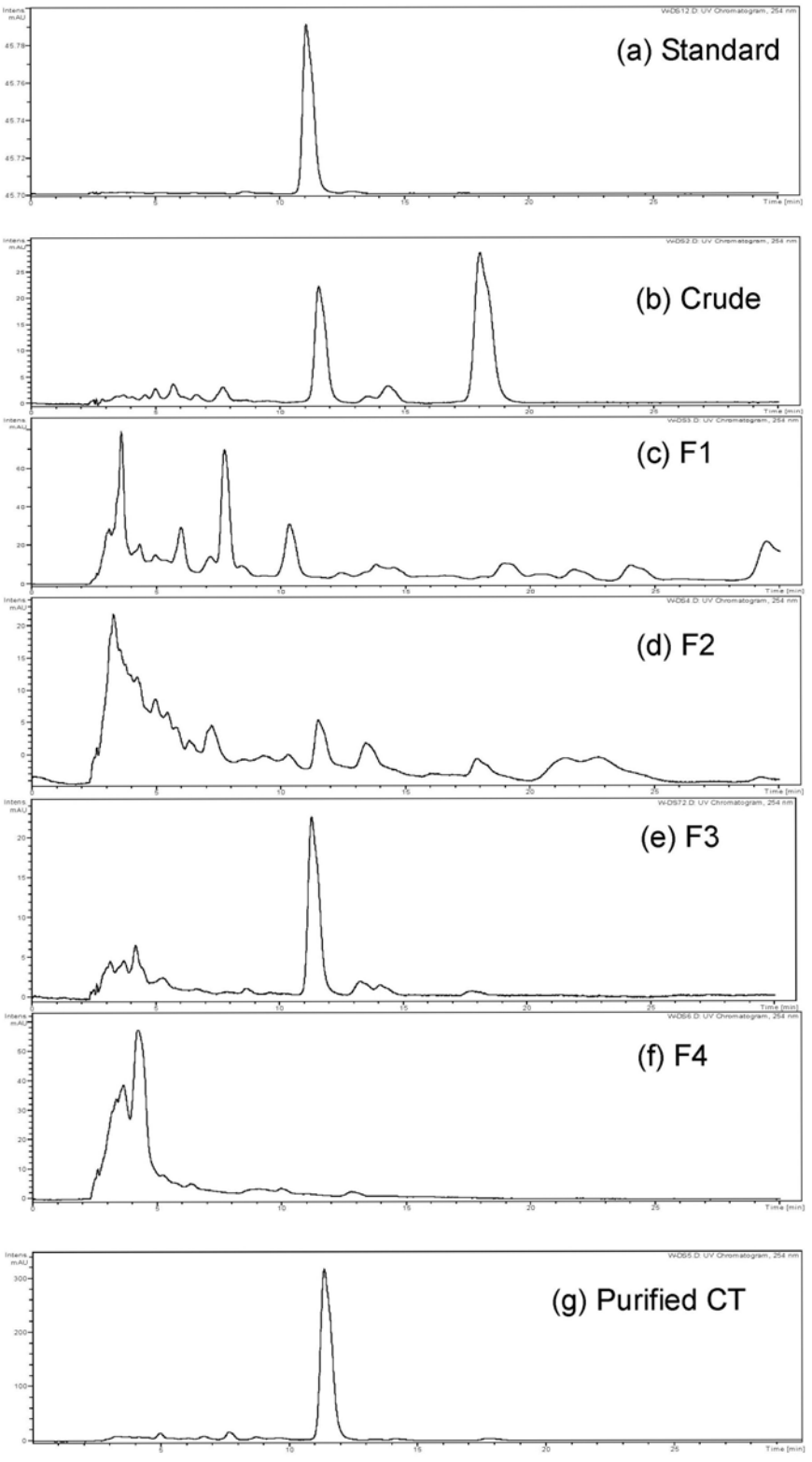

Fig 2.2 HPLC chromatograms of (a) standard CT compound; (b) Danshen Sc-CO2 extract; (c)-(f) fractions collected from silica-gel column purification; (g) final CT obtained after two rounds of column purification

Compound List:

#	RT [min]	Range [min]	Height	Area	Area %
1	8.6	8.3 - 9.1	2	47	1.4
2	11.1	10.6 - 12.5	114	3344	97.7
3	12.9	12.6 - 13.6	1	32	0.9

Chromatograms:

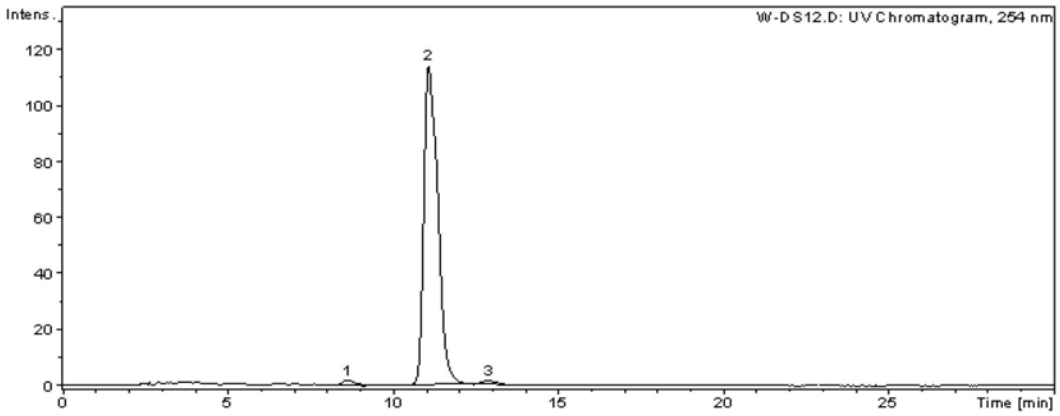

Fig 2.3 Peak integration of CT standard. CT's presence is indicated by peak at retention time 11.1 minute. Purity of CT calculated by peak integration is 97.7%.

Compound List:

#	RT [min]	Range [min]	Height	Area	Area %
1	3.2	2.7 - 3.4	2	47	5.1
2	3.7	3.4 - 4.0	1	20	2.1
3	4.2	3.9 - 4.7	4	69	7.4
4	5.3	4.7 - 5.9	1	25	2.7
5	8.7	8.4 - 9.2	1	15	1.6
6	11.3	10.8 - 12.7	22	678	72.2
7	13.3	12.8 - 13.8	1	42	4.5
8	14.1	13.8 - 14.9	1	20	2.1
9	17.8	17.3 - 18.5	1	23	2.4

Chromatograms:

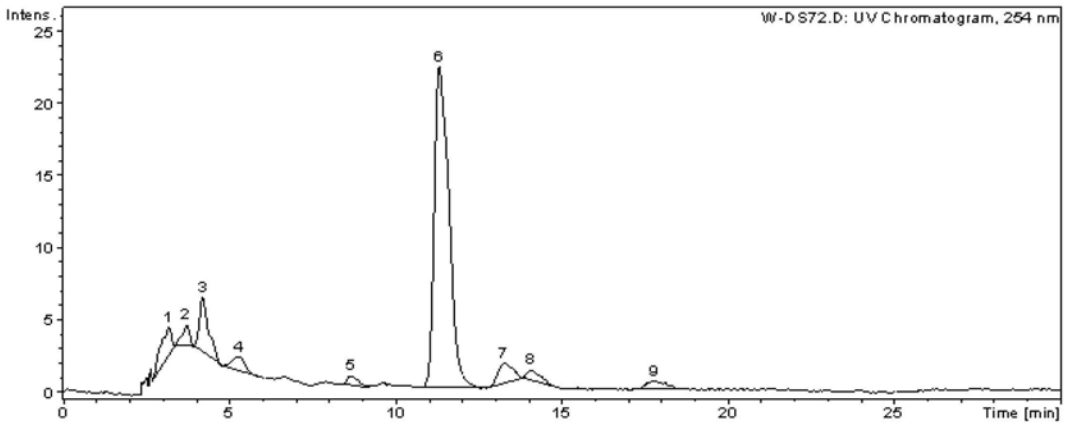

Fig 2.4 Peak integration result of fraction F3. CT's presence is indicated by peak at retention time 11.3 minute. Purity of CT calculated by peak integration is 72.2%.

Compound List:

#	RT [min]	Range [min]	Height	Area	Area %
1	5.0	4.8 - 5.3	8	112	1.1
2	6.7	6.4 - 7.3	6	115	1.1
3	7.6	7.3 - 8.1	14	288	2.8
4	8.7	8.5 - 9.2	3	48	0.5
5	11.4	10.8 - 12.8	314	9557	92.8
6	13.3	13.0 - 13.7	1	38	0.4
7	14.1	13.9 - 14.6	1	36	0.3
8	17.7	17.4 - 18.6	3	110	1.1

Chromatograms:

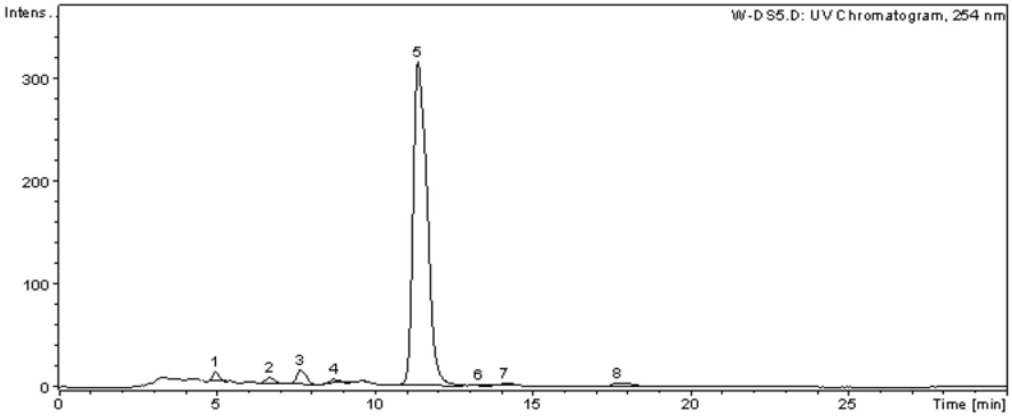

Fig 2.5 Peak integration result of purified CT. CT's presence is indicated by peak at retention time 11.1 minute. Purity of CT calculated by peak integration is 92.8%.

2.3.3 LC-MS and MS-MS analysis of fraction

Mass spectrometric analyses of the standard CT and purified CT were done by negative mode APCI. CT is a diterpenoid which has weak polarity and lipophilicity. It can be positively ionized in the APCI source. Therefore, APCI source was used as interface. The full product scan mass spectra and their fragmentation schemes of product ions from the parent ions $[M + H]^+$ are shown in Fig 2.6 (CT standard) and Fig 2.7 (purified CT). Precursor ion $[M + H]^+$ for the compound at retention time 11.3 min was found to be the same in both the CT standard and the purified CT, which has an *m/z* value = 279.1. This value agreed to previous report (Hu et al., 2005) of LC-MS analysis of CT. Characteristic of this precursor ion shown in the MS/MS spectra was identical in both the CT standard and the purified CT. This gives further evidence on the identity of our purified CT.

(a)

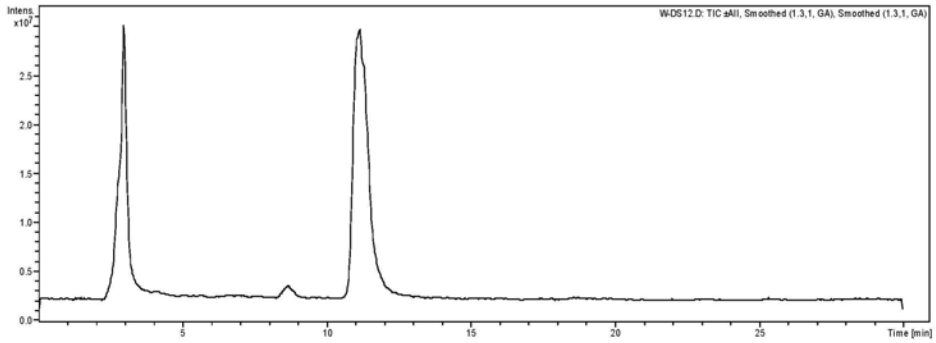

(b)

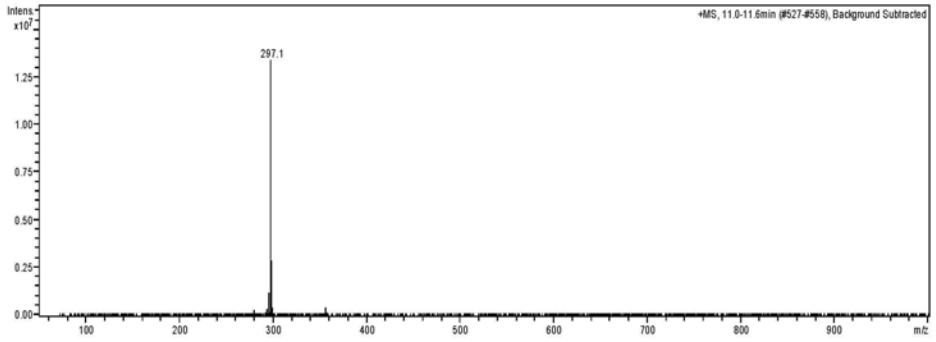

(c)

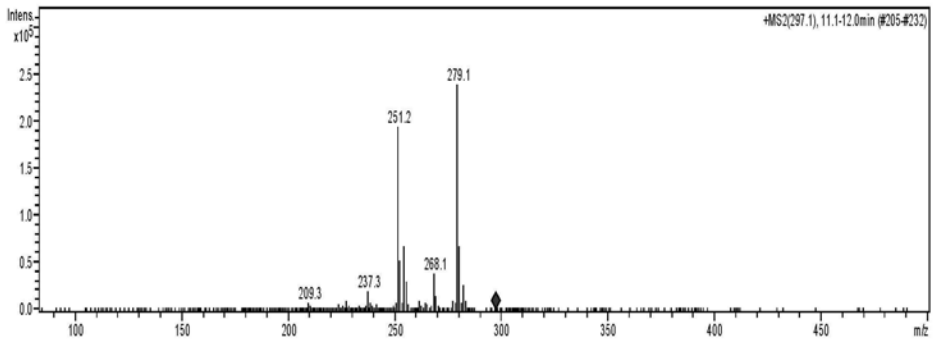

Fig 2.6 (a) LC-MS spectrum; (b) parent ion spectrum; and (c) product ion spectrum of the CT standard

(a)

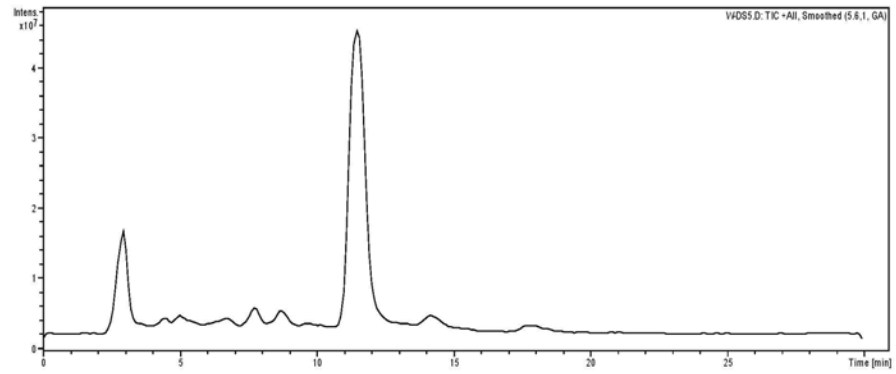

(b)

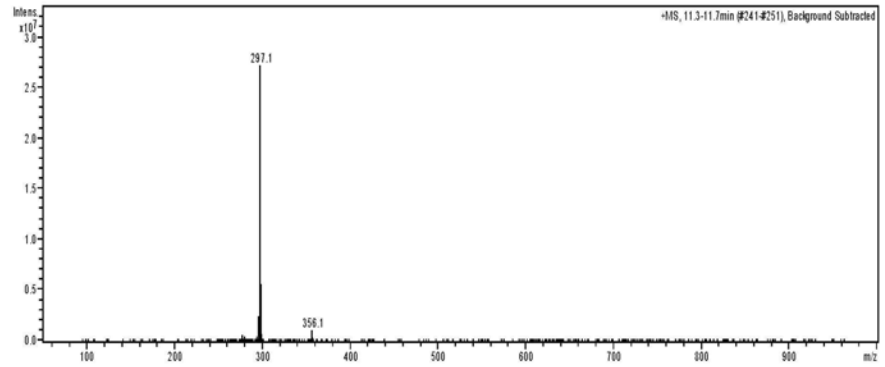

(c)

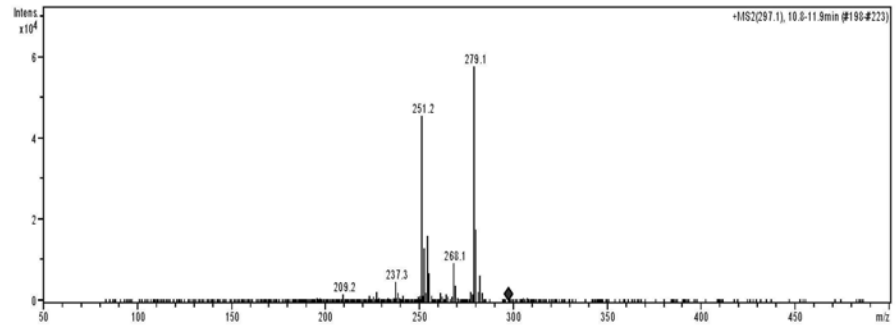

Fig 2.7 (a) LC-MS spectrum; (b) parent ion spectrum; and (c) product ion spectrum of the CT purified

2.4 Conclusion

A procedure of purifying CT from Sc-CO_2 extract of Danshen was established. The Sc-CO_2 extract originally got 48% CT in content. Content of CT was increased to 72.2%, as confirmed by HPLC analysis, after first round of silica gel column purification, and it was increased to 92.8% after second round of purification using the same protocol. Identity of purified CT was confirmed by LC-MS followed by MS/MS analysis. The purification started from 10 g Sc-CO_2 Danshen extract. It finally yield 2.6 g purified CT.

The above CT extraction protocol is different from previous protocol developed by other research group. Traditionally CT extracted was started with multiple extraction of Danshen powder with 95% ethanol, which produced extract with 0.4% CT content, and then followed by separation using silica gel column (Xu et al., 2006a). Whereas our extraction procedure started with Sc-CO_2 Danshen extract with relatively high CT content (48%). Further improvement on the current protocol could be done by filtering the column purified CT and allowing crystallization of CT, that could obtain a final purified product with higher purity up to 98% as reported (Xu et al., 2008).

Chapter 3 Inhibition of human AChE by cryptotanshinone

3.1 Introduction

CT was first found to possess AChE inhibitory activity in a large scale screening project by our team, which search for AChE inhibitors in Chinese Medicinal Material. To decide whether CT is able for treating AD, its inhibitory property towards AChE would be a major consideration. For example, irreversible AChE inhibitors, due to their property of strong inhibitory action and formation of covalent bond with AChE molecule, are considered highly toxic. This class of AChE inhibitor is usually used as pesticide or biological weapon rather than drug. Most of the anti-AD drugs, like tacrine, physotigmine, donepezil and galantamine (Gal) are reversible AChE inhibitors. Although in clinical usage, dose control and titration are necessary to avoid serious side effects, these AChE inhibitors are proven to be save (Inglis, 2002).

Butyrylcholinesterase (BuChE) is a homologue of AChE and a pseudo-cholinesterase. It shares 65% amino acid sequence homology with

AChE. Its molecular form and active centre structure are also similar to AChE (Allderdice et al., 1991). It is able to hydrolyze esters of choline including acetylcholine (Atack et al., 1986). BuChE pereferentially acts on butyrylcholine instead of ACh, and it also hydrolyzes a variety of ester-containing drugs, including aspirine (Schwarz et al., 1995). Unlike AChE which is mainly found in the CNS, muscle and erythocyte, BuChE is highly active in peripheral tissues such as liver, intestine, kidney, heart and lung. Therefore, BuChE has a physiological function of detoxification by its action of scavenging cholinesterase inhibitors including potent organophosphorus nerve agents before they reach their synaptic targets (Lenz et al., 2007). Due to its tissue distribution and substrate specificity, cross-inhibition of BuChE by AChE inhibitor was believed to be responsible for the peripheral side effect of AChE inhibitor treatment. However, there are more and more research that supports BuChE's role in the development and progression of AD. For example, amount of BuChE in AD patient's brain increase with the progression of disease (Perry et al., 1978a). Both AChE and BuChE are associated with the amyloid plaque in which elevated activity of both enzyme is detected (Geula and Mesulam, 1995b; Jang et al., 2008). Moreover, they both enhance the assembly of Aβ fibril and increase neurotoxicity triggered by

Aβ (Inestrosa et al., 2005). Therefore, AChE inhibitors that can also inhibit BuChE would have therapeutic advantage of memory improving and disease modifying (Ballard, 2002).

In this chapter, the inhibitory strength and inhibition type of CT towards AChE would be worked out. It is done in parallel with BuChE. Data produced is useful for determination of the mechanism of inhibition.

3.2 Materials and Methods

3.2.1 Ellman Assay

ChE inhibitory activity was measured by using the Ellman colorimetric method (Ellman et al., 1961). CT was dissolved in a solvent containing 30% methanol and 70% DMSO. Appropriate amount of CT or vehicle and 0.1 unit recombinant human AChE or BuChE were added to 90 μl 100mM sodium phosphate (pH7.4). The samples were incubated at r.t. for five min. The colorimetric reaction was started by adding 7 μl of 12.5 mM acetylthiocholine iodide (ACTI) (Sigma, China) or butrylcholine thio (Sigma, China) and 7μl of 10mM 5'5-dithio-bis-(2-nitrobenzoate) (DTNB) (Sigma, China). The absorbance at 415 nm was monitored by a spectrophotometric microplate reader (Biorad, USA) for 20 min at 1-minute interval. The rate of change of absorbance, reflecting the rate of hydrolysis of reaction substrate, was steady from 1 to 10 or in some cases 1 to 15 minutes depending on the presence or absence of inhibitor. Slope of straight line region, which reflects the apparent ChE activity, was calculated by linear curve fitting module of Prism 5.0 (GraphPad Software, USA). The percent inhibition was calculated by using the equation: (enzyme activity of control)−(enzyme activity of

sample)/(enzyme activity of control)×100.

3.2.2 Kinetic study

Various amount of CT and Gal was titrated against different amount of substrate (from 0.02 μM to 1.3 μM in final reaction mix), and the AChE activity of individual combination was assayed as described above. The kinetic data were analyzed and the kinetic constants were calculated by means of the non-linear curve fitting module of Prism 5.0 statistical software.

3.2.3 Reversibility study of CT inhibitory action by incubation time

The experimental approach to determine the reversibility of CT towards human AChE was to assay the cumulative effect over time. To begin the measurement of inhibition, 1 unit of AChE in 100 mM sodium phosphate (pH7.4) was equilibrated to 25°C for 5 minutes. CT solution was then added to the AChE solution. Aliquots were removed at 2 min intervals for 20 min, and the AChE activities of the aliquots were measured immediately by Ellman assays as described above. Malathion (Sigma, China), a known irreversible AChE inhibitor, was used as a control.

3.2.4 Reversibility study of CT inhibition by dialysis

The reversibility of CT inhibition towards human AChE was studied by dialysis. 1.5 units of enzyme and 3 μM CT were incubated in 0.1 M Na_2HPO_4 in final volume of 50 μl. After 15 min incubation at 25℃, the reaction was stopped by chilling in an ice bath, and 10 μl aliquot of mixture was taken out and activity was assayed in 300 μl buffer by the Ellman's method. Then the remaining mixture was dialyzed against 1 L buffer in micro-dialysis tubing (6000-8000 kD MWCO; Spectrum Laboratories, USA) at 4 ℃ or 25℃ respectively. After 24 hours, the remaining activity inside the dialysis tubing was measured. Control was taken the same procedure in the absence of inhibitor.

3.3 Result

3.3.1 Inhibition of CT towards AChE

To determine the IC_{50} of CT towards human AChE, 0.3 U of human AChE was incubated with increasing concentration of CT, from 0.1 to 30 μM . The ChE activities were determined by Ellman colormetric assay (Fig 3.1). The IC_{50} values of CT for human AChE calculated from non-linear regression was 4.67 μM.

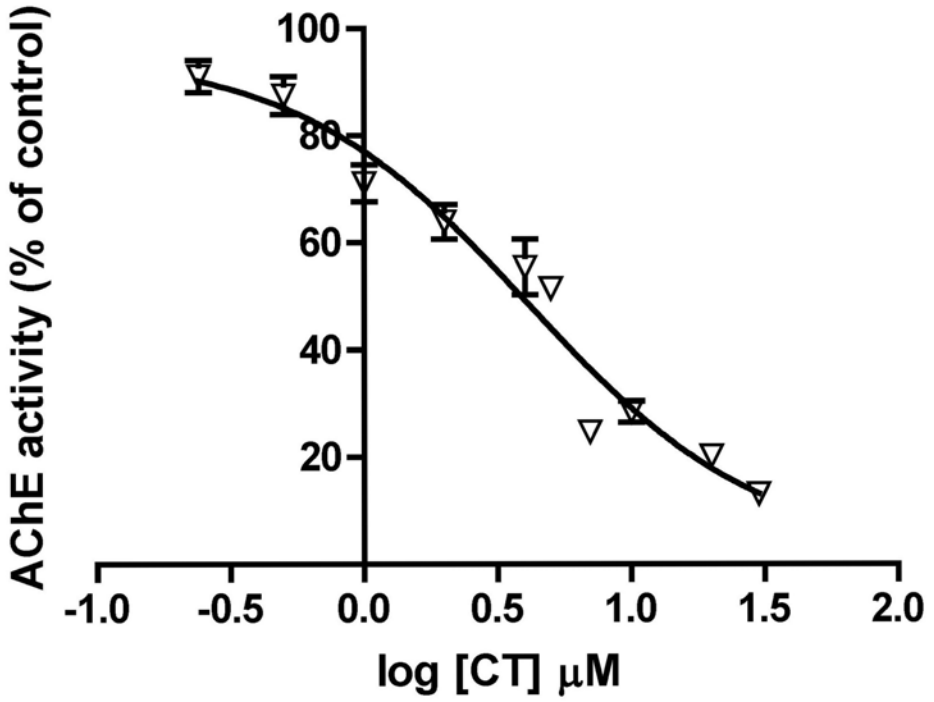

Fig 3.1 Inhibitory effect of CT on human AChE (▽).Data represents the mean ± SEM of AChE activity of three individual experiments.

3.3.2 Reversibility of CT inhibition towards AChE

To investigate the characteristics of inhibition, 3 μM CT was incubated with recombinant human AChE, and AChE activity was measured at 2 min intervals for 20 min. In the presence of CT, AChE activity decreased to 60% of the control after 6 min of incubation and was maintained at similar activity level throughout the incubation period (Fig. 3.2). In contrast, AChE activity was reduced continuously with the prolongation of incubation with 0.15 μM malathion, a known irreversible inhibitor of AChE.

The reversibility of CT for the inhibition of AChE was further studied by dialysis. After overnight dialysis at 4℃, AChE activity was not fully recovered. However, when enzyme-inhibitor complex was dialyzed at 25℃, AChE activity could be fully recovered (Fig 3.3). In contrast, AChE activity was dropped when incubated with irreversible inhibitor malathion. The above result indicated that CT is a tight-binding reversible inhibitor of AChE.

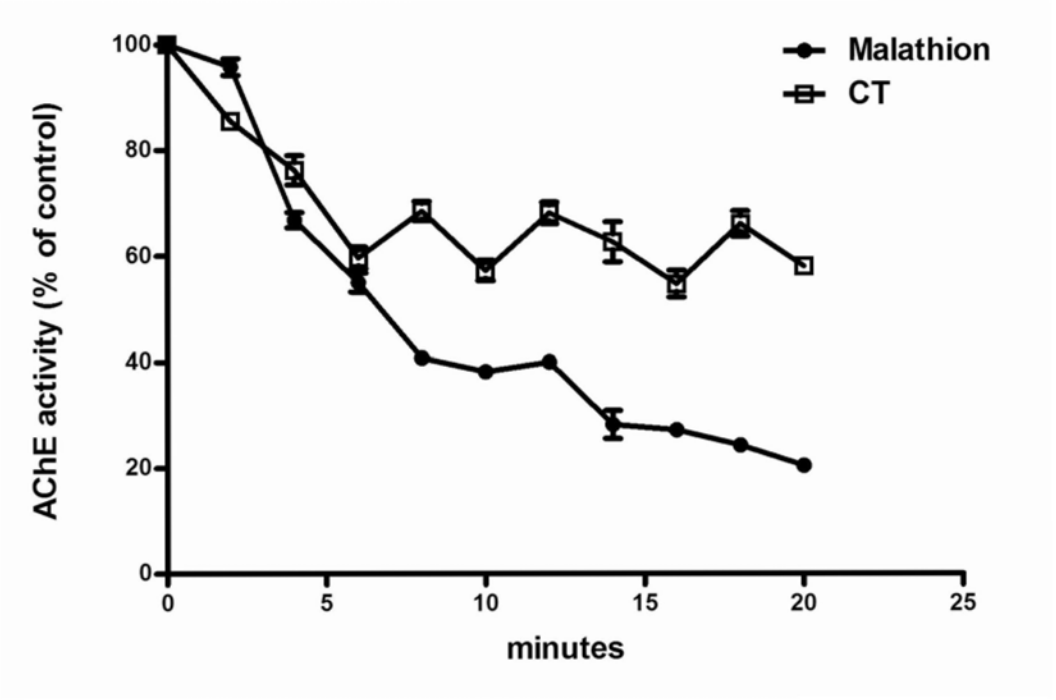

Fig 3.2 Study of reversibility of CT towards human AChE. Time course analysis of the inhibitory effect of CT (□) (3 μM) on human AChE. Data represents the mean ± SEM (n = 3). Malathion (•) (0.15 μM) was used as a control to demonstrate irreversible inhibition of human AChE.

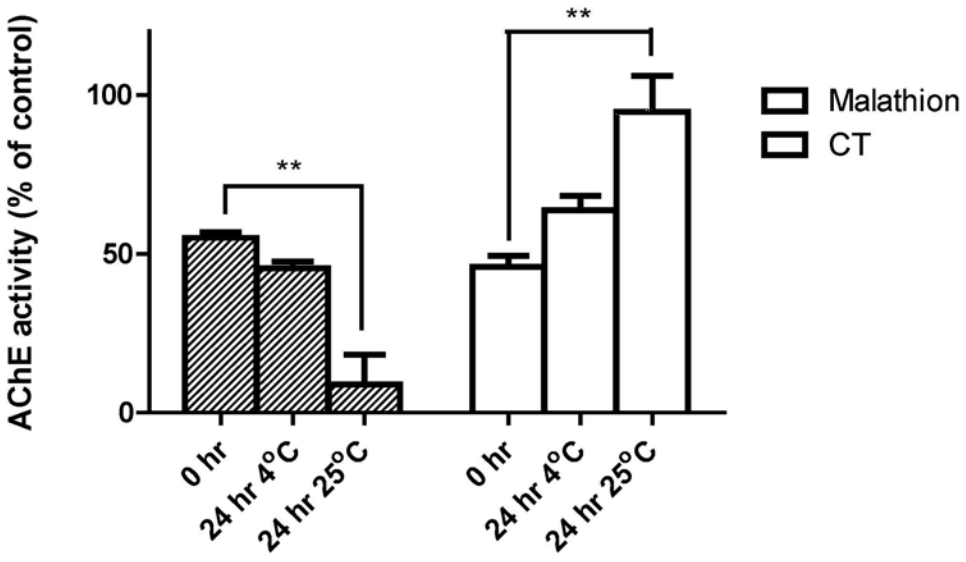

Fig 3.3 human AChE activity measured immediately after 15 minute (0 hr), 24hr at 4°C dialysis and 24 hr at 25°C dialysis, with addition of 0.15 μM malathion or 3 μM CT. Activity was expressed as percentage of control which prepared as the same procedure without the inhibitor. Values represent mean ± SEM of percentage of inhibition (n=3). One way ANOVA with post hoc Bonferroni tests; **= $P< 0.005$ for AChE activity of malathion and CT after dialysis at 25℃ overnight, compared with 15-min incubation without dialysis.

3.3.3 Inhibition of CT towards human BuChE

Specificity of CT inhibition was studied using pseudo-cholinesterase BuChE. Result showing that CT inhibited both human AChE and BuChE in a concentration-dependent manner (Fig 3.4). The IC_{50} values of CT towards human AChE and BuChE were 4.09 and 6.38 μM, respectively. The IC_{50} ratio between BuChE and AChE for CT was 1.56. Gal, which shows higher specificity towards AChE instead of BuChE was used as control. Result of Fig 3.4 is summarized in Table 3.1. With a low IC_{50} ratio, we can conclude that CT was relatively non-selective for human AChE and BuChE.

Table 3.1 Summary of IC_{50} of Fig 3.4

Compound	IC_{50} towards AchE (μM)	IC_{50} towards BuChE (μM)
CT	4.67 ± 0.41	6.66 ± 0.42
Gal	0.77 ± 0.33	7.85 ± 0.20

(a)

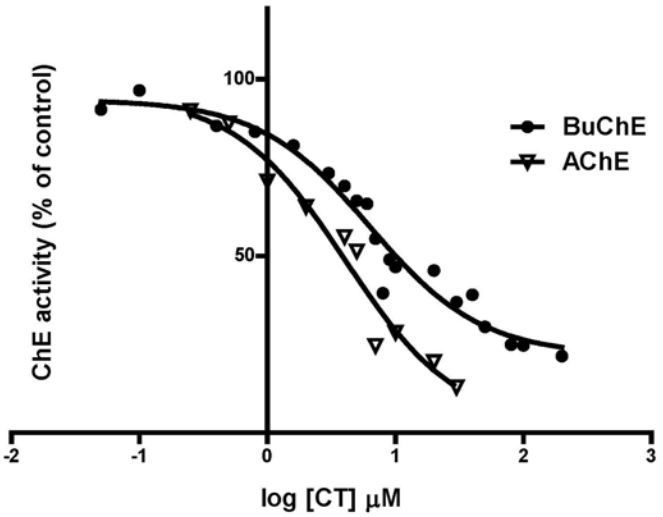

(b)

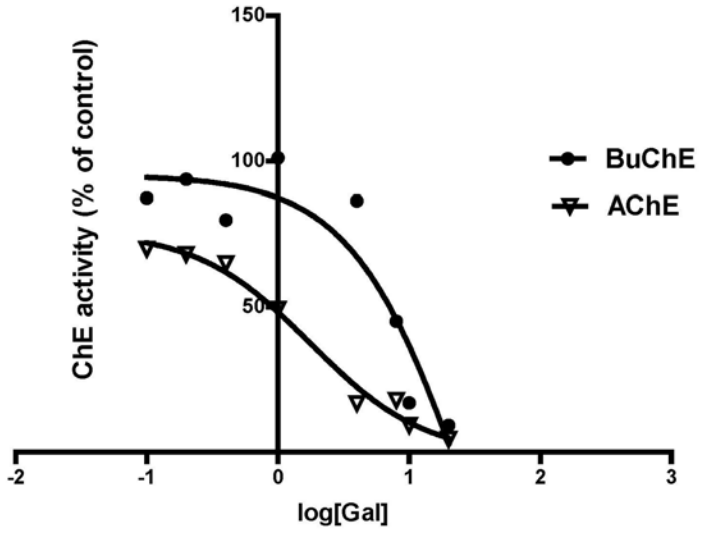

Fig 3.4 Inhibitory effect of (a) CT and (b) Gal on human AChE (▽) and human BuChE (•). Data represents the average value of two independent experiments performed in duplicate.

3.3.4 Type of inhibition of CT towards human AChE

To determine the mode of AChE inhibition by CT, enzyme kinetic experiments were carried out. Human AChE was incubated with different amount of ACTI in the presence of increasing amount of CT. Lineweaver-Burk plots showed that both K_m and V_{max} were altered by CT, indicating that the inhibition is a mixed-type (Fig. 3.5a). Re-plot of the K_m / V_{max} against different concentration of CT works out the apparent Ki which indicated by the X-axis intercept of the graph. The apparent K_i of CT for human AChE was 6.3 μM (Fig. 5b)

(a)

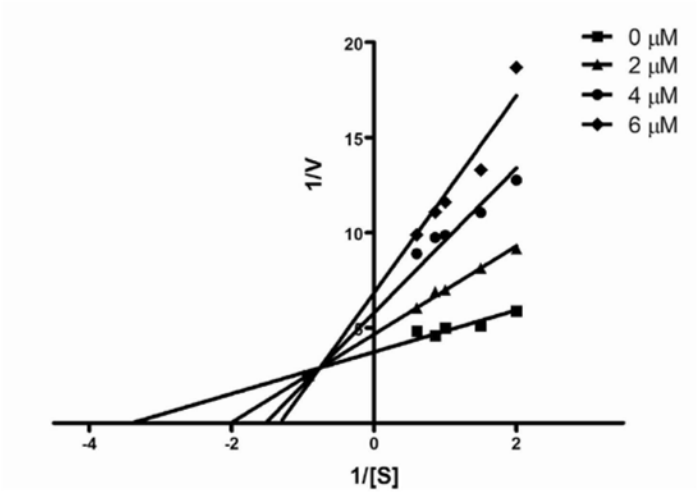

(b)

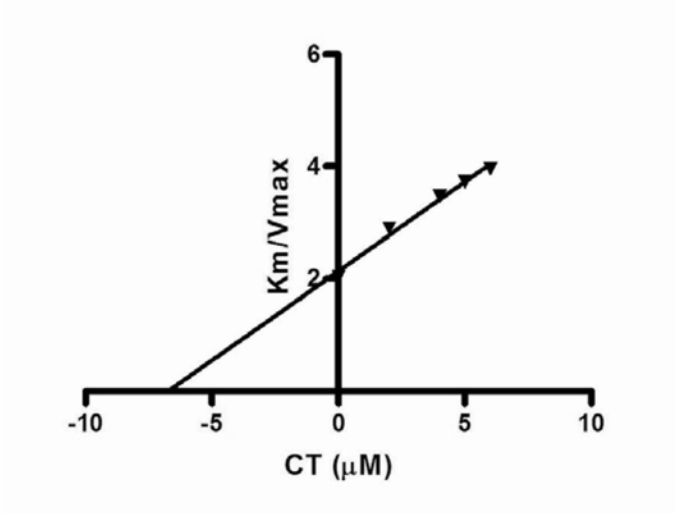

Fig 3.5 Kinetic study of the inhibition of human AChE by CT. AChE activity was measured by Ellman colorimetric assay as described in materials and methods. (a) The graph shows representative Lineweaver-Burk plots of human AChE with increasing amount of CT (b) Plot of K_m/V_{max} versus CT concentrations was obtained from Michaelis–Menten non-linear regression; apparent K_i calculated as the negative value of *x*-axis intercept was 6.20 μM.

3.3.5 Type of inhibition of CT towards human BuChE

Type of inhibition of CT towards human BuChE was worked out using similar condition. Lineweaver-Burk plots showed that both K_m and V_{max} were decreased by CT, showing characteristic of uncompetitive inhibition (Fig. 3.6a). Re-plot of the slope of Lineweaver-Burk plots at different substrate concentration against concentration of CT works out the apparent Ki which indicated by the intersection point of lines. The apparent K_i of CT for human BuChE was 2.17 μM (Fig. 5b)

(a)

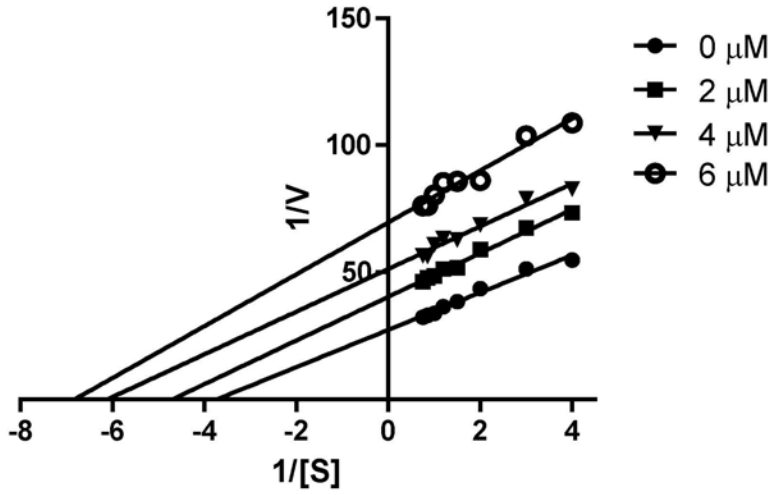

(b)

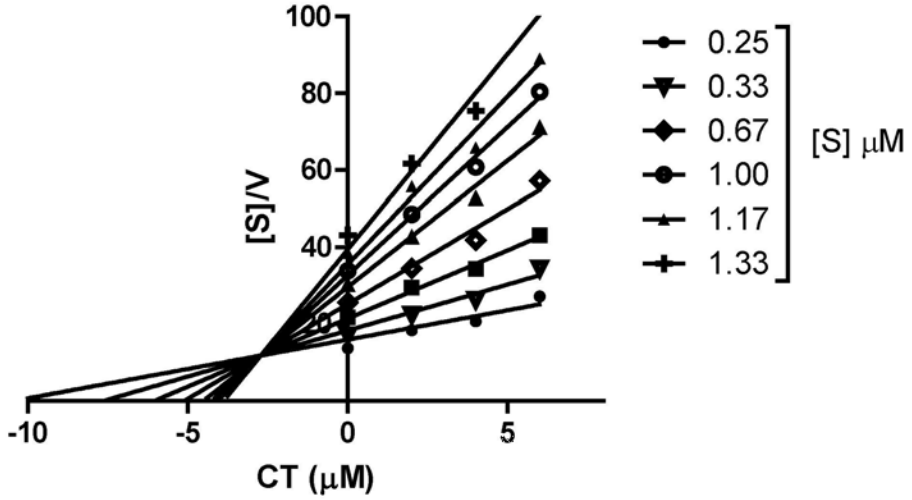

Fig 3.6 Kinetic study of the inhibition of human BuChE by CT. (a) The graph shows representative Lineweaver-Burk plots of human BuChE with increasing concentrations of CT (b) Plot of *s/v* versus CT concentrations at different substrate concentration was obtained from Michaelis–Menten non-linear regression; apparent K_i calculated as the x value of the intersection point was 2.17 μM.

3.4 Discussion

In the present study, we evaluated the AChE inhibiting property of CT, a natural compound isolated from the Danshen, root of *Salvia miltiorrhiza,* for the treatment of AD.

Although there is evidence to suggest that CT is a non-primate AChE inhibitor, it has been reported that there is difference in potency of AChE inhibitor towards AChE from different species (Alcala et al., 2003). Comparing with previous report, CT shows a higher inhibitory effect on human AChE rather than bovine erythrocyte AChE (7 μM as reported by Ren et al., 2004) and mouse brain AChE (100 μM causes 52% inhibition as reported by Kim et al., 2007), indicating that CT is a more potent inhibitor for human AChE than for mouse and bovine's.

Reversibility of the inhibitory action is also studied. The data indicates CT needs 6 minutes to reach its maximum inhibitory action towards human AChE. As the amount of inhibitor-enzyme complex in the reaction mix reached equilibrium, the degree of inhibition remains nearly the same throughout the

20 minutes incubation time. Reversibility of the binding of CT to human AChE is further confirmed by the method of dialysis. CT is a reversible inhibitor that its inhibitory action can be reversed by dialysis at 25℃ overnight. However, at 4℃ 24 hr CT failed to completely dissociate from the enzyme:inhibitor complex. The above data indicated a tight-binding reversible inhibition process could be involved.

In addition to the inhibition of AChE, CT was also found to inhibit human BuChE. BuChE is also known as pseudo-cholinesterase which is able to hydrolyze esters of choline including acetylcholine (Atack et al., 1986). Importantly, BuChE activity has been found to elevate in the brain of AD (Atack et al., 1986; Geula and Mesulam; Mesulam et al., 2002). Selective inhibition of BuChE has been shown to increase the level of acetylcholine and improve learning in rats (Giacobini, 2003). The IC_{50} ratio of hAChE/hBuChE is 1.56. This ratio is relatively low when comparing with some other well known AChE inhibitors like Huperzine A (=636), Galantamine (=9) and Donepezil (=186), while it is similar to Rivenstigmine (1.1) (Giacobini, 2003). In human brain, balance between these two regulatory enzymes is essential for healthy brain. In healthy individual, they are maintained in 0.2-0.5 BuChE:AChE ratio.

In AD patients, resulting BuChE:AChE can reach as high as 11 (Giacobini, 2003). As brain BuChE takes the role of hydrolyzing excessive ACh, the imbalance between these two enzymes would cause excessive hydrolysis of ACh. It is particularly important to consider the fact that in AD patient, while brain AChE activity continuously declines, BuChE activity increases continuously during disease progression (Perry et al., 1978). CT could be considered as a treatment for mild to advanced cases of AD due to its dual-inhibitory (AChE and BuChE) action. It was found that the IC_{50} ratio of CT between BuChE and AChE was 1.56 suggesting that CT possesses similar inhibition potency towards BuChE and AChE. As BuChE can catalyze the breakdown of acetylcholine, therapeutic agents that can inhibit both AChE and BuChE may give extra benefits in the treatment of AD when compare with agents that preferentially inactivate AChE.

To know more about the mechanism of inhibition, determination of the inhibition type of CT has been carried out. Results show that CT is a mixed-type inhibitor to human AChE. This type of inhibition is generally the result of combination of partially competitive and pure non-competitive inhibition. Binding of a mixed-type inhibitor, for example huperzine, inhibits

AChE through inducing conformation change that destroyed the oxyanion hole, which stabilizes substrate's tetrahedral intermediate during hydrolysis reaction (Raves et al., 1997). Its inhibitory activity is not achieved by occupying the aceyl-binding pocket or the choline binding site (Greenblatt et al., 1999). Interestingly, CT inhibits human BuChE in an uncompetitive manner. The mode of inhibition is different from AChE that CT only binds to enzyme-substrate complex in an uncompetitive mode of inhibition. One possible explanation is that CT has a higher affinity with the enzyme-substrate complex. But in the case of AChE, CT's binding to the enzyme-substrate complex is hindered because of the limited size of the aromatic gorge. However, the wider aromatic gorge in BuChE allows accomodation of larger substrate (Radic et al., 1993), thus favoring the binding of CT with AChE that a substrate has already bind to it. Nevertheless, as CT is either a mixed-type or uncompetitive ChE inhibitor, it is predicted that CT probably binds at the aromatic gorge sub-sites, in the presence or absence of substrate.

In conclusion, CT is found to be a tight-binding reversible inhibitor of AChE. It also inhibits BuChE with similar IC_{50}. CT inhibits AChE followed mixed-type of inhibition, while it is an uncompetitive inhibitor towards BuChE.

Chapter 4 In vitro study of cryptotanshinone in primary cortical neurons

4.1 Introduction

In previous chapter, it was found that CT is a reversible mixed-type inhibitor of AChE. A more in-depth study of CT on its characteristic and property of inhibition in viable cells are required for a better understanding of it before putting it into an *in-vivo* preclinical test model.

Cortical neurons isolated from brain of rats embryo is used as a model for studying the effect of CT. Isolated cells were grown in serum-free neural basal medium and selected by adding mitotic inhibitor. By this method, the final culture would contain approximately 99.5% neurons (Zhao et al., 2002). Apart from studying the AChE inhibitor property, this cultured neuron model can provide the biochemical study. Glutamate, a neurotransmitter and an excitotoxin that plays an important role in neuronal cell death in AD (Walton and Dodd, 2007), can induce apoptosis of cortical neuron. Some AChE inhibitors such as galantamine and tacrine have been found to protect

neurons from glutamate excitotoxicity in this cultured neuron model (Takada-Takatori et al., 2006). These AChE inhibitors are said to be disease-modifying because of their neuroprotective effect. In this chapter, the effect of CT on attenuating the glutamate excitotoxicity would also be investigated.

4.2 Materials and methods

4.2.1 Isolation of primary cortical neurons

Cortical neuron culture was prepared from S/D rat embryos at embryonic day 18 (E-18). Pregnant rats were obtained from the Laboratory Animal Services Center, The Chinese University of Hong Kong. The rat was anesthetized with diethyl either (Peanreac Quimica, Italy). Embryos were removed by a cesarean section. The head of the embryos was cut with sterile instruments and transferred to a large culture dish containing HBSS medium without calcium (Sigma, China). The skin and the skull were removed with fine pincers. The whole brain was extracted and immediately transferred to another dish containing HBSS medium. The two hemispheres were cut with scalpel and placed medial side up. The frontal and occipital parts of the cortex were removed in order to unroll the hemisphere. Blocks of neocortex could be obtained by progressive dissection eliminating presumptive hippocampus and white matter. Blocks of neocortex were stored in HBSS medium without calcium and supplemented with 1 mM sodium pyruvate (Sigma).

4.2.2 Preparation of dissociated neurons

The following procedures were performed in a laminar flow culture hood using sterile technique. All dissected cortices were transferred to a 50 ml centrifuge tube (Falcon, USA). 5 ml of 0.05% trypsin/EDTA (Gibco, USA) was added to the dissected tissue and incubated at 37℃ for 10 min with constant shaking. After incubation, cortices were triturated gently with a 5 ml pipette 3 times. It was then allowed to settle down for 3 min and the cloudy supernatant was transferred to a tube containing 25 ml plating medium: DMEM with 10% horse serum and 5% Glutamax (all purchased from Gibco, USA). The serum was used to neutralize trypsin. The above trypsinization, trituration and neutralization procedures were repeated 3 times with another 10 ml of trypsin/EDTA. Cloudy supernatant collected was filtered through a 100 μm cell strainer (Falcon, USA).

4.2.3 Cell plating

After filtered through cell strainer, cells were centrifuged at 450 x *g* for 5 min and supernatant was discarded. Cells were resuspended in HBSS containing

calcium and supplemented with 1 mM sodium pyruvate. 10 μl aliquot of the cell suspension was mixed thoroughly with 10 μl Trypan blue solution (Gibco, USA). Cell number was counted and correct amount of cortical neurons was aliquoted. Cells were then centrifuged 450 x *g* for 5 min and resuspended in plating medium and transferred to 6-well or 24-well plates pre-coated with 0.01 mg/ml poly-L-lysine (Sigma, China). For AChE activity assay and Western blot analysis, cells were plated on 6-well plate (Ikwaki, Japan) at a density 1 x 10^7 / well. For Cell viability assay, cells were plated on 24-well plate (Ikwaki, Japan) at a density 1.5 x 10^6 /well. Cells were incubated at 37°C in a humidified incubator with 5% CO_2/95% air.

4.2.4 Cell maintenance

Medium was changed to neurobasal medium supplemented with 2% B27, 0.5 mM Glutamax (all purchased from Gibco, USA). Culture medium was replaced every other day. On day 3 after cell plating, 2.5 μM cytosine arabinonucleoside (Sigma, China) was added to inhibit mitotic cell growth. Experiments were performed on days 7 to 10 of cultures in neurobasal medium containing 2% antioxidant free B27 supplement.

4.2.5 AChE activity assay

Medium was removed from the cells by aspiration and cells were washed 3 times with HBSS. Cell content was extracted by adding 0.4 ml of High Ionic Strength buffer (10 mM $NaHPO_4$, pH 7.0-8.0, 1 M NaCl, 10% Triton X-100, 1 mM EDTA) to each well. After 5 min incubation in room temperature, cell lysate was collected and centrifuged at 12,000 rpm in a 1.5 ml microfuge tube for 20 minutes. Supernatants were collected and protein concentration was determined by Bradford color reagent (Biorad, USA). Equally 100 μg protein from each sample was used as enzyme source for Ellman assay

4.2.6 Measurement of cell viability

Cell viability after treatment was by MTT (3-(4,5-dimethyltiazol-2-yl)-2, 5-diphenyl-tetrazolium) proliferation test. After drug treatment, the medium was replaced with 5 mg/ml of MTT (Sigma, China) solution in HBSS and the cells were incubated at 5% CO_2 37℃ for 2 hours. After incubation, MTT was aspirated and DMSO was added to each well to dissolve crystals formed. The purple color produced was measured spectrometrically at absorbance 540 nm with a microplate reader (Bio-Rad, Model 3550).

4.2.7 Glutamate challenge on cortical neuron

Seven-day old cortical neurons were pretreated with various doses of CT diluted in neural basal medium. Before treatment, neurons were washed twice with Krebs HEPES buffer containing 100 mM NaCl, 2 mM KCl, 2.5 mM $CaCl_2$, 1 mM $MgSO_4$, 1 mM $NaH2PO_4$, 4.2 mM $NaHCO_3$, 12.5 mM HEPES, and 10 mM glucose. Glutamate challenge was carried out by 10-minute room temperature treatment in Krebs HEPES buffer containing 1 mM glutamic acid, with CT or galantamine diluted into it. Following glutamate exposure, cultures were washed twice with Krebs HEPES buffer and replaced with CT/galantamine containing neurobasal medium. Cultures were returned to the incubator and allowed to incubate for 2 hrs prior to MTT measurement.

4.2.8 Western blot analysis

Proteins were separated by SDS-PAGE on a Mini-Protean III electrophoresis cell (Bio-Rad, USA). A 10% gel was used for analysis. The volume of the resolving-gel mix needed per gel was about 3.2 ml if 0.75 mm thickness gel was made. After the resolving-gel mix was pipetted to the gel gap at one side, a thin layer (approximately 1 cm) of isopropanol was added. While waiting for the hardening of resolving-gel, stacking-gel mix without TEMED (Biorad, USA)

was also prepared according to the recipe. After the resolving layer was formed, isopropanol was removed from the gel top. The stacking-gel mixture was added with TEMED and pipetted on top of the resolving gel. Finally, the comb for sample slots was inserted into the stacking-gel layer immediately. The gel was ready to use after 30 min. The gel setup was put in the gel tank. Fresh SDS-PAGE running buffer was poured to the cavity formed by electrode-unit and to the surrounding space. Protein samples were mixed with SDS sample loading buffer and boiled for 10 min. Five to twenty microlitres of each sample was loaded into the sample slots. The gel was run at a constant voltage of 150 V for 50 min or until the tracking dye reaching at the end of the gel. After SDS-PAGE, the stacking gel was discarded and the resolving gel was equilibrated in transfer buffer for at least 15 minutes. PVDF nitrocellulose membrane (Millipore, China) and 6 pieces of Whatman 3-mm filter paper were cut to slightly larger than the gel. For PVDF membrane, it was presoaked in methanol for activation and then 3 minutes in transfer buffer for equilibration. The 3mm filter papers were stacked into two stacks of 3 pieces each and wetted with transfer buffer. Electroblotting was carried out using a semi-dry electroblotter Trans-Blot Cell (BioRad, USA). The gel was placed on top of the membrane and between the 2 stacks of prepared filter papers. The semi-dry

blotting was operated at a constant voltage of 10 V for 1 hour. Then the membrane was removed and kept wet in TBST solution. To block the non-specific binding of antibodies to the membrane, it was immersed in blocking solution (5% non-fat milk in TBST) and shaken for 1 hour at room temperature. Antibody of appropriate dilution as applied to the membrane and incubated at 4 °C for 16 hours with constant shaking. The membrane was then washed in TBST solution for 3 times each for 15 minutes. Appropriate secondary antibody conjugated with horseradish peroxidase (HRP) was diluted in TBST in a concentration suggested by the manufacturer with the membrane at room temperature for 1 hour, followed by washing in TBST solution 3 times each for 15 minutes. ECL (enhanced chemiluminescence) detection kit (GE Healthcard, USA) was used to obtain signal from the membrane. The membrane was exposed to Fuji Medical X-ray Film (Fuji, Japan). Compositions of reagents used in this section are listed in Appendix. Antibodies used in this study include Anti-AChE (Santa Cruz, USA), Anti-Tau (DAKO, USA), Anti-phospho-tau AT270 (Thermo Fisher Scientific, USA).

4.2.9 RNA extraction and quantitive real-time PCR

RNA samples was collected from treated cell by TRIZOL reagent (Invitrogen,

USA). Briefly, TRIZOL was added directly to the HBSS washed cells on culture plate. For the amount of reagent added, 1 ml/ 25 cm^2 flask was assayed to be optima. The plate was incubated for 5 min at room temperature and then the total cell lysate was transferred to a sterile 1.5 ml microfugue tube. 0.5 ml chloroform was added and shaken vigorously for 15 sec. The mixture was incubated at room temperature for 3 min. To separate the aqueous and organic phases, the mixture was centrifuged at 12000 xg for 15 min at 4°C. The aqueous top layer was sucked carefully and transferred to fresh and sterile tube. Approximately 0.25 ml of isopropanol was than added to the aqueous RNA solution and incubated for 30 min on ice. The RNA pellet was obtained by centrifugation at 12000 xg for 10 min. The supernatant was discarded carefully without disturbing the pellet. The RNA pellet was washed with 75% ethanol at room temperature by gentle mixing. The RNA was recovered by centrifugation at 7500 xg for 5 min at 4°C and ethanol was discarded by pipetting. The total RNA was then dissolved in 15 μl of sterile RNase-free water. For the synthesis of first strand cDNA, volume equivalent to 5 μg RNA was mixed with 1 μl 0.5 mg/ml oligo(dT) primer and 1 μl 10mM dNTP mix. Then the mixture was preheated to 65°C for 5 min and then quick chill on ice. 4 μl 5X first strand buffer and 2 μl dithiothreitol (DTT) were added

to the reaction mix. Then the mixed contents were incubate at 42°C for 2 min. 1 μl (200 units) of SuperScript II RT (Invitrogen, USA) was added to start the reaction. Mixture was incubated at 42°C for 50 min. The reaction was stopped by heating at 70°C for 10 min.

AChE level in cDNA samples were determined by SYBR Green–based quantitative PCR method. For quantitive real-time PCR, primers for mouse GAPDH (forward primer: CCCCCATGTTTGTGATGGGT, nucleotide 453-472; backward primer: TGTGGTCATGAGCCCTTCCA , nucleotide 601-582; GeneBank accession number: NM_017008.3), and AChE (forward primer: TGCCCCATGGCTATGAAATC, nucleotide 1427-1446; backward primer: CGGGCAAAATTGGTCCAGTA , nucleotide 1547-1528; GeneBank accession number: NM_172009.1) were purchased from Invitrogen, Hong Kong. Briefly, in 25 μl reaction mixture containing SYBR Green RT mix, 0.1 μg cDNA and 1 μM forward and backward primers were mixed in MicroAmp 96-well reaction plate (Applied Biosystem, USA). An ABI 7500 fast real-time PCR instrument (Applied Biosystems, USA) was used to perform quantitive PCR. The amplification conditions were as follows: 94 °C for 10 min, followed by 40 cycles of denaturation at 94 °C for 15 s, and annealing and extension at

60 °C for 1 min. Concentrations of kDNA that were not within the linear range were estimated using Sequence Detection System Gene-Amp 7500 data analysis software (Applied Biosystems) that allows assessment of the dissociation curve and the fluorescence intensity of the samples. The fluorescence intensity of each sample, which proportional to the amount of DNA present, was expressed in terms of the PCR threshold cycle (C_T) defined as the number of PCR cycles required for the fluorescence signal to exceed the detection threshold. Results were reported as the mean ±SEM log2 fold change relative to control from 3 independent experiments. The fold change of treatment group relative to control group was calculated as $-\log2(\Delta C_T$ control group - ΔC_T treatment group)

4.3 Results

4.3.1 Inhibition of AChE from rat cortical neuron by CT

Inhibitory action of AChE from rat cortical neuron by CT was determined using cell lysate from 10-day cortical neurons isolated from E18 rat fetuses. Cell lysate was treated with various concentrations of CT. The AChE activity was determined by Ellman colorimetric assay (Fig 4.1). IC_{50} of CT towards AChE from cell lysate was 8.41±0.21 μM.

4.3.2 AChE activity of CT treated cortical neurons

The efficacy of CT-treatment on intracellular AChE activity of neuron was also investigated. Cell lysate from cortical neuron treated with 0-20 μM CT or 10 μM galantamine for 24 hrs, 48 hrs and 4 days were assayed for AChE activity (Fig 4.2). CT (20 μM) treatment at 48 hrs significantly reduced cell AChE activity to ~60% of control. The above result suggests that CT treatment is able to inhibit AChE activity of living cells.

Further investigation of the cellular AChE amount of these 4-day CT-treated cells showed that there was a little drop in AChE protein expression in 20 μM

cells (Fig 4.3). As detected by optical density measurement, cellular amount of AChE 20 μM group has dropped to 74% of the control, which similar with the AChE activity in the lysate (70%, Fig 4.2c). On the other hand, 10 μM galantamine treatment also decrease cellular AChE amount to 81% of the control, and the AChE activity was reduced to 59%. Therefore, part of the drops in AChE activity in these samples may be due to the effect of CT on decreasing the cellular AChE amount.

In addition the fold of change in AChE expression was detected by quantitative real-time PCR. The fold change in the expression of AChE in 20 μM CT treated group was 0.75 ± 0.10 (n=3 in triplicate) fold relative to vehicle control group. This result is consistent with the western blot analysis.

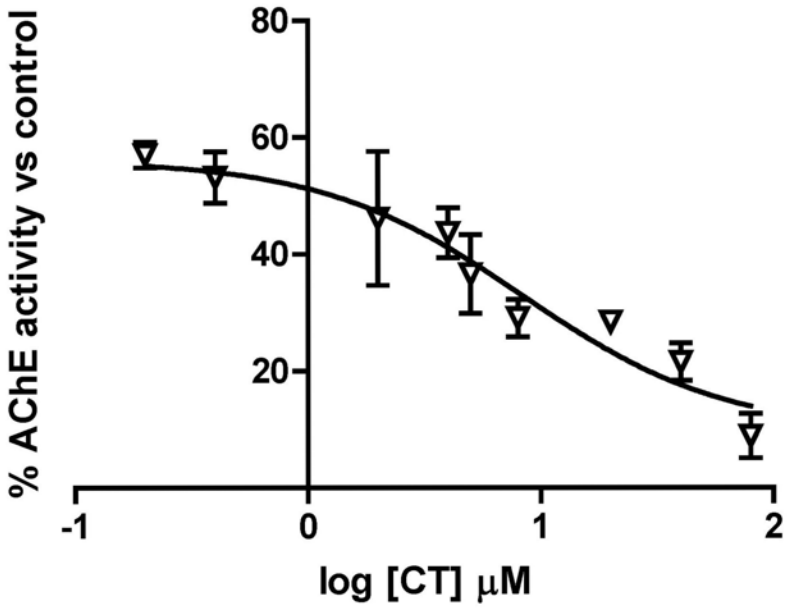

Fig 4.1 Inhibitory effect of CT on AChE from rat cortical neuron(∇). Data represent the average value of three independent experiments performed in triplicates.

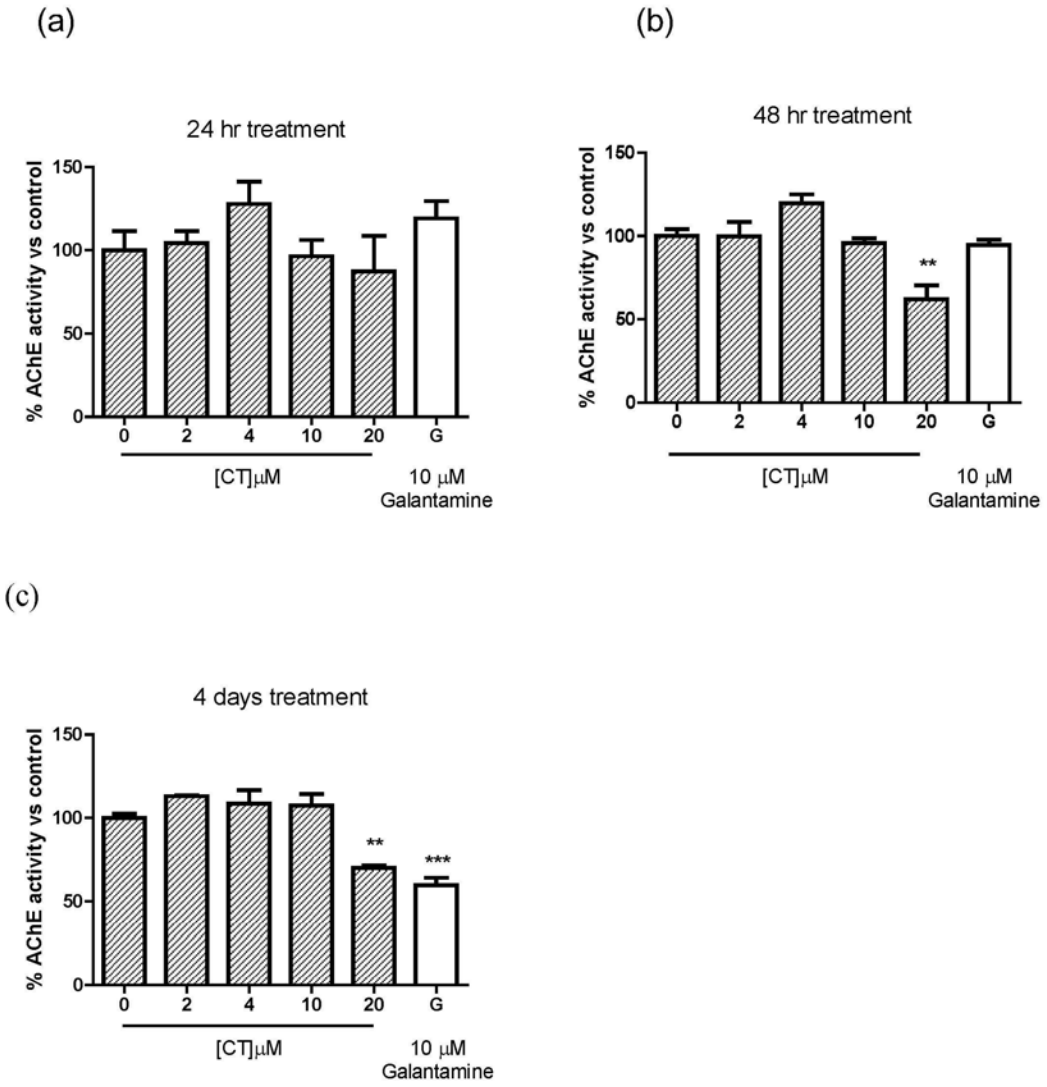

Fig 4.2 Effect of CT treatment on AChE activity of cell lysate. Primary cortical neurons were pretreated with 0-20 μM CT(stripped bar) or galantamine (white bar) for 24-hrs, 48 hrs and 4 days. AChE activity of cell lysate from sample that equally containing 100 μg total protein was assayed by Ellman's method. Values represent mean ± SEM of percentage of inhibition (n=3). One way ANOVA with post hoc Dunnet's test; ** = $P < 0.005$, *** = $p < 0.001$ for AChE activity significantly differ with control (0 μM CT).

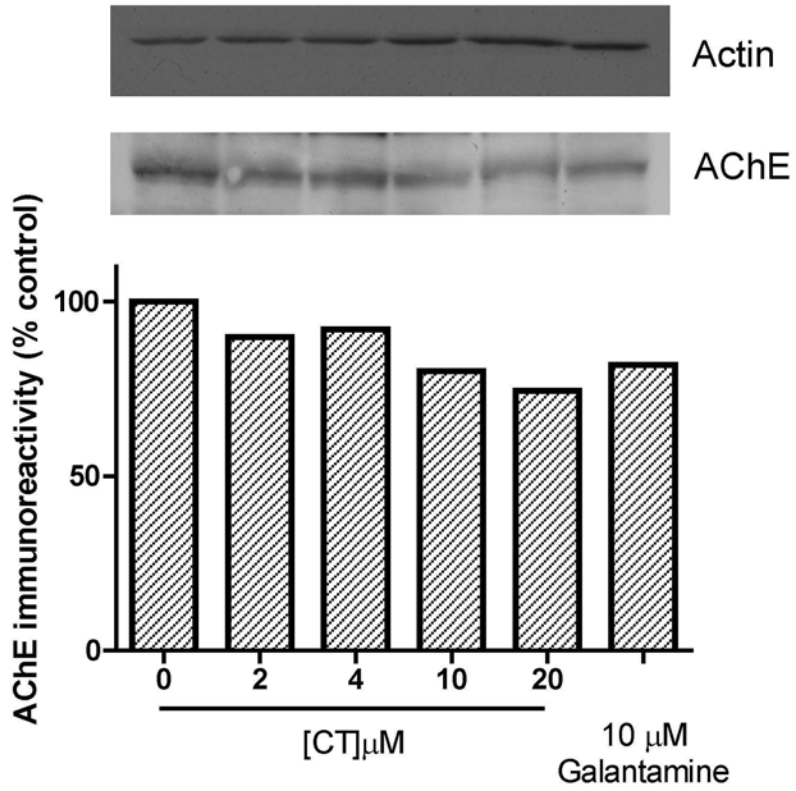

Fig 4.3 Effect of 4 days CT treatment on cell AChE amount. Total lysate from primary cortical neuron treated with 0-20 μM CT/ 10 μM galantamine was analyzed by Western blot using anti-AChE/ anti-actin antibodies. Western blot bands of AChE immunoblot was analyzed with densitometer and the relative amount of AChE in samples were presented as percentage of control (bar chart), which was treated with vehicle only.

4.3.3 Effect of CT on protecting neuronal cells from glutamate excitotoxicity

Effect on CT on protecting neurons from glutamate excitotoxicity was studied by exposing cortical neuron culture pretreated with CT to 1 mM glutamate challenge. Glutamate treatment induces apoptosis in cortical neuron by inducing calcium influx (Zhao et al., 2002), and it significantly reduces cell viability. Viability of glutamate challenged cell dropped to 60%-70% of untreated cells. Toxicity of glutatmate was ameliorated by 24 hrs of galantamine pretreatment (Fig 4.4b), which has been reported to protect neuron from glutamate challenge (Takada-Takatori et al., 2006). Cells pretreated with 10 and 20 μM CT for 24 hrs (Fig 4.4a) does not have observable toxicity effect.

Tau hyper-phosphorylation is one of the consequences of glutamate excitotoxicity (Chohan and Iqbal, 2006), phosphorylation state of tau in CT-treated cells was also investigated. Fig 4.5 shows there is a decrease in the mean value of tau phosphorylation detected by anti-tau AT270 on phospho-epitope T181. Dephosphorylation of tau protein was also evident by the shift in electromobility of tau as detected in the total tau blot. Putting this together, although the difference of result suggested that the effect of CT on

ameliorating glutamate excitotoxicity might counteracting by the blockade of the downstream actor of glutamate excitotoxicity, which is tau phosphorylation.

(a)

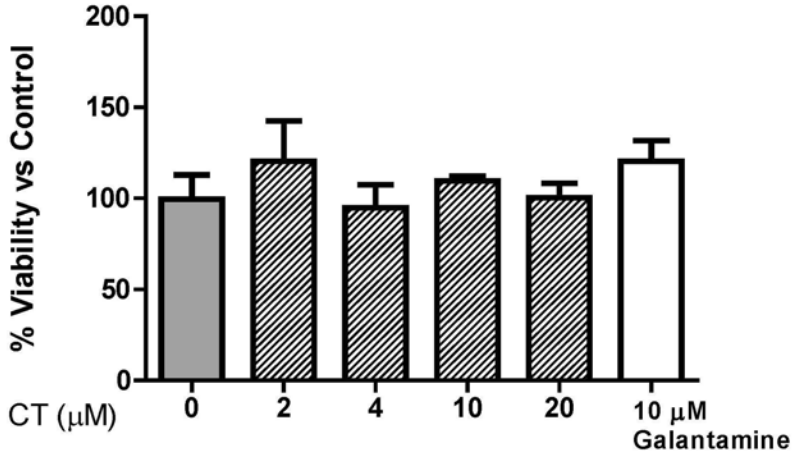

(b)

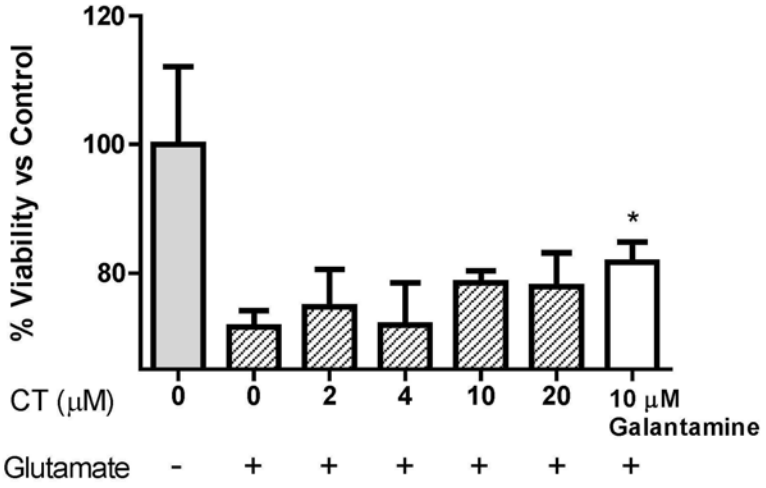

Fig 4.4 Viability of primary cortical neurons measured with MTT assay. (a) Primary cortical neurons were pretreated with different concentration of CT as indicated for 24 hrs. (b) Culture were pretreated with different concentration of CT for 24 hrs and then exposed to 1 mM glutamate for 10 min and then incubated with glutamate-free medium for 1 hr. Data represent mean ± SEM of 3 individual treatment.

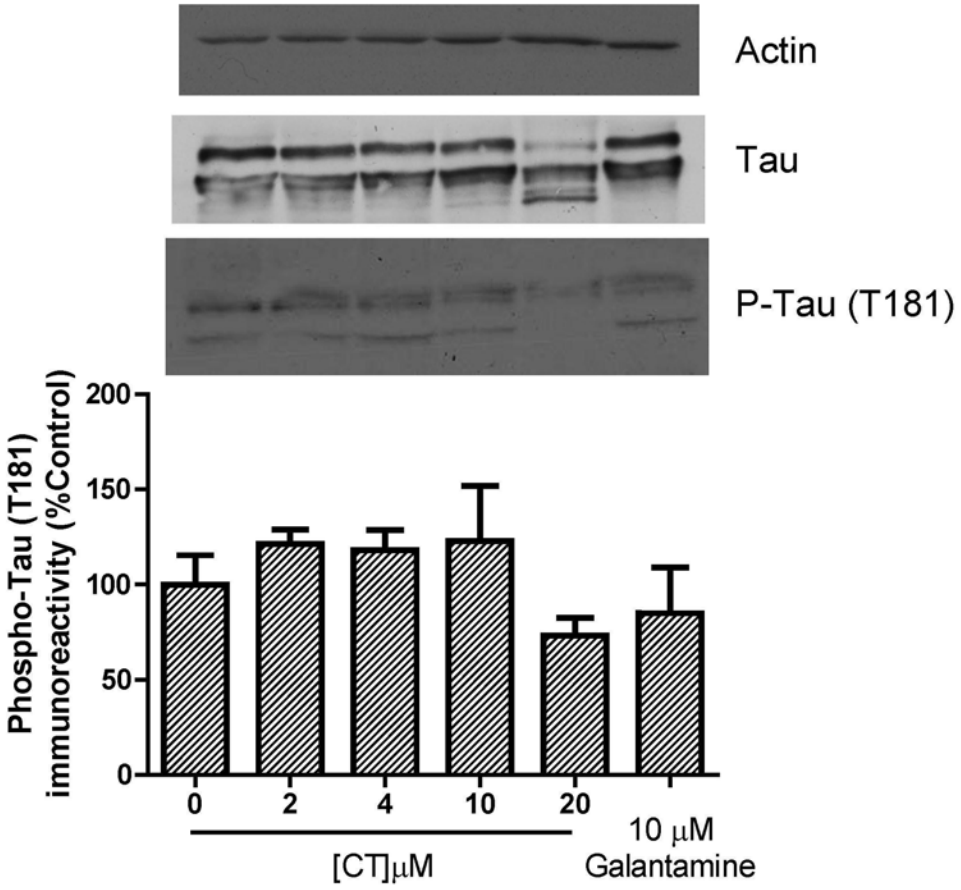

Fig 4.5 Effect of 4 days CT treatment on tau phosphorylation. Total lysate from primary cortical neuron treated with 0-20 μM CT/ 10 μM galantamine were analyzed by Western blot using anti-actin/anti-tau/anti-phospo-tau antibodies. Western blot bands of phospho-tau T181 immunoblot was analyzed with densitometer. Data represents mean ± SEM of three individual treatment. Immunoreactivity of phosphor-tau blot was normalized with total tau immunoreactivity of the same sample.

4.4 Discussion

In this chapter, CT was shown to inhibit the AChE from cultured rat cortical neuron. When directly mixing CT with total lysate of the neuron culture, it inhibited the AChE activity in the lysate with IC_{50} 8.47 μM. However when CT was diluted into culture medium and incubated with cortical neurons, the incubation time needed to provide significant inhibition on AChE activity was prolonged. There was no significant inhibition in 24-hrs treatment groups, not even the positive control galantamine. On the other hand, significant reduction in AChE activity in the lysate was observed in 48-hrs and 4 days treatment groups (Fig 4.2), while reduction in AChE activity was accompanied by decrease in cellular AChE amount (Fig 4.3). There is no literature report that long-term AChE inhibitor treatment could reduce AChE amount. In fact, most studies emphasized on the change in brain AChE activity after long-term administration of AChE inhibitors, without mentioning the effect of inhibitor treatment on AChE expression (Davidsson et al., 2001). Whether the reduction in cellular AChE was associated with the decrease in AChE activity could not be concluded from the current data, because there was not much decrease in AChE activity of the 10 μM treatment group (Fig 4.2c) but the

immunoactivity of AChE in lysate was decreased 20%. At this point, it can be concluded that the reduced AChE activity and reduced AChE expression might be two separate events. Further investigation of this relationship in CT-treated isolated cortical neuron is needed.

One pathological hallmark of AD, the Aβ protein, exerts its cytotoxic effect on triggering a number of signaling cascades. Major mechanisms include the activation of glutamate receptor (Harkany et al., 2000) and stimulation of glutamate release by microglia (Harris et al., 1996). Glutamate excitotoxicity is mediated through NMDA receptor. Antagonist like mementine can protect cell from glutamate excitotoxicity and reduce tau phoshporylation (Song et al., 2008). In AD, Aβ toxicity is acting through multiple pathways, either by disturbing protein phosphorylation balance (Alvarez et al., 2002) or through *N*-methyl *D*-aspartate (NMDA) receptor activation (Fig 4.6). The linkage between these mechanisms is tau protein, a downstream event that causes neuron death (Roberson et al., 2007). Result in this chapter suggested that CT is not only an AChE inhibitor, but it can also ameliorate glutamate excitotoxicity by reducing intracellular tau hyperphosphorylation at phosphorylation site T181, which is heavily phosphorylated in PHF-tau

(Goedert et al., 1994). This finding made CT a potential AChE inhibitor that has disease modifying effect against AD pathology.

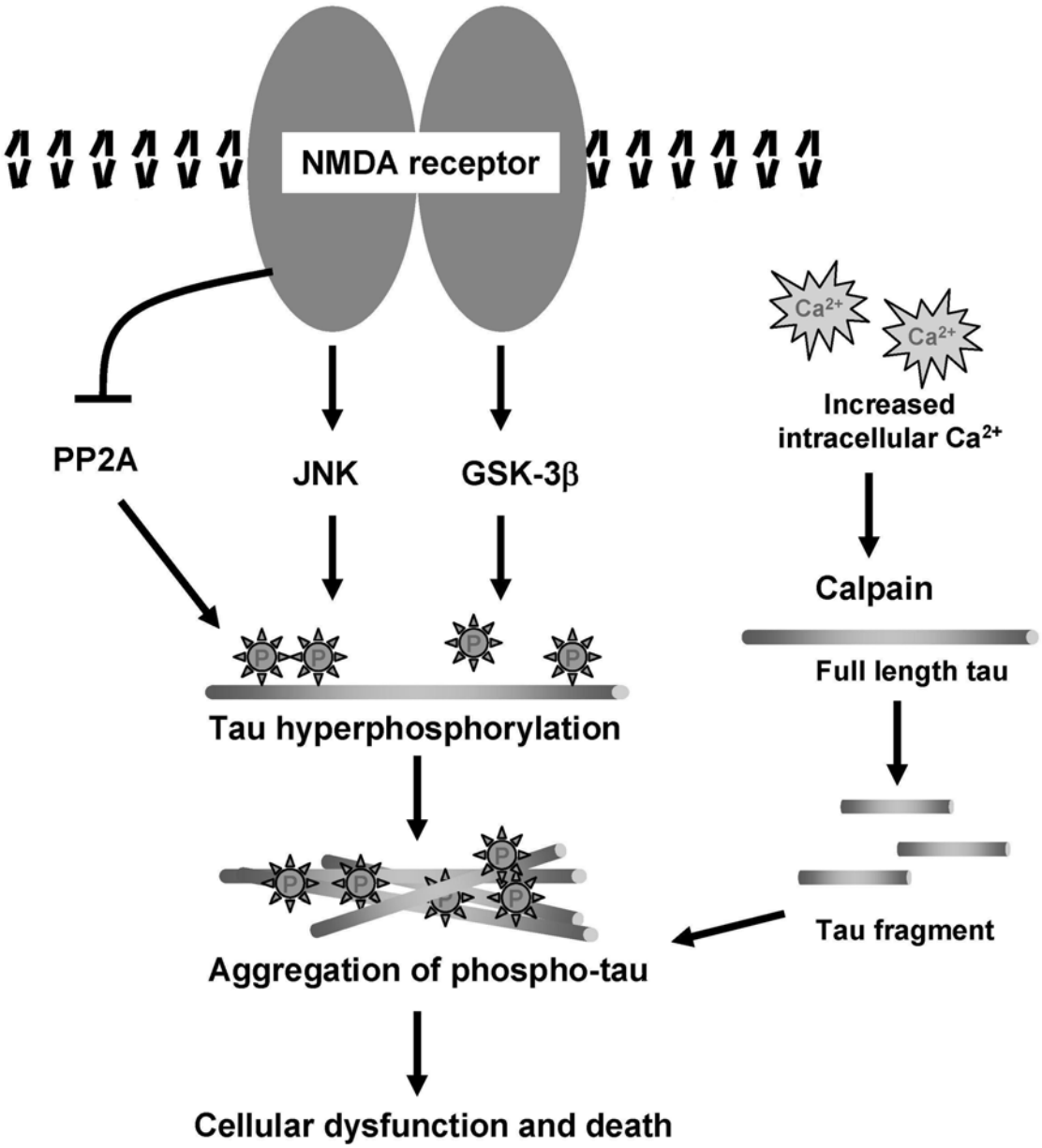

Fig 4.6 Proposed mechanism of NMDA receptor-induced neurotoxicity in AD that related to tau phosphorylation. Activation of NMDA receptor inhibits protein-phosphatase 2A (PP2A), which in turn increase the phosphorylation of tau. Tau kinase c-Jun-N-terminal kinase (JNK) and GSK-3β, are activated by

NMDA receptor (Chohan and Iqbal, 2006; Tolosa et al., 2008). The above events cause tau hyperphosphorylation and leads to a change in its secondary structure that brings about its dissociation from the microtubules. In addition, the increased intracellular Ca^{2+} activates calpain, which cleaves non-hyperphosphorylated tau into fragments that are toxic to the cell. The aggregated tau proteins cause cellular dysfunction and finally cell death.

Chapter 5 Study of amnesic effect of cryptotanshinone in Morris Water Maze task

5.1 Introduction

As CT has proven its AChE inhibitory action *in situ* and *in vitro*, the next step is to test its pharmacological effect on a preclinical model. In this chapter, we study the effect of CT in the Morris Water Maze animal model. This animal model is proven to be sensitive to cholinergic system, and it has been used as the choice among animal models that used on testing AChE (Fadda et al., 2000; Fadda et al., 1996)

5.1.1 Behavioral model for AD

In order to facilitate pre-clinical assessment of novel drugs for treating AD, a number of animal models have previously been developed. Many of these models involve the generation of cognitive deficits in rodents by genetic manipulations or by pharmacological means so as to reproduce some typical AD symptoms such as spatial memory decline. Transgenic mice model of amyloidosis by genetic modifications was well developed. Several transgenic

lines were produced which express human APP, Aβ, or APP genes carrying familial AD mutation. These transgenic mice exhibit some degree of pathological changes that include amyloid deposit, neuritic plaque formation, synaptic loss and astrocytosis, although none of these animals showed obvious neuronal loss as consistently observed in AD (Yamada and Nabeshima, 2000). Other models include the transgenic rodents with human tau or GSK-3β in the hope to increase tauopathy phenotype (Lucas *et al.,* 2001; Hernandex *et al.*, 2002; Arendt *et al.,* 1995). Transgenic mice that mimic cholinergic deficit in AD by overexpressing human acetylcholinesterase (Berri *et al.,* 1995) or generating lesions to the basalis magnocellularis (Winker *et al.,* 1995) were also produced. Despite extensive use of these models in pharmaceutical industries and academic research, there is however no perfect animal model that could mimic all the cognitive and behavioral abnormalities observed in patients with AD. The most common animal model based on pharmacological manipulations was produced by the administration of anti-cholinergic drug, scopolamine (Scop) (Beatty et al., 1986). Scopolamine is a muscarinic receptor antagonist which blocks ACh receptor thus mimicking a cholinergic deficit condition in animal model. These Scop-treated animals produce deterioration in memory test performance,

which could be reversed by pre-treatment with AChE inhibitors (Smith *et al.,* 1990), This model is commonly used to assess the drug efficacy for improving memory deficit.

5.1.2 Introduction to Morris water maze task

The memory deficit in rodents could be assessed based on Morris water maze task. Originally developed by R. Morris in 1984, this task is based upon the premise that animals have evolved an optimal strategy to explore their environment and escape from the water after a minimum amount of training (Morris, 1984). Experimentally, mice are released in a pool of water and allowed them to be rescued by reaching a hidden platform. Their spatial memory and learning can be reflected by their strategy to search the platform by memorizing the distant visual cues. The mice that learn and remember the spatial cues would find the platform in the shortest time. With the help of computer and tracking software, the gain in spatial accuracy of the mice can be measured as parameters generated from the captured swimming path. By comparing parameters between different treatment groups, we can assess the effect of drug to the mice behavior.

As CT has proven to be an AChE inhibitor *in-situ* and *in-vitro*. This raises the opportunity that CT could be used as an anti-AD drug. In order to explore this possibility, the effect of CT on Scop induced spatial memory impairment was studied in the present thesis. An in-house water maze system was set up to test the *in vivo* efficacy of CT.

5.2 Material and methods

5.2.1 Reagents

Purified CT (>90% purity) was obtained by the method described in chapter 2. Huperzine A (HupA) was purchased from Calibiochem. Scopolamine hydrobromide (Scop) were purchased from Sigma.

5.2.2 Animals

Male S/D rats (400 ± 50 g, 12 weeks old,) were supplied by Laboratory Animal Services Center, The Chinese University of Hong Kong. The S/D rats were housed in five per cage and kept in a temperature controlled room maintained at 22 °C with a 12 h light-dark cycle. Food and water were available *ad libitum*. Before water maze training, the rats were allowed 2 days acclimatization to the environment. Rats were handled according to experimental procedures approved by the Animal Experimentation Ethics Committee of the Chinese University of Hong Kong.

5.2.3 Water maze setup

Water maze setup (Fig 5.1) consists of a circular black-painted pool (160 cm

diameter x 70 cm height filled with water (temp 24-27℃). The setup was surrounded by black curtains. The pool was conceptually divided into four equal sized quadrants. Four bright colored geometric cue cards were placed at four corners above the pool. A black cylinder platform (10 cm diameter x 30 cm height) was submerged at depth about 1 cm and was placed at the centre of a randomly selected quadrant. The position of the submerged platform would not change during all training session. Swim paths of the animals were monitored by a video camera which was placed at two meters above the center of the pool. The camera was connected to a computer equipped with a video tracking system. The video capturing system, mule capture 1.5 was provided by John Cheng of System Engineering at The Chinese University of Hong Kong.

a)

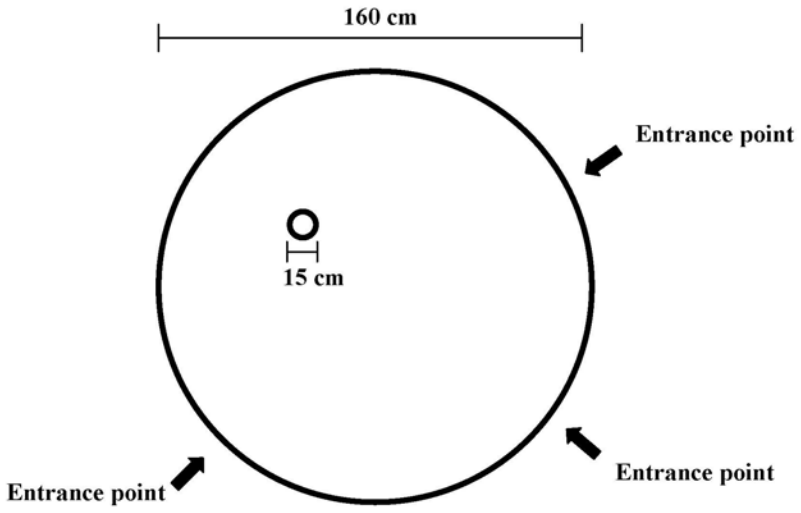

Fig 5.1 Water maze setup. A removable hidden platform with 10 cm diameter was placed inside the 160 cm diameter swimming pool. Three entrances by which the rats were put into the water maze during training session and probe trial are indicated. The setup was surrounded by black curtain, with highly visible cues attached on it.

5.2.4 Drug treatment

56 male S/D rats were randomly divided into seven groups (n=8). Stock solution of CT was prepared by dissolving completely in DMSO with 20% N,N –dimethylacetamide (Sigma) in concentration 20 mg/ml. Then the stock solution was diluted into feeding vehicle containing distilled water with 5% Polysorbat-80 (Sigma) making final concentration 0.1, 0.5, 1 and 2 mg/ml). Drugs were administered by oral garvaging. Rats were fed daily according to their body weight (10 ml/kg), and the final dosing would be 1, 5, 10 and 20 mg/kg. Rats in positive control group were treated with 1 mg/kg HupA.

5.2.5 Water maze procedure with visible platform

At the last day of treatment a visual acuity test was performed at the end to assure that the animals did not have any visual defects. Rats allowed to swim to a red platform protruded from water. One trial with no time limit would be given to the rats to familiar with the setup. Its latency to climb onto the platform and its swimming activities were recorded on the second trial.

5.2.6 Water maze procedure with hidden platform

Rats treated with drugs were injected intraperitoneally either with saline (10

ml/kg) or 0.5 mg/kg Scop in saline. A pre-training probe test was performed 20 minutes post-injection. In the probe test, the rats were given 60s to swim without the escape platform. The swimming paths of the rats were recorded by the video camera placed above the maze. A 4-trial training session was given to the rats. In each training trial, the rats were loaded by hand into the pool, facing the inside wall of the tank, at one of the four pseudo-randomly varied starting points. The same starting point was not used more than twice in each session. Once the rats reached the platform, they were allowed to remain on the platform for 30 seconds. Those rats could not find the submerged platform within 90 seconds were guided to the platform and placed there for 30 seconds. All trials were performed between 11:00-18:00 h on each day. A post-training probe test was carried out immediately after the 4th training trial. The swimming paths of the rats from the pre-training probe test and the post-training probe test were analyzed by Nolduls ColourPro software (version 3.1, Noldus Information Technology, The Netherlands) to determine the memory performance of the rats. Performance was expressed as the average distance travelled by the rat during swimming to the spatial location at which escape platform was located during training.

5.2.7 Search strategy analysis

Swim path for each probe test was plotted using mule pros-processing 1.8, provided by John Cheng of System Engineering at The Chinese University of Hong Kong. The search strategy was assigned to each trial using a categorization scheme similar those developed previously (Brody and Holtzman, 2006; Janus, 2004). The categorization scheme was modified to fit the probe test assessment. The searching scheme was divided into spatial, non-spatial (including scanning, random searching and chaining) and no-searching (including wall hugging and thigmotaxis) categories. Typical examples of each category or subcategory are shown in Fig 5.2

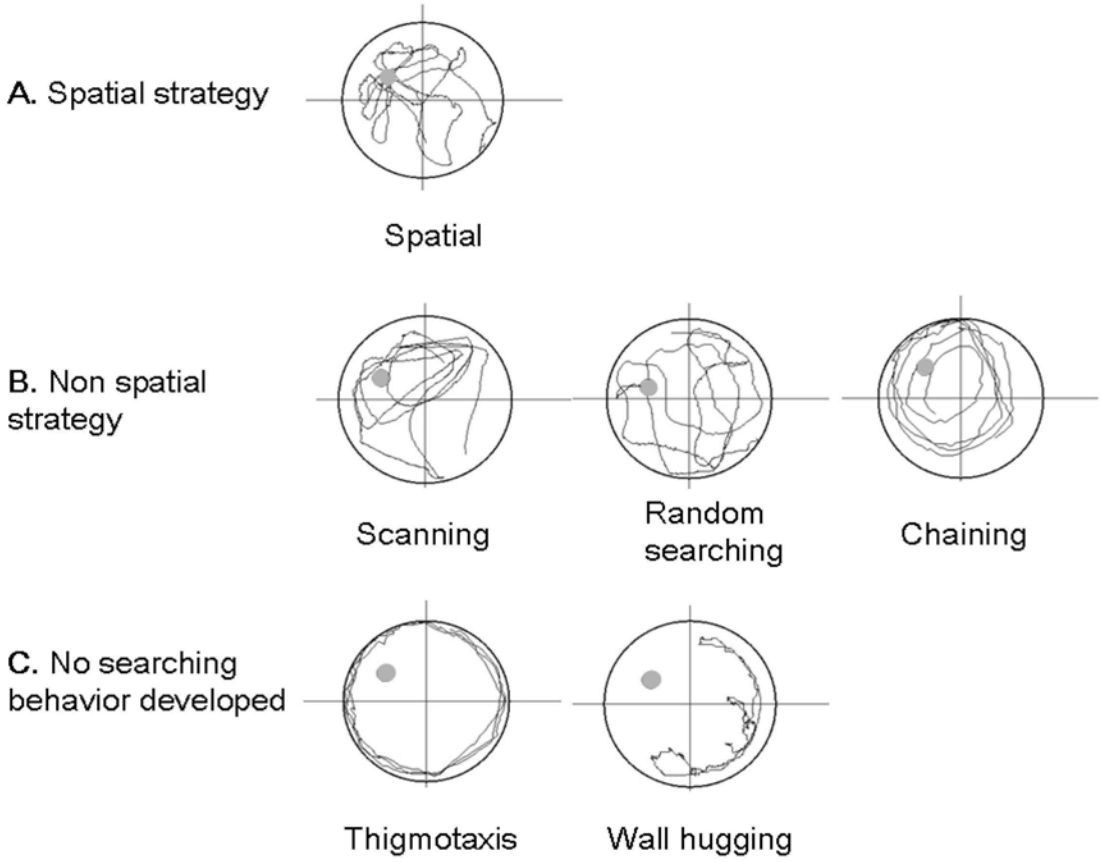

Fig 5.2 Search strategy examples exhibited by S/D rats in the probe test. The location of the hidden platform is indicated by the black circle at upper left quadrant. **A.** Spatial strategies. Paths were confined to the area where platform was located, characterized by searching behaviors such as occasional sharp turning and rearing. **B.** Non-spatial systematic strategy: Scanning- repetitive searching path, with a bias to the platform location; Random searching - searching the entire tank without bias towards any portion; Chaining- repetitive looping at the inner area of the pool. **C.** No searching behavior developed: Thigmotaxis- looping along the side of pool; Wall hugging: stay near the wall with less motivation to move.

5.2.8 Plasma alanine aminotransferase (ALT) assays

ALT assays were performed from the rats either fed with vehicle and CT. In brief, blood samples were collected from the rats by tail-bleeding in tubes containing heparin (0.5% w/v). The blood samples were centrifuged at 2,000 rpm for 10 min at room temperature. The upper plasma layers were collected and assayed for ALT activities. Plasma ALT activity was assessed using an alanine aminotransferase kit (BioSystems) according to the manufacturer's instructions.

5.2.9 Brain AChE/ BuChE activity assay

Rats were sacrificed by decapitation. Rat whole brain were rapidly removed and weighted. The whole brain was then perfused with isotonic saline. The whole brain was homogenized in three volume of ice cold homogenizing buffer containing 50 mM Tris-HCl, pH 7.4 and 300 mM sucrose. Homogenate was then centrifuged at 1000 x *g* for 20 min. Supernatants were collected and protein concentration were determined by Bradford color reagent (Biorad, USA). Equally 100 μg protein from each sample was used as enzyme source for Ellman assay.

5.3 Results

5.3.1 Drug treatment does not impair visual function of rats

Visible platform test which also called visual acuity test was performed at the day after 1-month drug treatment. This test does not involve the use of cognitive but visual function. Performance in the visible platform test is affected by factors such as vision, swimming ability, and motivation to escape from water. All the abilities above are essential for normal cognitive function, and they are prerequisites for carrying out any cognitive function test. Mice that cannot swim a direct path to the visible platform in the visual acuity test would be discarded from the data. In this test, all rats can reach the protruding platform within 30 seconds on second trial. Test result show that drug treatment did not cause visual impairment to rats in all treatment group.

5.3.2 Effect of CT treatment on escape latency of Scop treated rats during training session

The *in-vivo* efficacy of CT was studied using the water maze acquisition test. CT (0, 1, 5, 10, and 20 mg/kg) or the control drug 1 mg/kg HupA were administered for a month. Rats were then subjected to a 4-trial water maze training. Escape latency for each trial was recorded as a measure of performance. As shown in Fig 5.3, while comparing the escape latency of trial 1 with trial 4, a significant decrease was observed in the control (Veh+Saline, group 1) group, which indicated a normal memory acquisition process. The Scop treated group (Veh+Scop, group 2), which under the influence of Scop, was failed to acquire memory through the training session, and no significant decrease in escape time was resulted. For the groups pretreated with CT, they showed different degree of improvement in escape latency (group 5-7). Among different CT treated groups, the most significant improvement was observed in group 5, which pretreated with 5 mg/kg CT. Since there were a general decreasing trend in escape time of CT pretreated groups after the 4-trial training, we can conclude that CT has a reversing effect on the memory acquisition ability impairment brought by Scop. In this experiment, known AChE inhibitor (Xu et al., 2006b) was used as a positive control, and it also

showed reversal effect on Scop memory acquisition impairment.

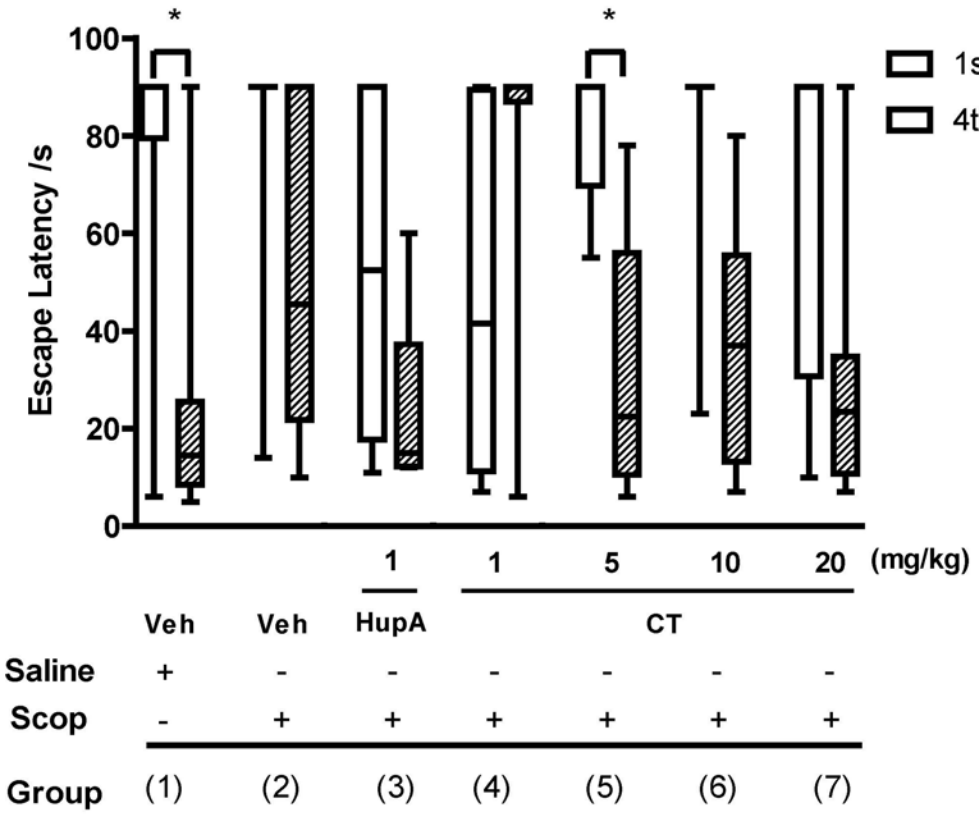

Fig 5.3 Effect of chronic oral administration of CT on escape time of rats in escape latency distribution of training trial 1 (white bars) and training trial 4 (stripped bars). Rats were administered with vehicle (Veh), HupA or CT for one month. Saline or Scop was administrated intraperitoneally 30 min before the test. Values represent mean ± SEM of escape time (n=8). One way ANOVA with post hoc Bonferroni tests.; *p < 0.05 significantly different between the escape latency of trial 1 and trial 4.

5.3.3 Effect of CT treatment on memory acquisition of Scop-treated rats in probe trial

In probe trial, rats were given 1 minute to swim freely in the pool without platform. Their swimming path was captured for analyzing search strategy. The decrease in mean distance to platform was used as an index to demonstrate the task learning ability of the rats (Gandhi et al., 2000). As shown in Fig 5.4, the Scop-injected control group 2 showed a significant decrease in task learning ability in comparison with the saline-injected control ($p<0.05$). The Scop-induced impairment was reversed in the CT-treated rats, and a maximum reversal was observed at 5 mg/kg ($p<0.05$; Fig. 6). Higher doses of CT (> 10 mg/kg) only slightly improved the task learning ability of the rats.

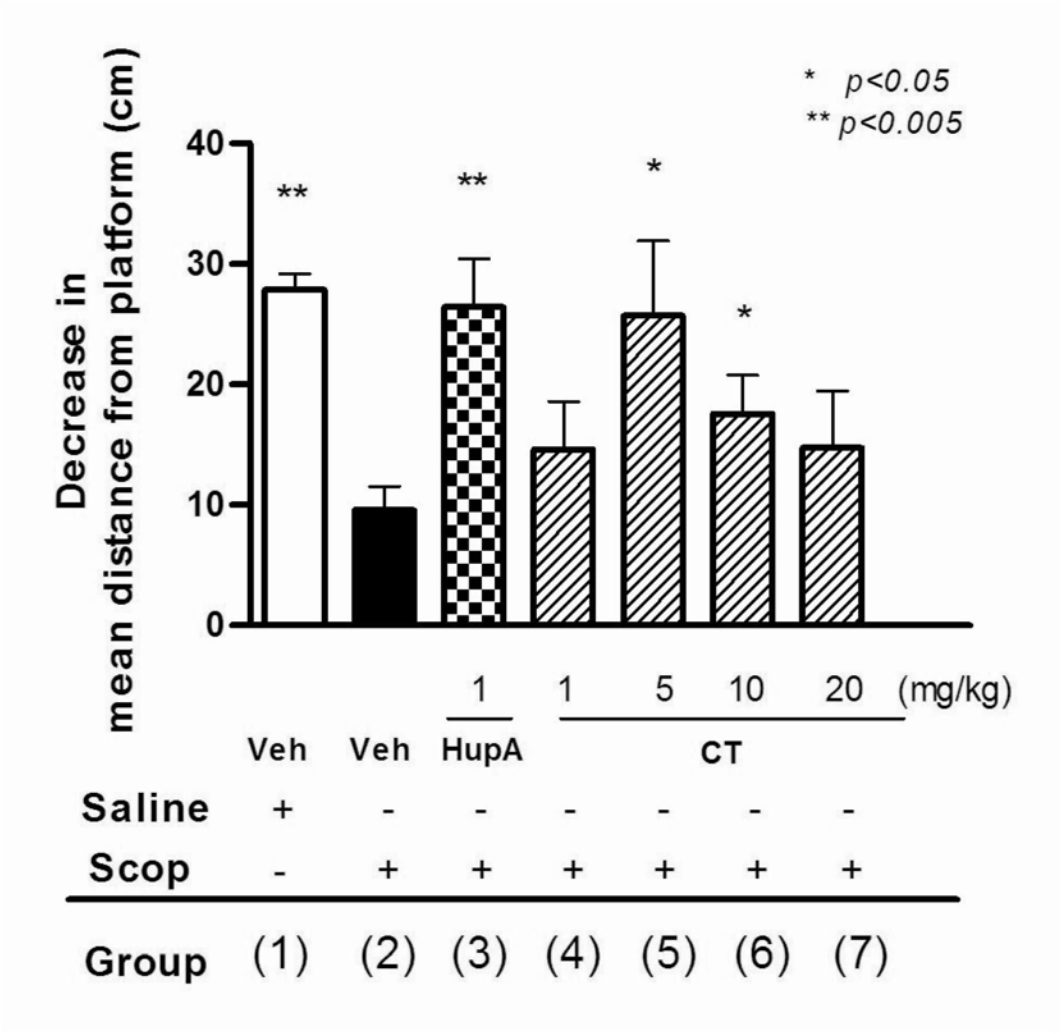

Fig 5.4 Effect of chronic oral administration of CT on the performance of probe test. Rats were administered with Veh, HupA or various doses of CT for one month. Saline or Scop was administrated intraperitoneally 30 min before the test. Values represent mean ± SEM of differences (n=8) between the mean distance to target in pre-training probe trial and post-training probe trial. One way ANOVA with post hoc Bonferroni tests; *$p < 0.05$, **$p < 0.005$ significantly different from the vehicle group injected with Scop.

5.3.4 Effect of CT on strategy selection of the Scop-treated rats

The search strategies used by the rats in the water maze acquisition test are summarized in Fig 5.2. Search strategies can be classified in three major types – spatial, non-spatial and no-searching. The distribution of search strategies performed by the rats are shown in Fig 5.5. In the pre-training probe test (Fig 5.5a), nearly all the rats (98.21%) showed no searching strategy, which indicated by thigmotaxic (80.36%) and wall-hugging (17.85%) behavior. It has already been known that rodents would try to search the wall for the exit of water maze when they are unfamiliar with the task (Whishaw, 1985). After the hidden platform training, 75 % of rats in the saline-injected control group developed a spatial search strategy (Fig 5.5b). Consistent with other reports, the Scop-administrated rats exhibited deficits in acquiring spatial strategy (0% of incidence) during their navigation but 62.5% of rats exhibited thigmotaxis. All doses of CT used in this study could improve the search performance of the Scop-treated rats. The maximum effect was observed in rats treated with 5 mg/kg of CT, and the rats adopted a high proportion of spatial strategy (50%) along with some non-spatial (25%) and no-searching (25%) strategies. HupA also improved the search performance of the Scop-treated rats.

(a)

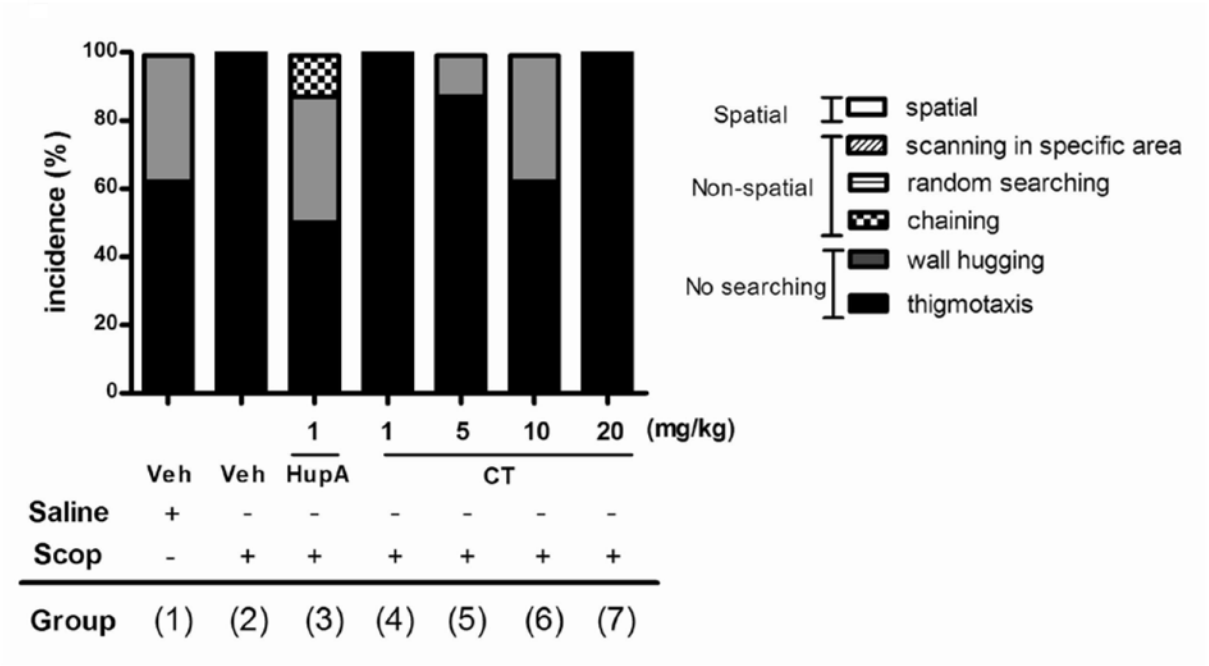

(b)

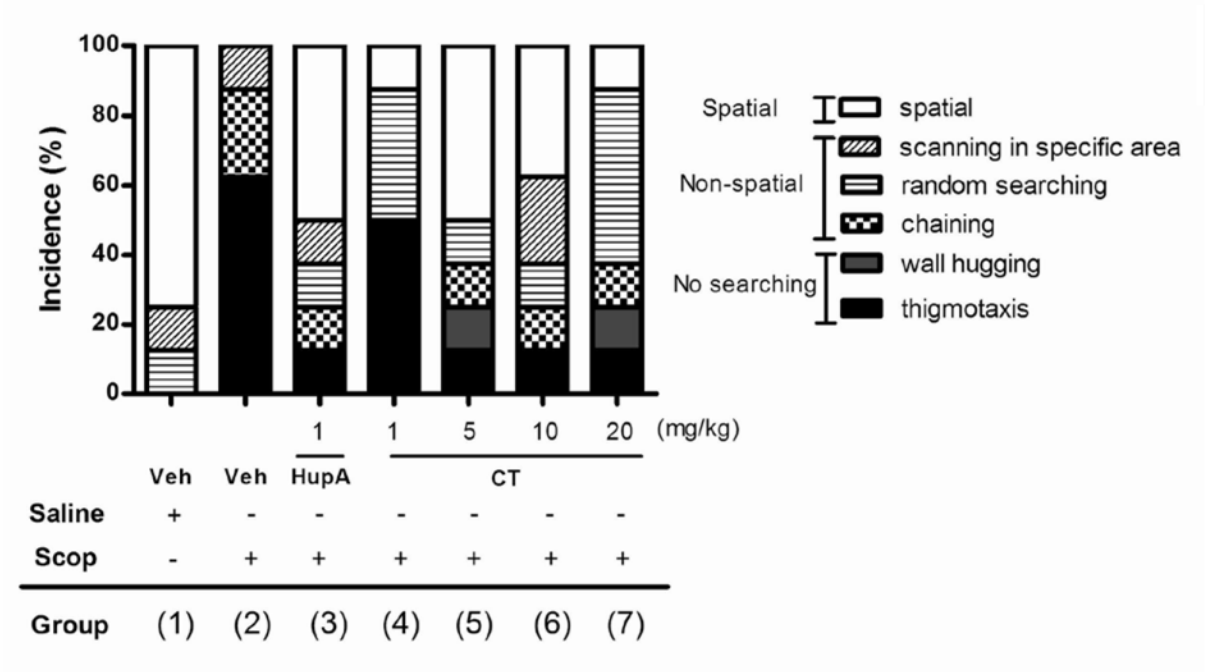

Fig 5.5 Search strategies distribution of the rats. Search strategy used by the rats (a) in the pre-training probe test (b) in the post-training probe test. Strategy types were defined as described in Fig 5.2.

5.3.5 Effect of CT on the swimming speed of rats

One of the concerns of water maze task is whether the animal is in good condition. In the case of drug test, if the treatment applied has made them too weak to swim, their task performance would be independent of their ability of learning and memory. Therefore swimming speed of rats in probe test was also investigated. Fig 5.6 shows the swimming speed of rats of different treatment groups in the after-training probe test. Significant increase in swimming speed was observed in group 1, 4, 5 and 7, which corresponds to Veh, 1, 5, or 20 mg/kg CT treated with Scop. Previous research reported that Scop treatment would slightly increase swimming speed of animals (von Linstow et al., 2007). More than that, CT treated group except 10 mg/kg increased the swimming of rats in a greater extend than the Scop+Veh group. By observation, the CT-treated rats were more active and energetic while swimming or inside their cages. Together with the general increase of swimming speed, CT might have some effect on increasing the locomotor activity of animals.

(a)

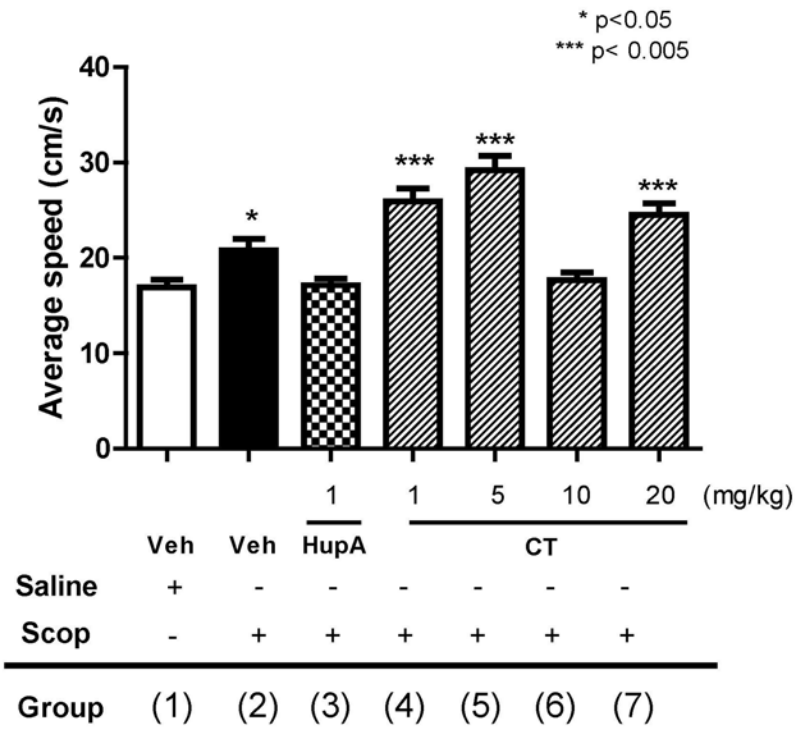
* p<0.05
*** p< 0.005
Average speed (cm/s)
40
30
20
10
0
*
***
***
***
1
1
5
10
20
(mg/kg)
Veh
Veh
HupA
CT
Saline
+
-
-
-
-
-
-
Scop
-
+
+
+
+
+
+
Group
(1)
(2)
(3)
(4)
(5)
(6)
(7)

(b)

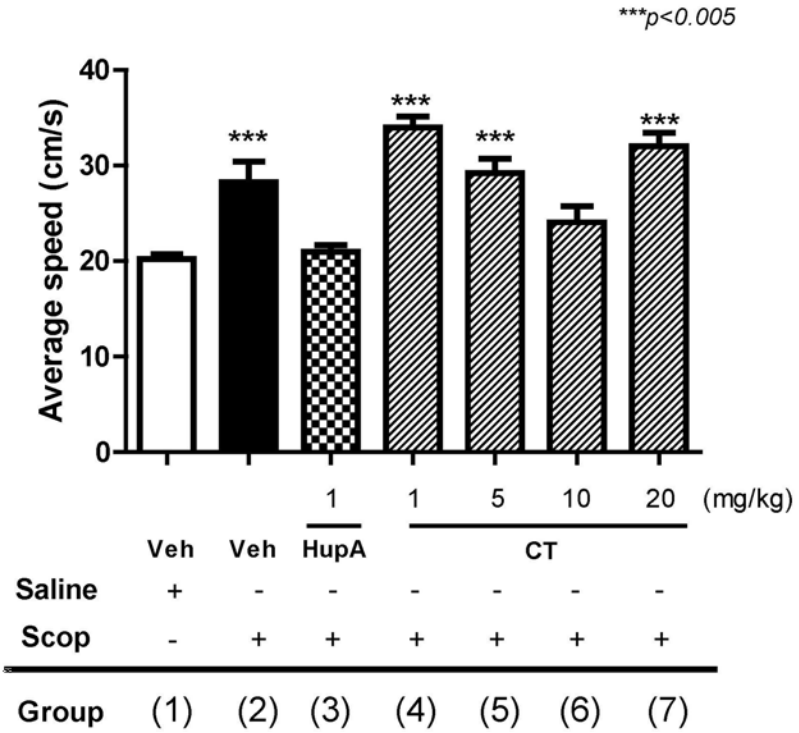
***p<0.005
Average speed (cm/s)
40
30
20
10
0
***
***
***
***
1
1
5
10
20
(mg/kg)
Veh
Veh
HupA
CT
Saline
+
-
-
-
-
-
-
Scop
-
+
+
+
+
+
+
Group
(1)
(2)
(3)
(4)
(5)
(6)
(7)

Fig 5.6 Swimming speed of rats in the probe trial (a) before and (b) after training. Values represent mean ± SEM of swimming speed within group (n=8). One way ANOVA with post hoc Dunnett's multiple comparison test; ***$p < 0.005$ significantly different from the vehicle group injected with saline (group 1).

5.3.6 Effect of CT treatment on plasma ALT of rats

Hepatotoxicity is one of the side effects of some AChE inhibitors like Tacrine and tetrahydroaminoacridine (Kumar and Becker, 1989; Watkins et al., 1994). Therefore we would like to monitor the plasma ALT activity of the treated animals. Plasma from group 5 to 7, which correspond to treatment dose 5, 10 ad 20 mg/kg were examined (Fig. 5.7). There was no significant change in the level of plasma ALT activities in groups treated with 5 and 10 mg/kg in comparison to the controls. Remarkable elevated plasma ALT activity was observed in 20 mg/kg group.

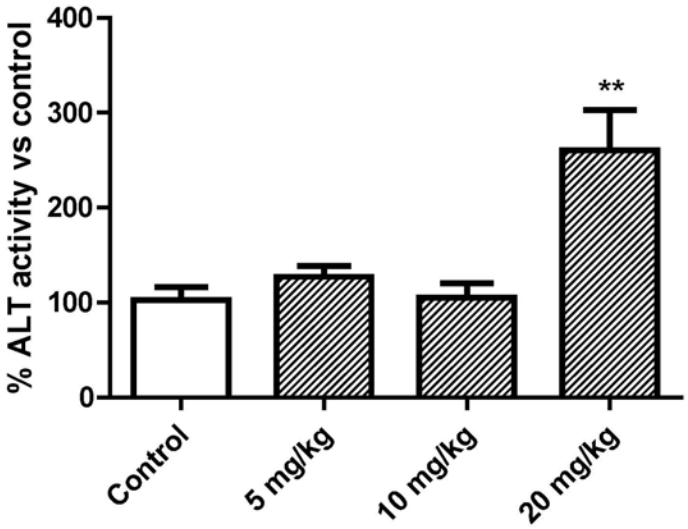

Fig 5.7 Effect of CT treatment on the animal plasma ALT. ALT activity of plasma samples collected from S/D rats treated for 1 month with various dose of CT were assayed. Result expressed in percentage of ALT activity of Veh samples of corresponding treatment group. Bars indicate mean ±SEM (n=8). One way ANOVA with post hoc Dunnett's multiple comparison test; $^{**}p < 0.005$ significantly different from the control group.

5.3.7 Brain AChE activity of CT-treated rats

In order to know if the improved performance in water maze acquisition task correlated with the brain AChE activity, brains of rats from Veh group, and the groups showing positive result on reversing Scop treatment were collected. Brain homogenates were prepared and assayed for AChE activity. Fig 5.8 shows the AChE and BuChE activity in total brain homogenate of Veh, 5 mg/kg and 10 mg/kg groups. A slight but not significant (verified by one way ANOVA with post hoc Dunnet's test versus Veh group) increase in brain AChE activity was observed. There was a significant increase in brain BuChE activiy in the 10 mg/kg group. From this result, it seems there is no correlation between the brain AChE/BuChE activity and the improvement in water maze task performance.

(a)

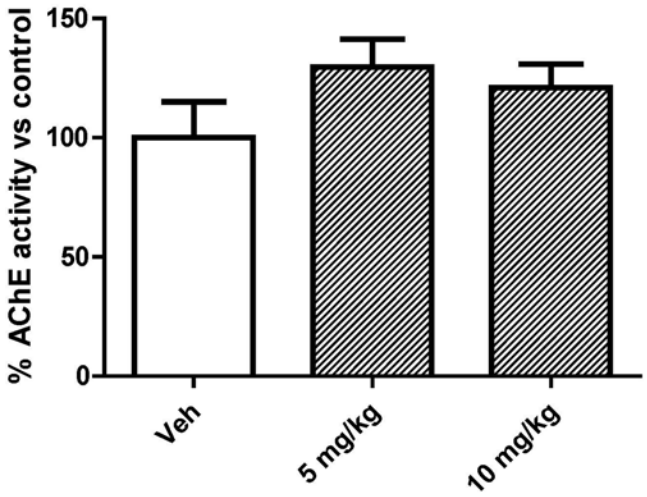

(b)

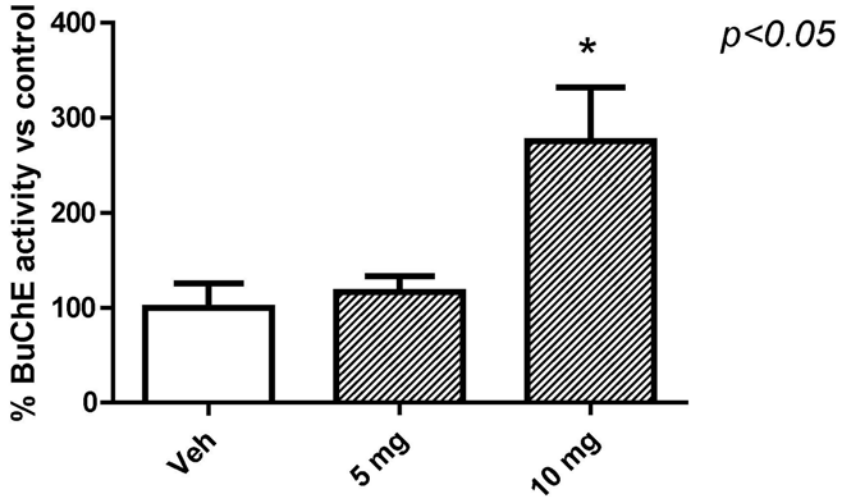

Fig 5.8 Brain (a) AChE and (b) BuChE activity of rats chronically fed with 5 mg/kg/day and 10 mg/kg/day CT. Values represent mean ± SEM of percentage of AChE activity versus control rats which fed with Veh only (n=8). One way ANOVA with post hoc Dunnett's multiple comparison test.; *$p < 0.05$ significantly different from the Veh group.

5.4 Discussion

Therapeutic effect of CT against Scop-induced cognitive lesion was evaluated by water maze acquisition test. In this study, performance of rats in water maze task was assessed during training and probe trial. Efficacy of CT on reversing Scop-induced cognitive dysfunction was shown by either reduced escape latency during training session (Fig 5.3) or increased spatial accuracy in probe trials (Fig 5.4). The dose of CT resulting in the maximum reversal effect of the Scop-induced cognitive lesion was 5 mg/kg. However, higher doses of CT failed improving the task learning performance of the Scop-treated rats. Such a U-shape dose response phenomenon has been reported with other cholinesterase inhibitors in rodents (Braida et al., 1996; Wang et al., 1999a).

An explanation to this phenomenon is that a high dose of cholinergic drug could cause an adverse effect on motor function of tested subject. Animals treated with different AChE inhibitors in high dose suffered a reduction in swimming speed in water maze task (Van Dam et al., 2005). However, this is not the case in our experiment. Swimming speed of rats does not decrease by

CT treatment, but instead, a general increase in swimming speed was observed in CT treated animal (Fig 5.6). Although Scop-treated rats also have a significant increase in swimming speed, which due to the disturbance of sensorimotor function (Beiko et al., 1997). Swimming speed of CT treatment group is even higher than Scop-Veh group. This is an interesting observation. As in clinical case, one of the side effects of long term administration of AChE inhibitor was neuromuscular weakness and deterioration (Lev-Lehman et al., 2000). Whereas in our case, CT could even increase locomotor activity of treated rats. Further experiment on the effect of CT on animal's muscular strength will be discussed in next chapter.

Another explanation on the adverse effect on high dose treatment is the toxicity caused. The effective doses, 5 mg/kg and 10 mg/kg treatment, did not show obvious adverse effect on the liver function of the rats. At 20 mg/kg treatment, significant liver toxicity is observed (Fig 5.7). Although from our result, 20 mg/kg treatment shows no impairment on the sensorimotor function of the rats (Fig 5.6), we don't know if it may have some disturbance on the other functions that is essential to spatial learning ability.

We also analyzed the search strategies of the rats and found a pronounced difference in the search strategy used by the CT-dosed rats as compared to the vehicle controls. A major effect of CT was to increase the incidence of spatial searching strategies especially in the group treated with 5 mg/kg of CT. It has been reported that CT inhibits AChE activity in the mouse brains (Kim et al., 2007). Therefore CT may improve the spatial memory by restoring the cognitive function impaired by Scope presumably through inhibiting cholinesterase activities. We also observed an increase in the usage of non-spatial strategies in all groups of the CT-treated rats, including those treated with 10 and 20 mg/kg. It was apparent from our studies and from previous work that rodents using non-spatial strategies, always had low scores in various assessment schemes such as average distance to target (Baldi et al., 2003). This may explain why the groups dosed with 10 and 20 mg/kg of CT had low scores in the water maze acquisition test. However, the switch from thigmotaxic and wall-hugging strategies to non-spatial strategies is also considered as a memory acquisition process (Saucier et al., 1996), and which is related to brain cholinergic system (von Linstow et al., 2007). This is an evident of unimpaired memory function.

From the brain AChE and BuChE activity assay of treated animal, the improvement on cognitive function cannot correlate with the degree of inhibition of brain AChE/BuChE activity. At 5 mg/kg and 10 mg/kg groups, which were the effective doses, CT treatments slightly increased brain AChE activity and significantly increase brain BuChE activity at 10 mg/kg group. This agrees with some studies on long term administration of ChE inhibitors. AChE and sometimes BuChE levels founds elevate in subjects treated with ChE inhibitors like tacrine, donepenzil and galantamine (Parnetti et al., 2002). Prolonged exposure to ChE inhibitor would cause a general increase of brain AChE activity due to negative feedback mechanism. Yet, the increase in brain AChE activity does not necessarily correlated with the improvement in memory performance (Davidsson et al., 2001). The mechanism lies behind this phenomenon is very complicated. Some research groups say it is due to the increase in expression of neuroprotective retro-AChE isoform by drug (Nordberg, 2006). Another research group found that long term drug treatment increase nicotinic ACh receptor expression, thus increase the sensitivity of cholinergic signal (Reid and Sabbagh, 2003). Further experiment on the working mechanism of CT should be carried to solve this phenomenon.

Chapter 6 Effect of cryptotanshinone on animal's locomotor activity

6.1 Introduction

As the purpose of AChE inhibitor treatment is to increase the amount of ACh available for neural and neuromuscular transmission throughout the body, pharmacological adverse effects would be expected if cholinergic system is overstimulated. One of the adverse effects is that prolonged treatment of AChE inhibitor may cause muscle weakness or muscle cramp. Muscle cramp is a sign of ACh poisoning caused by excessive inhibition of peripheral AChE causing overstimulation of nicotinic ACh receptor at the neuromuscular junction. Case of muscle cramp was reported with donepenzil treatment and muscle weakness with metrifonate (Gauthier, 2001). Prolonged tacrine treatment would disturb neuromuscular transmission and evoke muscle twitched tension (Ibebunjo et al., 1997). Neuromuscular adverse effect would lead to respiratory distress resulting in AChE inhibitor induced anesthesia. In fact, case of anesthesia has been reported from patients on AChE inhibitor treatment and muscle relaxant co-treatment is required (Baruah et al., 2008).

In previous chapter, during water maze experiment, it was found that CT treatment generally increased swimming speed of treated animals, without disturbing their cognitive function. This observation gives support that chronic CT treatment did not induce neuromuscular side effect on the animals.

To more precisely test if CT would cause cholinergic poisoning and to further confirm if CT treatment could really improve exercise performance of animal, behavioral tests on the motor function of animals were performed. Muscle coordination and balance would be tested by rotorod setup in which the mice were placed on a running rotorod. Latencies for the mice to fall from the rotating drum were recorded. On the other hand, exercise performance in terms of endurance was tested by the forced swimming test. In order to assess the potential mechanisms of CT bioactivity, we also measured liver starch, blood urea nitrogen and lactic acid in the animal.

6.2 Materials and methods

6.2.1 Animals

Male NIH mice (25 ± 5 g, 4 weeks old,) were supplied by Guangdong Medical Laboratory Animal Center, China. Mice were housed in ten per cage and kept in a temperature controlled room maintained at 22 °C with a 12 h light-dark cycle. Food and water were available *ad libitum*. Before the start of experiment, the mice were allowed 1 hour acclimatization to the environment.

6.2.2 Drug treatment

Fifty male NIH mice were randomly divided into five groups (n=10). Stock solution of CT was prepared by dissolving completely in DMSO with 20% N,N –dimethylacetamide (Sigma, China) in a concentration of 20 mg/ml. Then the stock solution was diluted into feeding vehicle containing distilled water with 5% Polysorbat-80 (Sigma, China) making final concentration. The drug CT at 0.5, 1 and 2 mg/ml were administered by oral garvaging. Mice were fed daily according to their body weight (0.1 ml/10 g), and the final dosing would be 5, 10 and 20 mg/kg. For the drug control group, 10 mg/ml Creatine (Sigma) was prepared in the same Vehicle as CT.

6.2.3 Measurement of motor function by rotorod

Rotorod test was performed after two weeks of drug treatment. During rotorod experiment, mice were loaded onto the rotorod apparatus (model YLS-4C, FlyDe, China) rotating at 1 rpm. The speed was then increased from 1 rpm to 30 rpm within 1 minute. Time was taken when the mice fell off. Mice were given a two-minute trial to become acquainted with the apparatus. Retention of fall on the second trial will be taken as data.

6.2.4 Measurement of swimming endurance

At the day of experiment, drug or Vehicle were fed to mice 2 hours prior to the swimming test. Body temperature was measured at 1 hour after drug treatment. Swimming endurance of drug treated mice was evaluated by a forced swimming test. In forced swimming test, a plastic tank (20x15x17 cm) tank filled with water to a depth of 12 cm was used (Fig 6.1). The water temperature was maintained at 25℃. Prior to each test, mice were weighted and a load which equal to 5% of the mice body weight was attached to its tail. Mice were then set free into the water. Swimming time was taken when the mice exhausted, which is defined by stopping all coordinated movements and failure

to return to surface of the water to breathe within 7-second period. At this point they were immediately rescued from the tank. The swimming test was carried out during 11:00am to 5:00pm in order to avoid circadian variations in physical activity.

(a)

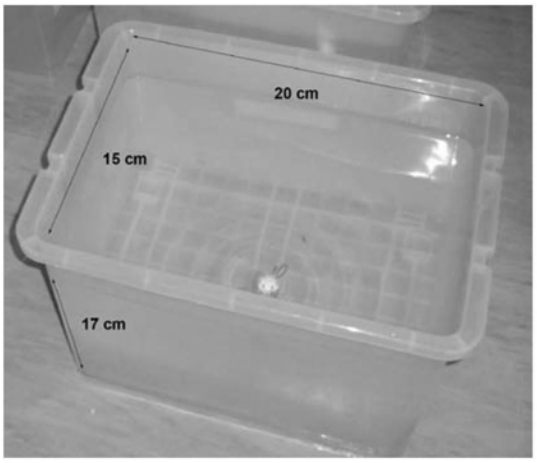

(b)

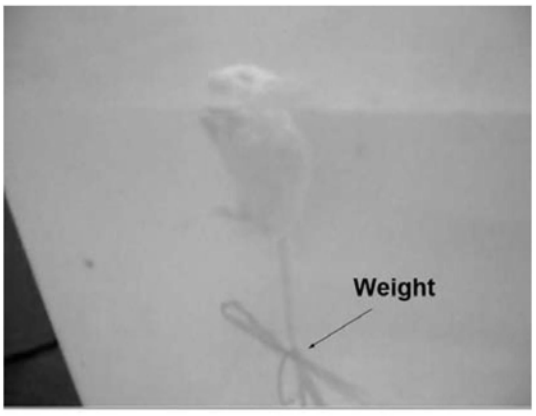

Fig 6.1 Forced swimming test setup. (a) 20x15x17 cm plastic tank filled with water (24-27℃) to a depth of 12 cm was used. (b) Loading equivalent to 5% of the mice body weight was tied to its tail.

6.2.5 Analysis of biomedical parameters

One week after the swimming endurance test, mice were allowed to swim without weight for 30 minutes, and were allowed to rest for 30 min. Blood was collected from the orbital sinus. Blood sample collected was divided into two portions. Serum was isolated from one portion and blood urea nitrogen level and blood cholesterol lever were determined by a commercial kit with an automated biochemistry analyzer. In the meanwhile another portion of blood sample was sonicated in hypotonic buffer, and lactic acid level in blood was determined by an automated analyzer. After blood collection, mice were immediately sacrificed by cervical dislocation and liver was isolated. Liver samples were homogenized in 100 mg/ml volume of trichloroacetic acid and centrifuged in 3000 rpm. Supernatant collected was mixed with 4x volume of 95% ethanol. After sedimentation, upper layer was removed and glycogen content of the lower layer was assayed by the Anthracene Ketone reagent. Glycogen weight (mg) per 100 mg of liver was calculated according to the following formula: Glycogen weight = DU/DS × 0.5 × homogenization liquid volume/liver weight (g) × 100 × 0.9, where DU represents the absorbency of the sample and DS represents the absorbency of the standard. The chemicals and the automatic analyzer for the above analysis were provided by the

Guangdong Medical Laboratory Animal Center.

6.3 Results

6.3.1 Effect of CT on motor coordination of mice

Overstimulation of cholinergic system would cause cholinergic poisoning which would lead to uncontrolled muscle contraction. Motor coordination defect is one of the adverse side effects of AChE inhibitor treatment (Gauthier, 2001). The disability of body balance and motor coordination in rodents can be reflected in rotorod behavioral test. The latency that the CT treated mice was able to maintain on the rotating drum until falling was analyzed (Fig 6.2). Data were analyzed by One way ANOVA and there was no significant difference between fall latency of different CT treated groups. Although 20 mg/kg CT treated group show an increase in latency of falling off the rotorod, no general trend of increase or decrease of fall latency was observed. From this result, no sign of motor defect caused by cholinergic poisoning was due to CT treatment.

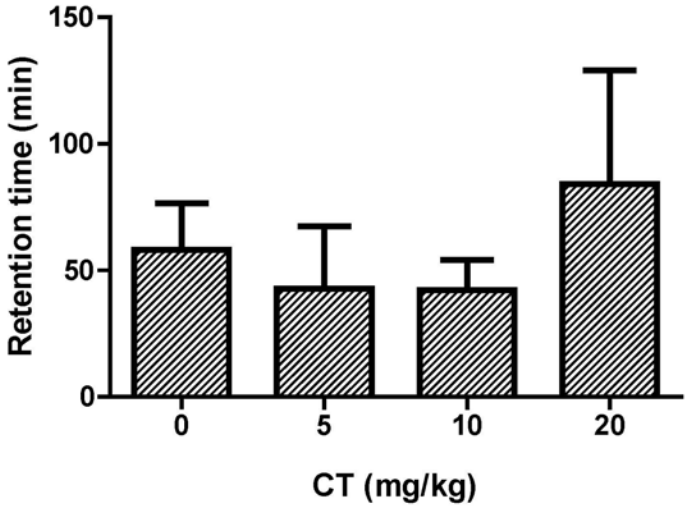

Fig 6.2 Effect of CT treatment on rotorod performance. NIH mice were fed orally with various dose of CT for 2 weeks. The mice were put onto the rotorod drum rotating at 1 rpm/min. Speed of the drum was increased to 30 rpm/min within 1 min. Values represent mean ± SEM of retention time that mice fell from the rotorod apparatus rotation at speed 30 rpm.

6.3.2 Effect of CT on swimming endurance of mice

Endurance of CT treated mice was tested by forced swimming test. In forced swimming test, the mice have to swim until exhaust. A load which equal to 5% of body weight was attached to the mice in order to shorten investigation time. Retention times for different treatment groups are listed in Fig 6.3. The average retention time shows a general increasing trend with treatment dose although changes are not significant when tested by One way ANOVA. In this experiment, a group treated with 100 mg/kg creatine was served as the positive control. Creatine can increase muscle strength and endurance in rodent and in human (Derave et al., 2003) . From our result, creatine treatment also increased average retention time in forced swimming test.

Increase in thermogenesis may improve exercise performance (Kline et al., 2007). The body temperatures of mice were examined 1 hour before the test (Fig 6.4). There was no significant difference in body temperature between different treatment groups. Therefore, the enhancing exercise performance of CT was not through increasing thermogenesis.

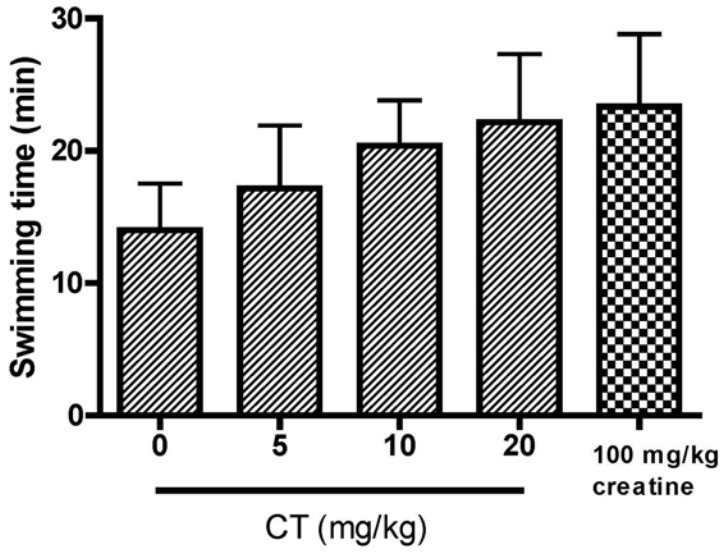

Fig 6.3 Effect of CT treatment on swimming time of mice in forced swimming test. Various doses of CT were administered for 30 continuous days. Mice were put to swim in a plastic tank filled with water (24-27°C). Loading equivalent to 5% of mice body weight was tie onto it. Mice swam until exhausted, defined by unable to return to the water surface to breathe within a 7-second period. Values represent ± SEM of maximum swimming time of mice (n=10).

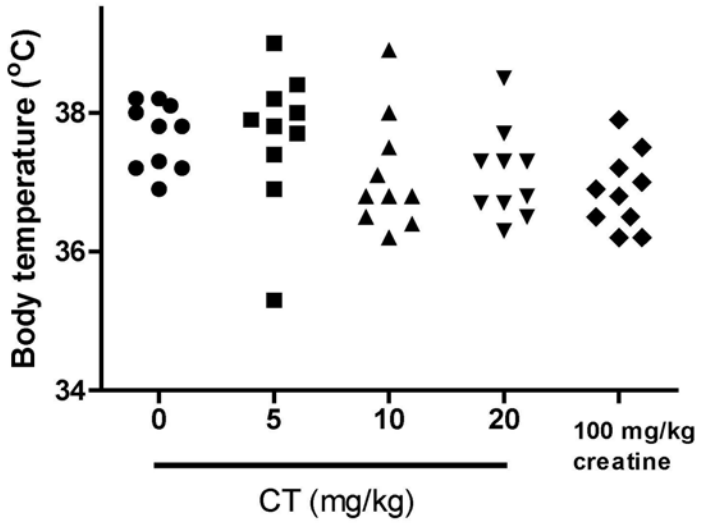

Fig 6.4 Body temperature of mice before forced swimming test. Body temperature was measured at 1 hour after drug administration and 1 hour before forced swimming test.

6.3.3 Study of biochemical markers of mice after exercise

Longer swimming time in forced swimming test can be interpreted as a reduced susceptibility to fatigue. Biochemical parameters related to anti-fatigue and energy metabolism were tested to further reveal the effect of CT on animal.

Accumulation of blood urea and blood lactic acid increases the risk of fatigue. Chronic CT oral administration dose dependently decrease blood lactic acid level after endurance exercise (Fig 6.5), where 10 mg/kg and 20 mg/kg groups show significant effect. Creatine treatment has the same effect on reducing lactic acid after exercise as reported by literature (Ceddia and Sweeney, 2004). Urea is another index used to measure endurance ability. The body preferentially uses sugar and fat as energy source. When there is continuous exercise, the body cannot obtain enough energy from sugar and fat catabolic metabolism, protein would be used as a source of energy and therefore urea as metabolic byproduct would be produced. Mice treated with CT and creatine did not show a significant decrease in blood urea after exercising for 30 minutes (Fig 6.6).

The main energy source of metabolism is carbohydrate. It is stored in our body as glycogen. Glycogen storage would deplete when under endurance exercise. Fatigue would happen after glycogen storage has been depleted. Therefore glycogen storage can be an index of degree of development of fatigue. From the result (Fig 6.7), CT treatment did not increase liver's glycogen storage.

In general, increase in endurance exercise performance of CT treated mice could be explained by its ability of reducing blood lactic acid accumulation after exercise, but not reducing blood urea accumulation nor increasing liver glycogen storage.

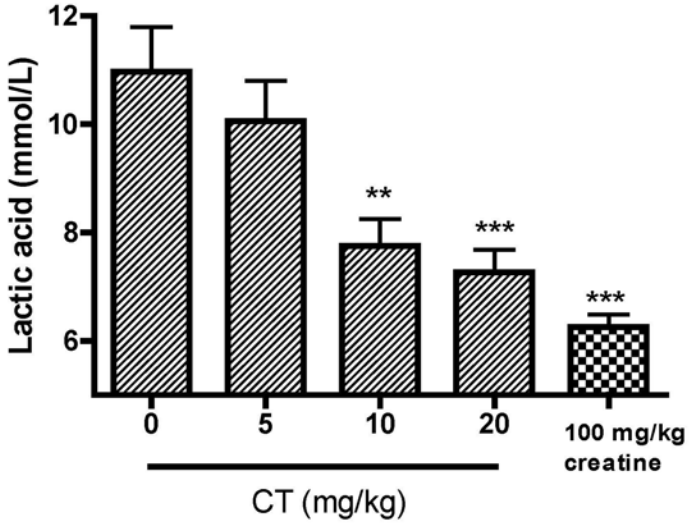

Fig 6.5 Blood Lactic acid of treated animals. Samples were collected after 30 min swimming. Values represent ± SEM of blood lactic acid of mice (n=10). One way ANOVA with post hoc Dunnet tests; $^{**}p < 0.005$, $^{***}p < 0.001$ significantly different with 0 mg/kg CT (control) group.

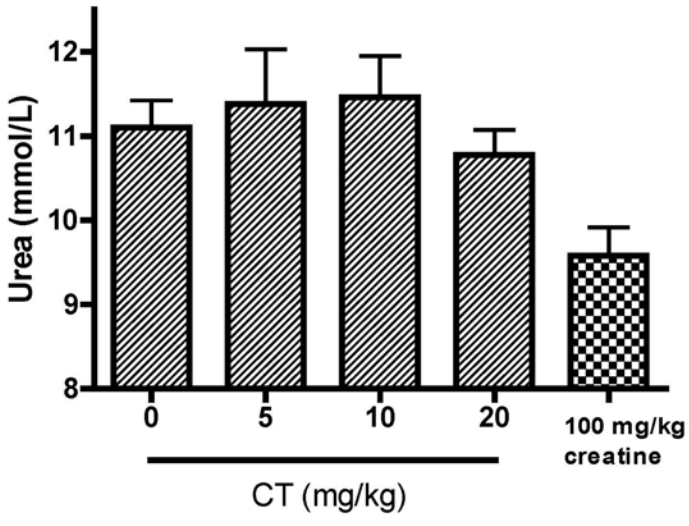

Fig 6.6 Blood urea of treated animals. Serum samples were collected after 30 min swimming. Values represent ± SEM of blood urea of mice (n=10).

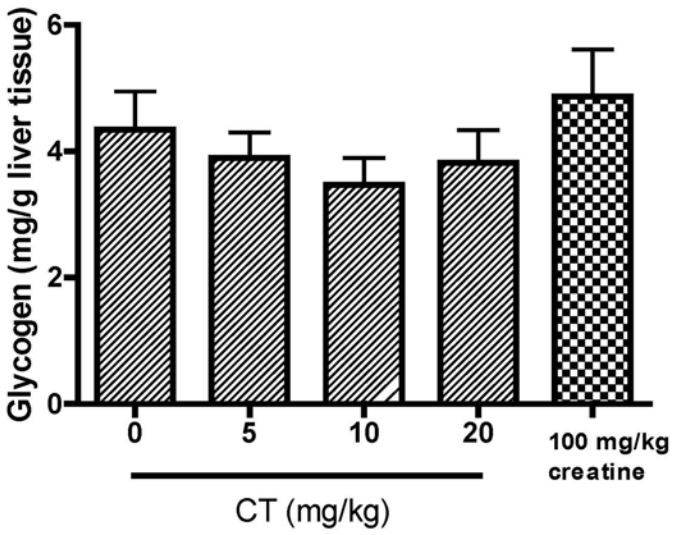

Fig 6.7 Liver glycogen of treated animals. Liver was collected from animals after 20 mins wimming. Values represent ± SEM of liver glycogen content (n=10).

6.4 Discussion

In this study, effect of CT treatment on the locomotor function of NIH mice was investigated. As observed in the previous water maze experiment, CT treatment does not cause motor defect, a common adverse effect of ChE inhibitor treatment. This is further confirmed by the unaffected performance of CT-treated mice in the rotorod test. From the result, muscle coordination of CT-treated rats is not affected. Therefore, chronic CT treatment does not acquire muscle weakness or uncontrolled muscle contraction as reported in the other AChE inhibitors (Gauthier, 2001; Ibebunjo et al., 1997). This data gives further support for the potential use of CT as an anti-AD drug.

The ability of CT on improving exercise performance was studied and CT shows a dose dependent effect on increasing the maximum swimming time of treated mice. Although general increasing trend in maximum swimming time observed in CT groups does not reach statistical significance when verified by One way ANOVA, the increase in average swimming time in creatine control group dose not reach statistical significance too. It appears both CT and creatine offer only subtle improvement to the performance. Further

modification to the forced swimming test protocol is needed to obtain a clearer picture of the drug effect.

Improvement in the exercise performance can be interpreted as the ability of anti-fatigue ability. Blood lactic acid is increased during exercise and is an indicator of fatigue. Removal of lactic acid from circulation is done by skeletal muscle, liver and heart. When under intense exercise, the rate of lactic acid production would excess the rate of removal, which results in fatigue. Result showing that CT is able to lower blood lactic acid after exercise. That means CT is able to attenuate the production or to enhance the clearance of lactic acid in circulation. Previous research showing that CT is able to phosphorylate and active AMP-activated protein kinase (AMPK), which is a key regulator of glucose uptake and energy metabolism in muscle cells (Kim et al., 2007). Interestingly, the positive control drug, creatine, also reported to activate AMPK (Ceddia and Sweeney, 2004). AMPK activation stimulates fatty acid production, ATP production, and on the other hand inhibiting protein and lipid synthesis (Suchankova et al., 2009). It also changes the cell metabolic state by increasing glucose oxidation (Ceddia and Sweeney, 2004). As the increase in glucose oxidation provides more energy source to the muscle cell, a

corresponding reduction in lactate production would be resulted for compensation. It is possible that CT reduces lactic acid production through the activation of AMPK. Recent research found that exercise can elevate the level of AMPK in association with brain-derived neurotrophic factor (BDNF), which plays an important role in synaptic plasticity (Kovalchuk et al., 2002). This in turn improves the synaptic plasticity and thus cognitive function (Gomez-Pinilla et al., 2008). As a potential anti-AD drug, the ability of CT to activate AMPK could therefore bring beneficial effect on the cognitive function.

In addition to AMPK activation, CT has been reported to benefit circulation. CT improves microcirculation (Han et al., 2008), and it is also a vasorelaxant, which causes vasodilation of coronary artery (Lam et al., 2008). Putting the above findings and results of this chapter together, the effect of CT on blood lactic acid clearance can be speculated. Vasodilation of coronary artery can improve overall circulation, and the effect of CT on microcirculation facilitates the clearance of lactic acid from muscle tissue. The above findings and speculations are summarized in Fig 6.8.

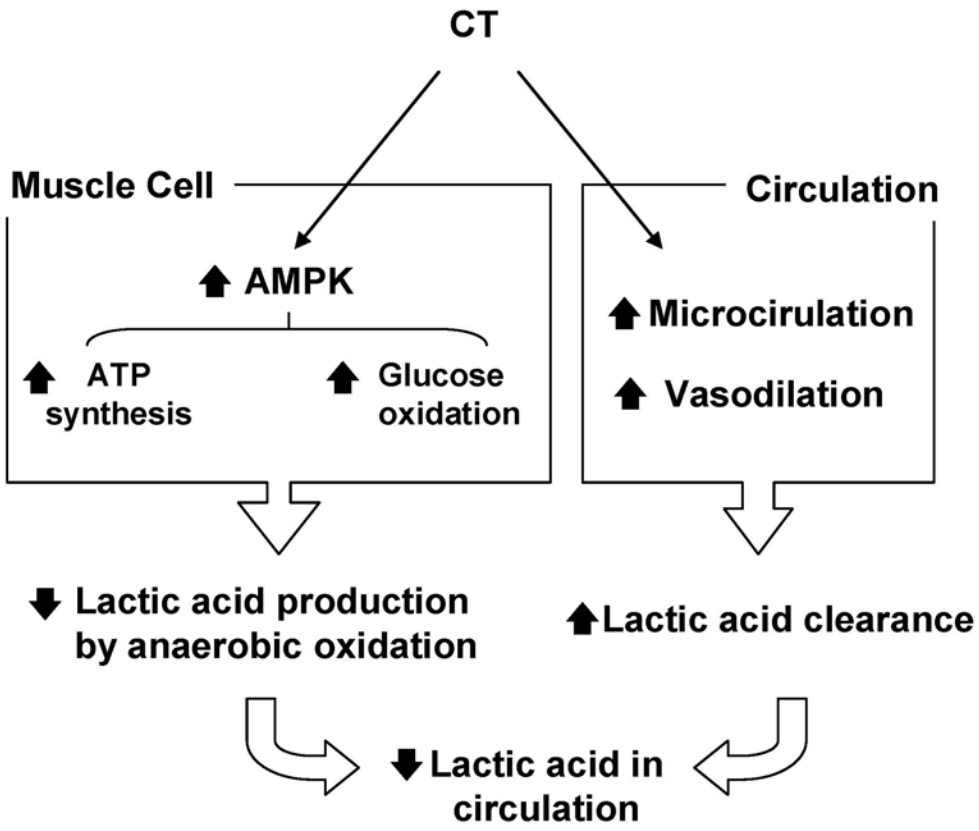

Fig 6.8 Schematic diagram of the effect of CT on reducing blood lactic acid.

In conclusion, tested by rotorod experiment, CT treatment does not cause motor defect. In addition, CT has the effect of enhancing the performance of rats through reducing the lactic acid in the circulation during exercise.

Chapter 7 General discussion and outlook

CT is a diterprene extracted from Danshen, the root of *Salvia miltiorrhiza* Bunge. The present study provides information on characterizing the AChE inhibiting property of CT *in-vitro*, and studying the *in-vivo* efficacy of CT on protecting scopolamine-induced memory impairment of rats in Morris water maze task. In addition, effect on the animal locomotor function has been revealed.

Many AChE inhibitors extracted from plants are alkaloid. Examples like huperzine-A and galantamine, which are a quinolizidine alkaloid, and a steroidal alkaloid respectively (Mukherjee et al., 2007). CT is a diterpenoid. So far, not many terpene-type AChE inhibitors have been reported. There is a monoterpene from the leaf of *Centella asiatica* and a diterpenoid from *Lsodon wightii* possessing AChE inhibiting property (Howes and Houghton, 2003); (Thirugnanasampandan et al., 2008). However, their potencies are low with IC_{50} towards human AChE in milli-molar level. The outstanding potency of CT and unique molecule class makes it a special class for the development of anti-AD drug.

Diterpenoids extracted from Danshen contain four major active constituents: tanshinone I, tanshinone IIA, dihydrotanshinone and CT. Apart from CT, another three compounds also showed anti-AChE activity. Tanshinone I and tanshinone IIA have a very weak anti-AChE activity with IC_{50} >50 μM. Among them, only CT and dihydrotanshinone are the most potent inhibitor. IC_{50} value of dihydrotanshinone, was 1 μM, which was the most potent AChE inhibitor among the four dipernoids (Ren et al., 2004). However, the amount of dihydrotanshinone in Danshen is far lower than CT (Hu et al., 2005; Li et al., 2002) and large scale extraction of dihydrotanshinone is difficult since it would be firstly extracted with dichloromethane:methanol in 4:1 ratio (Hu et al., 2005), or back extracted many times with 95% ethanol (Luo et al., 2006) and followed by column purification or preparative scale HPLC. Up till now, there is no method available for large scale preparation of dihydrotanshinone. Industrial scale preparation of CT by Sc-CO_2 extraction cannot be applied for the extraction of dihydrotanshinone since the amount of dihydrotanshinone inside the extract is very low (Li et al., 2004). Moreover, form a preliminary test of drug toxicity in neuroblastoma cell culture, dihydrotanshinone is highly toxic when comparing to CT (Fig 7.1). Considering all the above shortcomings, the

capability of developing dihydrotanshinone as potential anti-AD drug is lower than that of CT. The structure of dihydrotanshinone and CT differ in the way that the aromatic A ring in dihydrotanshinone is replaced by the hexane A ring in CT (Fig 7.2) and this might contribute to the higher potency of dihydrotanshinone on AChE inhibition. This little difference can be a hint for further modification of CT molecule to improve its potency.

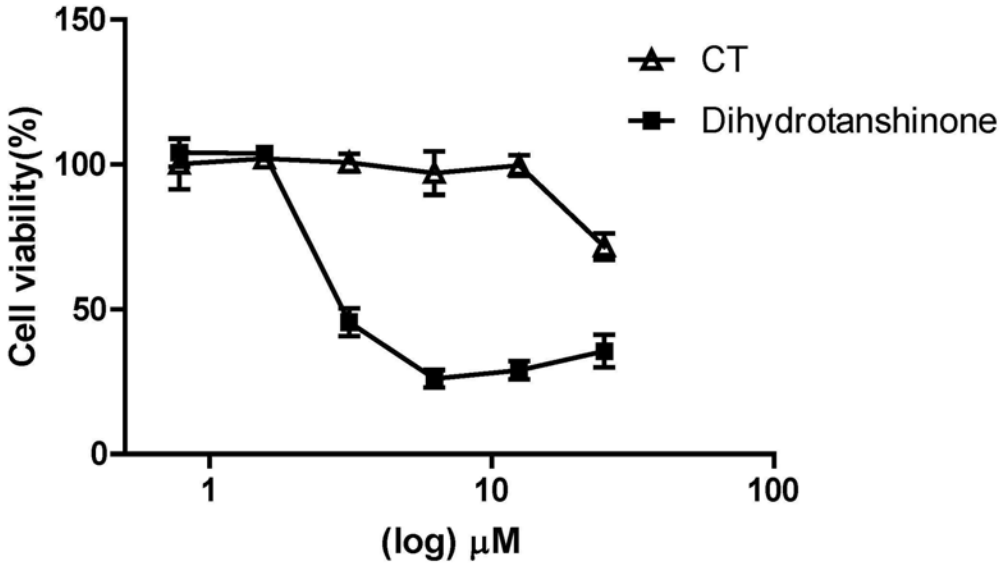

Fig 7.1 Viability of neuroblastoma SHSY-5Y cells measured with MTT assay. Neuroblastoma SHSY-5Y cells matained in culture medium (DMEMF-12 supplemented with 10%FBS) were treated with different concentration of CT (△) and Dihydrotanshinone (∎) for 4 hours. Data represent mean ± SEM of 3 individual treatment.

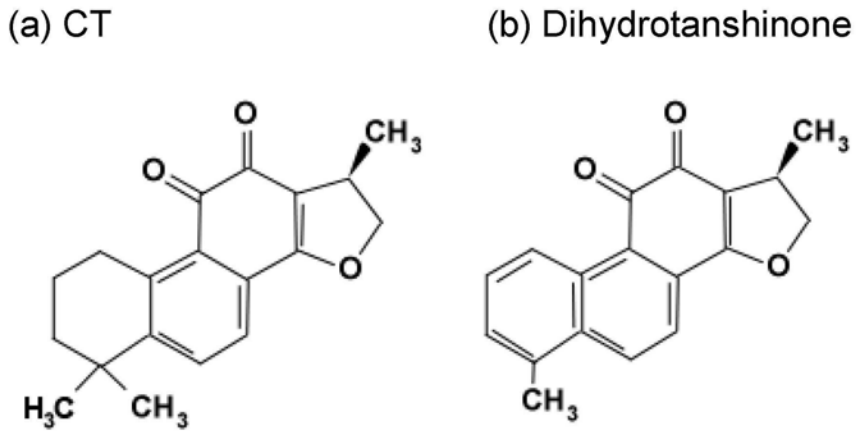

Fig 7.2 Structure of (a) CT and (b) dihydrotanshinone

As no data is so far available on the interacting site between CT and AChE molecule, kinetics assays were carried out to characterize how CT interacts with AChE. CT was found to be a reversible mixed-type inhibitor of human AChE and a reversible uncompetitive inhibitor of human BuChE. CT obeys first-order of inhibition, which indicated by the linear reactive curve of inhibited enzyme. From the mode of inhibition, it can be predicted that CT does not compete with AChE/BuChE for binding to their substrate. CT is a lipophilic diterpenoid. It probably binds with AChE/BuChE molecule through hydrophobic interactions. Hydrophobic interacting site of AChE molecule inside the active gorge includes the choline anionic site and the peripheral anionic site (Sussman et al., 1991). As CT is not a competitive inhibitor, the possibility that CT binds to the choline anionic site can be excluded. Difference in sequence in peripheral anion site residue between AChE and BuChE may be responsible to the difference in the observed mode of inhibition. In the future, details of binding of CT may be solved by co-crystallization with AChE molecule. Nowadays, bivalent AChE inhibitors that also target the peripheral binding site becomes a new approach for AD drug design (Munoz-Ruiz et al., 2005). Further modification of CT can be done by connecting to a competitive AChE inhibitor molecule by a linker with a suitable length.

Cholinergic therapies initially focus on the finding of anti-AChE drug because in healthy individual, AChE is responsible for the hydrolysis of ACh. However, as AD progresses, the regulation of ACh depends more on BuChE (Giacobini, 2003; Perry et al., 1978a). It is proven in clinical case that patients treated with AChE-selective inhibitors, galantamine and donepenzil, in early AD stage has developed tolerance in late stage. Switching to the non-selective inhibitor rivastigmine can restore the drug efficacy (Inglis, 2002). As CT is found to be a non-selective ChE inhibitor of both AChE and BuChE with similar potency, clinically, it may be more effective than a selective inhibitor along the progression of AD. Unfortunately, however, comparing with selective inhibitors, non-selective inhibitor rivastigmine has more adverse side effects such as vomiting, nausea and body weight loss in clinical cases (Farlow and Lilly, 2005; Gauthier, 2001) and this may be the consequence of inhibiting the peripheral BuChE. Data from chapter 6 suggested that long term CT treatment does not cause observable adverse effect like muscle weakness and body weight loss. It may due to the difference of molecular structures of CT and rivastigmine, so that CT can inhibit the esterase activity of BuChE/AChE but without blocking other functions. Another explanation to the cholinergic side effects is the rate

of inhibition. ChE inhibitors that inhibit the enzyme in fast rate results in a rapid rise in the body's ACh level, which may result in the adverse effect (Darvesh et al., 2003). CT is found not a fast acting inhibitor, which is indicated by the increase in inhibitory action during the course of incubation (Fig. 3.2),

Glutamate induced excitotoxicity was ameliorated by CT pretreatment. CT pretreatment was found to reduce tau phosphorylation, which is a downstream process of cell apoptosis mediated by glutamate excitotoxicity. Several tau kinases are involved in the pathology of the Aβ-mediated toxicity and the glutamate induced excitotoxicity: glutamate mediated calcium influx leads to the stimulation of ERK1/2 (Wenk et al., 2006); downregulation of phosphatidylinositol 3-kinase/ Akt (PI3/Akt) signaling pathway leads to activation of GSK-3β (Tolosa et al., 2008). Further investigation on the activation/deactivation of these tau kinases will help to clarify the CT-mediated neuroprotective effect. For further study, the upstream cause of glutamate excitotoxicy in AD, Aβ, may also be investigated in cultured cortical neuron.

Another possible mechanism of neuroprotective effect of AChE inhibitors is through antagonizing NMDA receptor (Song et al., 2008) and activating

nicotinic receptor α-7 subtype (Kihara et al., 2001) which's protective effect are mediated through reducing tau phosphorylation in the downstream (Kihara et al., 2001). Therefore, study of the effect of CT treatment on the regulation or activation/deactivation of the NMDA and nicotinic receptor may also be carried out to gain a more in-depth study on the neuroprotective effect of CT.

Several aspects on the effect of CT remain unexplored in the current study. The first one is the profile of CT on inhibiting different AChE isoforms, as AChE inhibitors like rivastigmine preferentially inhibits G1 isoform (Rakonczay, 2003), which is responsible for most of the brain AChE activity in AD patient (Siek et al., 1990). Another one is the differential expression of AChE isoforms. Different proportion of neuroprotective isoform AChE-R and neurodegenerative isoform AChE-S was reported in patients treated with rivastigmine, and the ratio of AChE-R:AChE-S was found to correlate with cognitive performance (Nordberg, 2006). In general, there was an increase in brain AChE activity in treated animals together with the improvement in cognitive function (chapter 5, Fig 5.8). Further investigation on the effect of CT on AChE isoform expression may give an answer on the above contradictive observation: if the increase in brain AChE activity is brought by the increase in

AChE-R isoform, the improvement in cognitive performance and the increase in TOTAL brain AChE activity would appear at the same time. On the other hand, although increase in brain AChE activity after prolonged inhibitor treatment has been reported in many other studies (Parnetti et al., 2002), a better correlation between improvement in cholinergic activity and improvement in cognitive performance can be tested by directly measure the CSF ACh level (Liang and Tang, 2004).

In conclusion, the present study provides data on the *in-vitro* and *in-vivo* efficacy of CT as an AChE inhibitor. The data suggested that CT is a reversible mixed-type and uncompetitive inhibitor for human AChE and BuChE repectively. CT treatment is able to inhibit AChE activity in cortical neuron culture, and protects neurons from glutamate challenge, by reducing the cellular tau phosphorylation. Data also showed that chronic oral administration of CT could reverse scopolamine-induced cognitive impairments in the absence of toxicity. In addition to cognitive improvement, CT treatment can increase swimming endurance in treated mice through reducing lactic acid produced during intense exercise. These findings provide support on the ability of CT as a potential therapeutic drug for treating AD

References:

Alcala, M. M., Vivas, N. M., Hospital, S., Camps, P., Munoz-Torrero, D., Badia, A., 2003. Characterisation of the anticholinesterase activity of two new tacrine-huperzine A hybrids. Neuropharmacology 44, 749-755.

Allderdice, P. W., Gardner, H. A., Galutira, D., Lockridge, O., LaDu, B. N., McAlpine, P. J., 1991. The cloned butyrylcholinesterase (BCHE) gene maps to a single chromosome site, 3q26. Genomics 11, 452-454.

Alvarez, G., Munoz-Montano, J. R., Satrustegui, J., Avila, J., Bogonez, E., Diaz-Nido, J., 2002. Regulation of tau phosphorylation and protection against beta-amyloid-induced neurodegeneration by lithium. Possible implications for Alzheimer's disease. Bipolar Disord 4, 153-165.

Ashani, Y., Shapira, S., Levy, D., Wolfe, A. D., Doctor, B. P., Raveh, L., 1991. Butyrylcholinesterase and acetylcholinesterase prophylaxis against soman poisoning in mice. Biochem Pharmacol 41, 37-41.

Atack, J. R., Perry, E. K., Bonham, J. R., Candy, J. M., Perry, R. H., 1986. Molecular forms of acetylcholinesterase and butyrylcholinesterase in the aged human central nervous system. J.Neurochem. 47, 263-277.

Baldi, E., Lorenzini, C. A., Corrado, B., 2003. Task solving by procedural

strategies in the Morris water maze. Physiology and Behavior 78, 785-793.

Ballard, C. G., 2002. Advances in the treatment of Alzheimer's disease: benefits of dual cholinesterase inhibition. Eur Neurol 47, 64-70.

Baruah, J., Easby, J., Kessell, G., 2008. Effects of acetylcholinesterase inhibitor therapy for Alzheimer's disease on neuromuscular block. Br J Anaesth 100, 420.

Beatty, W. W., Butters, N., Janowsky, D. S., 1986. Patterns of memory failure after scopolamine treatment: implications for cholinergic hypotheses of dementia. Behav.Neural Biol. 45, 196-211.

Beiko, J., Candusso, L., Cain, D. P., 1997. The effect of nonspatial water maze pretraining in rats subjected to serotonin depletion and muscarinic receptor antagonism: a detailed behavioural assessment of spatial performance. Behav.Brain Res. 88, 201-211.

Bon, S., Coussen, F., Massoulie, J., 1997. Quaternary associations of acetylcholinesterase. II. The polyproline attachment domain of the collagen tail. J Biol Chem 272, 3016-3021.

Bores, G. M., Huger, F. P., Petko, W., Mutlib, A. E., Camacho, F., Rush, D. K., Selk, D. E., Wolf, V., Kosley, R. W., Jr., Davis, L., Vargas, H. M., 1996.

Pharmacological evaluation of novel Alzheimer's disease therapeutics: acetylcholinesterase inhibitors related to galanthamine. J Pharmacol Exp Ther 277, 728-738.

Bourne, Y., Taylor, P., Marchot, P., 1995. Acetylcholinesterase inhibition by fasciculin: crystal structure of the complex. Cell 83, 503-512.

Braida, D., Paladini, E., Griffini, P., Lamperti, M., Maggi, A., Sala, M., 1996. An inverted U-shaped curve for heptylphysostigmine on radial maze performance in rats: comparison with other cholinesterase inhibitors. European Journal of Pharmacology 302, 13-20.

Brody, D. L., Holtzman, D. M., 2006. Morris water maze search strategy analysis in PDAPP mice before and after experimental traumatic brain injury. Exp.Neurol. 197, 330-340.

Ceddia, R. B., Sweeney, G., 2004. Creatine supplementation increases glucose oxidation and AMPK phosphorylation and reduces lactate production in L6 rat skeletal muscle cells. J Physiol 555, 409-421.

Cheng, W., Ma, L., Toshihide, H., 2004. Treatment of Vascular Dementia by Naozhitong Capsule: A Clinical Observation of 18 Cases. New Journal of Traditional Chinese Medicine 1, 16-18.

Chohan, M. O., Iqbal, K., 2006. From tau to toxicity: emerging roles of NMDA

receptor in Alzheimer's disease. J Alzheimers Dis 10, 81-87.

Contestabile, A., Ciani, E., 2008. The place of choline acetyltransferase activity measurement in the "cholinergic hypothesis" of neurodegenerative diseases. Neurochem Res 33, 318-327.

Cutler, N. R., Polinsky, R. J., Sramek, J. J., Enz, A., Jhee, S. S., Mancione, L., Hourani, J., Zolnouni, P., 1998. Dose-dependent CSF acetylcholinesterase inhibition by SDZ ENA 713 in Alzheimer's disease. Acta Neurol Scand 97, 244-250.

Darvesh, S., Walsh, R., Kumar, R., Caines, A., Roberts, S., Magee, D., Rockwood, K., Martin, E., 2003. Inhibition of human cholinesterases by drugs used to treat Alzheimer disease. Alzheimer Dis Assoc Disord 17, 117-126.

Davidsson, P., Blennow, K., Andreasen, N., Eriksson, B., Minthon, L., Hesse, C., 2001. Differential increase in cerebrospinal fluid-acetylcholinesterase after treatment with acetylcholinesterase inhibitors in patients with Alzheimer's disease. Neurosci Lett 300, 157-160.

De Ferrari, G. V., Canales, M. A., Shin, I., Weiner, L. M., Silman, I., Inestrosa, N. C., 2001. A structural motif of acetylcholinesterase that promotes amyloid beta-peptide fibril formation. Biochemistry 40, 10447-10457.

Derave, W., Van Den Bosch, L., Lemmens, G., Eijnde, B. O., Robberecht, W., Hespel, P., 2003. Skeletal muscle properties in a transgenic mouse model for amyotrophic lateral sclerosis: effects of creatine treatment. Neurobiol Dis 13, 264-272.

Ellman, G. L., Courtney, K. D., Andres, V., Jr., Feather-Stone, R. M., 1961. A new and rapid colorimetric determination of acetylcholinesterase activity. Biochem Pharmacol. 7, 88-95.

Esiri, M. M., 1996. The basis for behavioural disturbances in dementia. J Neurol Neurosurg Psychiatry 61, 127-130.

Fadda, F., Cocco, S., Stancampiano, R., 2000. Hippocampal acetylcholine release correlates with spatial learning performance in freely moving rats. Neuroreport 11, 2265-2269.

Fadda, F., Melis, F., Stancampiano, R., 1996. Increased hippocampal acetylcholine release during a working memory task. Eur.J.Pharmacol. 307, R1-R2.

Fang, L., Appenroth, D., Decker, M., Kiehntopf, M., Lupp, A., Peng, S., Fleck, C., Zhang, Y., Lehmann, J., 2008. NO-donating tacrine hybrid compounds improve scopolamine-induced cognition impairment and show less hepatotoxicity. J Med Chem 51, 7666-7669.

Farlow, M. R., Lilly, M. L., 2005. Rivastigmine: an open-label, observational study of safety and effectiveness in treating patients with Alzheimer's disease for up to 5 years. BMC Geriatr 5, 3.

Fu, H., Li, W., Lao, Y., Luo, J., Lee, N. T., Kan, K. K., Tsang, H. W., Tsim, K. W., Pang, Y., Li, Z., Chang, D. C., Li, M., Han, Y., 2006. Bis(7)-tacrine attenuates beta amyloid-induced neuronal apoptosis by regulating L-type calcium channels. J Neurochem 98, 1400-1410.

Gandhi, C. C., Kelly, R. M., Wiley, R. G., Walsh, T. J., 2000. Impaired acquisition of a Morris water maze task following selective destruction of cerebellar purkinje cells with OX7-saporin. Behavioural Brain Research 109, 37-47.

Garcia-Ayllon, M. S., Silveyra, M. X., Saez-Valero, J., 2008. Association between acetylcholinesterase and beta-amyloid peptide in Alzheimer's cerebrospinal fluid. Chem Biol Interact 175, 209-215.

Gauthier, S., 2001. Cholinergic adverse effects of cholinesterase inhibitors in Alzheimer's disease: epidemiology and management. Drugs Aging 18, 853-862.

Geerts, H., 2005. Indicators of neuroprotection with galantamine. Brain Res Bull 64, 519-524.

Geula, C., Mesulam, M. M., 1995a. Cholinesterases and the pathology of Alzheimer disease. Alzheimer Dis.Assoc.Disord. 9 Suppl 2, 23-28.

Geula, C., Mesulam, M. M., 1995b. Cholinesterases and the pathology of Alzheimer disease. Alzheimer Dis Assoc Disord 9 Suppl 2, 23-28.

Giacobini, E., 2003. Cholinergic function and Alzheimer's disease. Int.J.Geriatr.Psychiatry 18, S1-S5.

Giacobini, E., 2004. Cholinesterase inhibitors: new roles and therapeutic alternatives. Pharmacol.Res. 50, 433-440.

Goedert, M., Jakes, R., Crowther, R. A., Cohen, P., Vanmechelen, E., Vandermeeren, M., Cras, P., 1994. Epitope mapping of monoclonal antibodies to the paired helical filaments of Alzheimer's disease: identification of phosphorylation sites in tau protein. Biochem J 301 (Pt 3), 871-877.

Gomez-Pinilla, F., Vaynman, S., Ying, Z., 2008. Brain-derived neurotrophic factor functions as a metabotrophin to mediate the effects of exercise on cognition. Eur J Neurosci 28, 2278-2287.

Greenblatt, H. M., Kryger, G., Lewis, T., Silman, I., Sussman, J. L., 1999. Structure of acetylcholinesterase complexed with (-)-galanthamine at 2.3 A resolution. FEBS Lett 463, 321-326.

Han, J. Y., Fan, J. Y., Horie, Y., Miura, S., Cui, D. H., Ishii, H., Hibi, T., Tsuneki, H., Kimura, I., 2008. Ameliorating effects of compounds derived from Salvia miltiorrhiza root extract on microcirculatory disturbance and target organ injury by ischemia and reperfusion. Pharmacol Ther 117, 280-295.

Harel, M., Kryger, G., Rosenberry, T. L., Mallender, W. D., Lewis, T., Fletcher, R. J., Guss, J. M., Silman, I., Sussman, J. L., 2000. Three-dimensional structures of Drosophila melanogaster acetylcholinesterase and of its complexes with two potent inhibitors. Protein Sci 9, 1063-1072.

Harkany, T., Abraham, I., Timmerman, W., Laskay, G., Toth, B., Sasvari, M., Konya, C., Sebens, J. B., Korf, J., Nyakas, C., Zarandi, M., Soos, K., Penke, B., Luiten, P. G., 2000. beta-amyloid neurotoxicity is mediated by a glutamate-triggered excitotoxic cascade in rat nucleus basalis. Eur J Neurosci 12, 2735-2745.

Harris, M. E., Wang, Y., Pedigo, N. W., Jr., Hensley, K., Butterfield, D. A., Carney, J. M., 1996. Amyloid beta peptide (25-35) inhibits Na+-dependent glutamate uptake in rat hippocampal astrocyte cultures. J Neurochem 67, 277-286.

Howes, M. J., Houghton, P. J., 2003. Plants used in Chinese and Indian traditional medicine for improvement of memory and cognitive function.

Pharmacol Biochem Behav 75, 513-527.

Hu, P., Luo, G. A., Zhao, Z. Z., Jiang, Z. H., 2005. Quantitative determination of four diterpenoids in Radix Salviae Miltiorrhizae using LC-MS-MS. Chem Pharm Bull (Tokyo) 53, 705-709.

Ibebunjo, C., Donati, F., Fox, G. S., Eshelby, D., Tchervenkov, J. I., 1997. The effects of chronic tacrine therapy on d-tubocurarine blockade in the soleus and tibialis muscles of the rat. Anesth Analg 85, 431-436.

Imahori, K., Uchida, T., 1997. Physiology and pathology of tau protein kinases in relation to Alzheimer's disease. J Biochem 121, 179-188.

Inestrosa, N. C., Sagal, J. P., Colombres, M., 2005. Acetylcholinesterase interaction with Alzheimer amyloid beta. Subcell Biochem 38, 299-317.

Inglis, F., 2002. The tolerability and safety of cholinesterase inhibitors in the treatment of dementia. Int J Clin Pract Suppl, 45-63.

Jang, M. H., Piao, X. L., Kim, J. M., Kwon, S. W., Park, J. H., 2008. Inhibition of cholinesterase and amyloid-beta aggregation by resveratrol oligomers from Vitis amurensis. Phytother Res 22, 544-549.

Jann, M. W., 2000. Rivastigmine, a new-generation cholinesterase inhibitor for the treatment of Alzheimer's disease. Pharmacotherapy 20, 1-12.

Janus, C., 2004. Search strategies used by APP transgenic mice during

navigation in the Morris water maze. Learn.Mem. 11, 337-346.

Jin, D. Z., Yin, L. L., Ji, X. Q., Zhu, X. Z., 2006. Cryptotanshinone inhibits cyclooxygenase-2 enzyme activity but not its expression. European Journal of Pharmacology 549, 166-172.

Jogani, V. V., Shah, P. J., Mishra, P., Mishra, A. K., Misra, A. R., 2008. Intranasal mucoadhesive microemulsion of tacrine to improve brain targeting. Alzheimer Dis Assoc Disord 22, 116-124.

Kaufer, D., Friedman, A., Seidman, S., Soreq, H., 1998. Acute stress facilitates long-lasting changes in cholinergic gene expression. Nature 393, 373-377.

Kihara, T., Shimohama, S., Sawada, H., Honda, K., Nakamizo, T., Shibasaki, H., Kume, T., Akaike, A., 2001. alpha 7 nicotinic receptor transduces signals to phosphatidylinositol 3-kinase to block A beta-amyloid-induced neurotoxicity. J Biol Chem 276, 13541-13546.

Kim, D. H., Jeon, S. J., Jung, J. W., Lee, S., Yoon, B. H., Shin, B. Y., Son, K. H., Cheong, J. H., Kim, Y. S., Kang, S. S., Ko, K. H., Ryu, J. H., 2007. Tanshinone congeners improve memory impairments induced by scopolamine on passive avoidance tasks in mice. European Journal of Pharmacology 574, 140-147.

Kline, C. E., Durstine, J. L., Davis, J. M., Moore, T. A., Devlin, T. M., Zielinski,

M. R., Youngstedt, S. D., 2007. Circadian variation in swim performance. J Appl Physiol 102, 641-649.

Knapp, M. J., Knopman, D. S., Solomon, P. R., Pendlebury, W. W., Davis, C. S., Gracon, S. I., 1994. A 30-week randomized controlled trial of high-dose tacrine in patients with Alzheimer's disease. The Tacrine Study Group. JAMA 271, 985-991.

Kosasa, T., Kuriya, Y., Matsui, K., Yamanishi, Y., 1999. Inhibitory effects of donepezil hydrochloride (E2020) on cholinesterase activity in brain and peripheral tissues of young and aged rats. Eur J Pharmacol 386, 7-13.

Kovalchuk, Y., Hanse, E., Kafitz, K. W., Konnerth, A., 2002. Postsynaptic Induction of BDNF-Mediated Long-Term Potentiation. Science 295, 1729-1734.

Kryger, G., Harel, M., Giles, K., Toker, L., Velan, B., Lazar, A., Kronman, C., Barak, D., Ariel, N., Shafferman, A., Silman, I., Sussman, J. L., 2000. Structures of recombinant native and E202Q mutant human acetylcholinesterase complexed with the snake-venom toxin fasciculin-II. Acta Crystallogr D Biol Crystallogr 56, 1385-1394.

Kumar, V., Becker, R. E., 1989. Clinical pharmacology of tetrahydroaminoacridine: a possible therapeutic agent Alzheimer's

disease. Int.J.Clin.Pharmacol.Ther.Toxicol. 27, 478-485.

Lam, F. F. Y., Yeung, J. H. K., Chan, K. M., Or, P. M. Y., 2008. Mechanisms of the dilator action of cryptotanshinone on rat coronary artery. European Journal of Pharmacology 578, 253-260.

Lee, D. S., Lee, S. H., Noh, J. G., Hong, S. D., 1999. Antibacterial activities of cryptotanshinone and dihydrotanshinone I from a medicinal herb, Salvia miltiorrhiza Bunge. Bioscience, Biotechnology, and Biochemistry 63, 2236-2239.

Lenz, D. E., Yeung, D., Smith, J. R., Sweeney, R. E., Lumley, L. A., Cerasoli, D. M., 2007. Stoichiometric and catalytic scavengers as protection against nerve agent toxicity: a mini review. Toxicology 233, 31-39.

Leon, R., Rios, C. d. l., Marco-Contelles, J., Huertas, O., Barril, X., Javier Luque, F., Lopez, M. G., Garcia, A. G., Villarroya, M., 2008. New tacrine-dihydropyridine hybrids that inhibit acetylcholinesterase, calcium entry, and exhibit neuroprotection properties. Bioorganic & Medicinal Chemistry 16, 7759-7769.

Lev-Lehman, E., Evron, T., Broide, R. S., Meshorer, E., Ariel, I., Seidman, S., Soreq, H., 2000. Synaptogenesis and myopathy under acetylcholinesterase overexpression. J Mol Neurosci 14, 93-105.

Li, X., Tang, Y., Zhao, X. F., Lu, H. B., H., Z. X., 2004. Active components in the extracts of Radix Salvia miltiorrhizae by supercritical carbon dioxide fluid. Journal of Xipan Jiaotong University (Medical Sciences) 25, 614-620.

Li, Y. C., Zeng, J. Q., Liu, L. M., Jin, X. S., 2002. [Extraction of three tanshinones from the root of Salvia miltiorrhiza Bunge by supercritical carbon dioxide fluid and their analysis with high performance liquid chromatography]. Se Pu 20, 40-42.

Liang, Y. Q., Tang, X. C., 2004. Comparative effects of huperzine A, donepezil and rivastigmine on cortical acetylcholine level and acetylcholinesterase activity in rats. Neurosci Lett 361, 56-59.

Liao, F., Li, Q., 1996. Clinical Observation on 31 Cases of Senile Dementia Treated by "Nao Li Kang". Journal of Chengdu University of Traditional Chinese Medicine 19, 20-25.

Luo, X. J., Liu, Y., Li, Y., He, Y., 2006. [Study on uniform-design for optimizing supercritical-CO2 fluid extraction technique of tanshinones in radix salviae]. Zhongguo Zhong Yao Za Zhi 31, 2042-2045.

Mandelkow, E. M., Biernat, J., Drewes, G., Gustke, N., Trinczek, B., Mandelkow, E., 1995. Tau domains, phosphorylation, and interactions

with microtubules. Neurobiol Aging 16, 355-362; discussion 362-353.

Mesulam, M., Guillozet, A., Shaw, P., Quinn, B., 2002. Widely spread butyrylcholinesterase can hydrolyze acetylcholine in the normal and Alzheimer brain. Neurobiol.Dis. 9, 88-93.

Morris, R., 1984. Developments of a water-maze procedure for studying spatial learning in the rat. J.Neurosci.Methods 11, 47-60.

Mukherjee, P. K., Kumar, V., Mal, M., Houghton, P. J., 2007. Acetylcholinesterase inhibitors from plants. Phytomedicine. 14, 289-300.

Munoz-Ruiz, P., Rubio, L., Garcia-Palomero, E., Dorronsoro, I., del Monte-Millan, M., Valenzuela, R., Usan, P., de Austria, C., Bartolini, M., Andrisano, V., Bidon-Chanal, A., Orozco, M., Luque, F. J., Medina, M., Martinez, A., 2005. Design, synthesis, and biological evaluation of dual binding site acetylcholinesterase inhibitors: new disease-modifying agents for Alzheimer's disease. J Med Chem 48, 7223-7233.

Nilsson, L., Nordberg, A., Hardy, J., Wester, P., Winblad, B., 1986. Physostigmine restores 3H-acetylcholine efflux from Alzheimer brain slices to normal level. J Neural Transm 67, 275-285.

Nordberg, A., 2006. Mechanisms behind the neuroprotective actions of cholinesterase inhibitors in Alzheimer disease. Alzheimer Dis Assoc

Disord 20, S12-18.

Nordberg, A., Svensson, A. L., 1998. Cholinesterase inhibitors in the treatment of Alzheimer's disease: a comparison of tolerability and pharmacology. Drug Saf 19, 465-480.

Parnetti, L., Amici, S., Lanari, A., Romani, C., Antognelli, C., Andreasen, N., Minthon, L., Davidsson, P., Pottel, H., Blennow, K., Gallai, V., 2002. Cerebrospinal fluid levels of biomarkers and activity of acetylcholinesterase (AChE) and butyrylcholinesterase in AD patients before and after treatment with different AChE inhibitors. Neurol Sci 23 Suppl 2, S95-96.

Perry, E. K., Gibson, P. H., Blessed, G., Perry, R. H., Tomlinson, B. E., 1977. Neurotransmitter enzyme abnormalities in senile dementia. Choline acetyltransferase and glutamic acid decarboxylase activities in necropsy brain tissue. J Neurol Sci 34, 247-265.

Perry, E. K., Perry, R. H., Blessed, G., Tomlinson, B. E., 1978a. Changes in brain cholinesterases in senile dementia of Alzheimer type. Neuropathol.Appl.Neurobiol. 4, 273-277.

Perry, E. K., Tomlinson, B. E., Blessed, G., Bergmann, K., Gibson, P. H., Perry, R. H., 1978b. Correlation of cholinergic abnormalities with senile plaques

and mental test scores in senile dementia. Br.Med.J. 2, 1457-1459.

Price, D. L., Sisodia, S. S., Borchelt, D. R., 1998. Genetic neurodegenerative diseases: the human illness and transgenic models. Science 282, 1079-1083.

Radic, Z., Pickering, N. A., Vellom, D. C., Camp, S., Taylor, P., 1993. Three distinct domains in the cholinesterase molecule confer selectivity for acetyl- and butyrylcholinesterase inhibitors. Biochemistry 32, 12074-12084.

Rakonczay, Z., 2003. Potencies and selectivities of inhibitors of acetylcholinesterase and its molecular forms in normal and Alzheimer's disease brain. Acta Biol Hung 54, 183-189.

Raves, M. L., Harel, M., Pang, Y. P., Silman, I., Kozikowski, A. P., Sussman, J. L., 1997. Structure of acetylcholinesterase complexed with the nootropic alkaloid, (-)-huperzine A. Nat Struct Biol 4, 57-63.

Reid, R. T., Sabbagh, M. N., 2003. Effects of donepezil treatment on rat nicotinic acetylcholine receptor levels in vivo and in vitro. J Alzheimers Dis 5, 429-436.

Ren, Y., Houghton, P. J., Hider, R. C., Howes, M. J., 2004. Novel diterpenoid acetylcholinesterase inhibitors from Salvia miltiorhiza. Planta Med. 70,

201-204.

Roberson, E. D., Scearce-Levie, K., Palop, J. J., Yan, F., Cheng, I. H., Wu, T., Gerstein, H., Yu, G. Q., Mucke, L., 2007. Reducing endogenous tau ameliorates amyloid beta-induced deficits in an Alzheimer's disease mouse model. Science 316, 750-754.

Rogers, S. L., Doody, R. S., Pratt, R. D., Ieni, J. R., 2000. Long-term efficacy and safety of donepezil in the treatment of Alzheimer's disease: final analysis of a US multicentre open-label study. Eur Neuropsychopharmacol 10, 195-203.

Rotundo, R. L., 1990. Nucleus-specific translation and assembly of acetylcholinesterase in multinucleated muscle cells. J Cell Biol 110, 715-719.

Rylett, R. J., Ball, M. J., Colhoun, E. H., 1983. Evidence for high affinity choline transport in synaptosomes prepared from hippocampus and neocortex of patients with Alzheimer's disease. Brain Res 289, 169-175.

Samochocki, M., Hoffle, A., Fehrenbacher, A., Jostock, R., Ludwig, J., Christner, C., Radina, M., Zerlin, M., Ullmer, C., Pereira, E. F., Lubbert, H., Albuquerque, E. X., Maelicke, A., 2003. Galantamine is an allosterically potentiating ligand of neuronal nicotinic but not of muscarinic acetylcholine

receptors. J Pharmacol Exp Ther 305, 1024-1036.

Saucier, D., Hargreaves, E. L., Boon, F., Vanderwolf, C. H., Cain, D. P., 1996. Detailed behavioral analysis of water maze acquisition under systemic NMDA or muscarinic antagonism: nonspatial pretraining eliminates spatial learning deficits. Behavioural Neuroscience 110, 103-116.

Savini, L., Campiani, G., Gaeta, A., Pellerano, C., Fattorusso, C., Chiasserini, L., Fedorko, J. M., Saxena, A., 2001. Novel and potent tacrine-related hetero- and homobivalent ligands for acetylcholinesterase and butyrylcholinesterase. Bioorganic & Medicinal Chemistry Letters 11, 1779-1782.

Schwarz, M., Glick, D., Loewenstein, Y., Soreq, H., 1995. Engineering of human cholinesterases explains and predicts diverse consequences of administration of various drugs and poisons. Pharmacol Ther 67, 283-322.

Siek, G. C., Katz, L. S., Fishman, E. B., Korosi, T. S., Marquis, J. K., 1990. Molecular forms of acetylcholinesterase in subcortical areas of normal and Alzheimer disease brain. Biol Psychiatry 27, 573-580.

Sisodia, S. S., Martin, L. J., Walker, L. C., Borchelt, D. R., Price, D. L., 1995. Cellular and molecular biology of Alzheimer's disease and animal models. Neuroimaging Clin.N.Am. 5, 59-68.

Song, M. S., Rauw, G., Baker, G. B., Kar, S., 2008. Memantine protects rat cortical cultured neurons against beta-amyloid-induced toxicity by attenuating tau phosphorylation. Eur J Neurosci 28, 1989-2002.

Suchankova, G., Nelson, L. E., Gerhart-Hines, Z., Kelly, M., Gauthier, M. S., Saha, A. K., Ido, Y., Puigserver, P., Ruderman, N. B., 2009. Concurrent regulation of AMP-activated protein kinase and SIRT1 in mammalian cells. Biochem Biophys Res Commun 378, 836-841.

Sugimoto, H., Ogura, H., Arai, Y., Limura, Y., Yamanishi, Y., 2002. Research and development of donepezil hydrochloride, a new type of acetylcholinesterase inhibitor. Jpn J Pharmacol 89, 7-20.

Suh, S. J., Jin, U. H., Choi, H. J., Chang, H. W., Son, J. K., Lee, S. H., Jeon, S. J., Son, K. H., Chang, Y. C., Lee, Y. C., Kim, C. H., 2006. Cryptotanshinone from Salvia miltiorrhiza BUNGE has an inhibitory effect on TNF-alpha-induced matrix metalloproteinase-9 production and HASMC migration via down-regulated NF-kappaB and AP-1. Biochemical Pharmacology 72, 1680-1689.

Summers, W. K., 2006. Tacrine, and Alzheimer's treatments. J Alzheimers Dis 9, 439-445.

Sussman, J. L., Harel, M., Frolow, F., Oefner, C., Goldman, A., Toker, L.,

Silman, I., 1991. Atomic structure of acetylcholinesterase from Torpedo californica: a prototypic acetylcholine-binding protein. Science 253, 872-879.

Svensson, A. L., Nordberg, A., 1998. Tacrine and donepezil attenuate the neurotoxic effect of A beta(25-35) in rat PC12 cells. Neuroreport 9, 1519-1522.

Takada-Takatori, Y., Kume, T., Sugimoto, M., Katsuki, H., Niidome, T., Sugimoto, H., Fujii, T., Okabe, S., Akaike, A., 2006. Neuroprotective effects of galanthamine and tacrine against glutamate neurotoxicity. Eur J Pharmacol 549, 19-26.

Thirugnanasampandan, R., Jayakumar, R., Narmatha Bai, V., Martin, E., Rajendra Prasad, K. J., 2008. Antiacetylcholinesterase and antioxidant ent-Kaurene diterpenoid, melissoidesin from Isodon wightii (Bentham) H. Hara. Nat Prod Res 22, 681-688.

Tolosa, L., Mir, M., Olmos, G., Llado, J., 2008. Vascular endothelial growth factor protects motoneurons from serum deprivation-induced cell death through phosphatidylinositol 3-kinase-mediated p38 mitogen-activated protein kinase inhibition. Neuroscience.

Van Dam, D., Abramowski, D., Staufenbiel, M., De Deyn, P. P., 2005.

Symptomatic effect of donepezil, rivastigmine, galantamine and memantine on cognitive deficits in the APP23 model. Psychopharmacology (Berl) 180, 177-190.

von Linstow, R. E., Harbaran, D., Micheau, J., Platt, B., Riedel, G., 2007. Dissociation of cholinergic function in spatial and procedural learning in rats. Neuroscience 146, 875-889.

Walton, H. S., Dodd, P. R., 2007. Glutamate-glutamine cycling in Alzheimer's disease. Neurochem Int 50, 1052-1066.

Wang, B., Wang, Z., Jiang, S., Pan, H., 2005. Effect of Chinese herbs of blood-activating and stasis-dissipating on learning and memory ability of rats with hippocampal ischemia injury. Chinese Journal of Clinical Rehabilitation 48.

Wang, H., Carlier, P. R., Ho, W. L., Lee, N. T., Pang, Y. P., Han, Y. F., 1999a. Attenuation of scopolamine-induced deficits in navigational memory performance in rats by bis(7)-tacrine, a novel dimeric AChE inhibitor. Zhongguo Yao Li Xue Bao 20, 211-217.

Wang, H., Carlier, P. R., Ho, W. L., Wu, D. C., Lee, N. T., Li, C. P., Pang, Y. P., Han, Y. F., 1999b. Effects of bis(7)-tacrine, a novel anti-Alzheimer's agent, on rat brain AChE. Neuroreport 10, 789-793.

Watkins, P. B., Zimmerman, H. J., Knapp, M. J., Gracon, S. I., Lewis, K. W., 1994. Hepatotoxic effects of tacrine administration in patients with Alzheimer's disease. JAMA 271, 992-998.

Wenk, G. L., Parsons, C. G., Danysz, W., 2006. Potential role of N-methyl-D-aspartate receptors as executors of neurodegeneration resulting from diverse insults: focus on memantine. Behav Pharmacol 17, 411-424.

Whishaw, I. Q., 1985. Cholinergic receptor blockade in the rat impairs locale but not taxon strategies for place navigation in a swimming pool. Behav.Neurosci. 99, 979-1005.

Woodruff-Pak, D. S., Vogel, R. W., 3rd, Wenk, G. L., 2001. Galantamine: effect on nicotinic receptor binding, acetylcholinesterase inhibition, and learning. Proc Natl Acad Sci U S A 98, 2089-2094.

Xie, M. Z., Shen, Z. F., 1983. [Absorption, distribution, excretion and metabolism of cryptotanshinone]. Yao Xue Xue Bao 18, 90-96.

Xu, Y., Xue, F., Jiao, X. N., Zhang, Y. Y., Wang, J. X., 2008. Experiment on extraction of cryptotanshinone from Radix salvia miltiorrhiza. Northwest Pharmaceutical Journal 23, 145-147.

Xu, Y., Yang, J. R., Liu, X., Lo, D. C., Wang, J. X., 2006a. Study on the

extraction process of cryptotanshinone from Radix salvia miltiorrhiza. Northwest Pharmaceutical Journal 21, 111-112.

Xu, Z., Zheng, H., Law, S. L., Dong, S. D., Han, Y., Xue, H., 2006b. Effects of a memory enhancing peptide on cognitive abilities of brain-lesioned mice: additivity with huperzine A and relative potency to tacrine. Journal of Peptide Science 12, 72-78.

Xue, M., Cui, Y., Wang, H. Q., Luo, Y. J., Zhang, B., Zhou, Z. T., 1999. Pharmacokinetics of cryptotanshinone and its metabolite in pigs. Acta Pharmaceutica Sinica 34, 81-84.

Yankner, B. A., 1996. Mechanisms of neuronal degeneration in Alzheimer's disease. Neuron 16, 921-932.

Zhang, J., Huang, M., Guan, S., Bi, H. C., Pan, Y., Duan, W., Chan, S. Y., Chen, X., Hong, Y. H., Bian, J. S., Yang, H. Y., Zhou, S., 2006. A mechanistic study of the intestinal absorption of cryptotanshinone, the major active constituent of Salvia miltiorrhiza. J Pharmacol Exp Ther 317, 1285-1294.

Zhao, L., Chen, Q., Diaz Brinton, R., 2002. Neuroprotective and neurotrophic efficacy of phytoestrogens in cultured hippocampal neurons. Exp Biol Med (Maywood) 227, 509-519.

Zimmermann, M., Borroni, B., Cattabeni, F., Padovani, A., Di Luca, M., 2005. Cholinesterase inhibitors influence APP metabolism in Alzheimer disease patients. Neurobiol Dis 19, 237-242.